

4

Applied Research Laboratory

DTIC FILE COPY

AD-A197 399

Technical Report

ACOUSTIC INTENSITY: ENERGY TRANSFER,
WAVE PROPERTIES AND APPLICATIONS

by

Julian Adin Mann III

DTIC
SELECTED
AUG 15 1988
S H D

PENN STATE



DISTRIBUTION STATEMENT A
Approved for public release;
Distribution Unlimited

4

The Pennsylvania State University
APPLIED RESEARCH LABORATORY
P. O. Box 30
State College, PA 16804

ACOUSTIC INTENSITY: ENERGY TRANSFER,
WAVE PROPERTIES AND APPLICATIONS

by

Julian Adin Mann III

N00024-85-C-6041

Technical Report No. TR 88-010

August 1988

DTIC
SELECTE
AUG 15 1988
S H D
H

Supported by:
Naval Sea Systems Command

L. R. Hettche, Director
Applied Research Laboratory

Approved for public release; distribution unlimited

Unclassified
SECURITY CLASSIFICATION OF THIS PAGE

A1973??

REPORT DOCUMENTATION PAGE

1a. REPORT SECURITY CLASSIFICATION Unclassified		1b. RESTRICTIVE MARKINGS	
2a. SECURITY CLASSIFICATION AUTHORITY		3. DISTRIBUTION / AVAILABILITY OF REPORT Unlimited	
2b. DECLASSIFICATION / DOWNGRADING SCHEDULE			
4. PERFORMING ORGANIZATION REPORT NUMBER(S)		5. MONITORING ORGANIZATION REPORT NUMBER(S)	
6a. NAME OF PERFORMING ORGANIZATION Applied Research Laboratory The Pennsylvania State University	6b. OFFICE SYMBOL (if applicable) ARL	7a. NAME OF MONITORING ORGANIZATION Naval Sea Systems Command Department of the Navy	
6c. ADDRESS (City, State, and ZIP Code) P. O. Box 30 State College, PA 16804		7b. ADDRESS (City, State, and ZIP Code) Washington, DC 20362	
8a. NAME OF FUNDING / SPONSORING ORGANIZATION Naval Sea Systems Command	8b. OFFICE SYMBOL (if applicable) NAVSEA	9. PROCUREMENT INSTRUMENT IDENTIFICATION NUMBER	
8c. ADDRESS (City, State, and ZIP Code) Department of the Navy Washington, DC 20362		10. SOURCE OF FUNDING NUMBERS	
		PROGRAM ELEMENT NO.	PROJECT NO.
		TASK NO.	WORK UNIT ACCESSION NO.
11. TITLE (Include Security Classification) Acoustics Intensity: Energy Transfer, Wave Properties, and Applications			
12. PERSONAL AUTHOR(S) Julian Adin Mann III			
13a. TYPE OF REPORT Ph. D. Thesis	13b. TIME COVERED FROM TO	14. DATE OF REPORT (Year, Month, Day) August 1988	15. PAGE COUNT 179
16. SUPPLEMENTARY NOTATION			
17. COSATI CODES		18. SUBJECT TERMS (Continue on reverse if necessary and identify by block number)	
FIELD	GROUP	SUB-GROUP	acoustic intensity; acoustic variables measurement; acoustic waves; acoustic wave effects; acoustic wave intensity; acoustic wave velocity; nearfield acoustics. (1, 2, 3)
19. ABSTRACT (Continue on reverse if necessary and identify by block number)			
<p>> This study explores the physical interpretations of the instantaneous intensity, active intensity, and reactive intensity vectors in terms of energy transfer and wave properties in the nearfield of a general monochromatic sound field. The time dependent energy transfer is described by the instantaneous intensity, which contains contributions by the active intensity and the reactive intensity. The time independent intensity vectors are directly related to wave form properties. The</p>			
20. DISTRIBUTION / AVAILABILITY OF ABSTRACT <input checked="" type="checkbox"/> UNCLASSIFIED/UNLIMITED <input type="checkbox"/> SAME AS RPT. <input type="checkbox"/> DTIC USERS		21. ABSTRACT SECURITY CLASSIFICATION Unclassified	
22a. NAME OF RESPONSIBLE INDIVIDUAL		22b. TELEPHONE (Include Area Code)	22c. OFFICE SYMBOL

UnclassifiedSECURITY CLASSIFICATION OF THIS PAGE

active intensity vector is shown to be perpendicular to the resultant wave fronts and the reactive intensity is shown to point in the direction of decreasing pressure amplitude. Time dependent instantaneous intensity flux lines are drawn to show that in general the energy does not propagate with the resultant wave fronts.

The speed of wave front propagation and the complex specific acoustic impedance are calculated from the nearfield measurements of the time independent intensity vectors and energy densities. Five measured examples are presented which show that the location of energy sources, resonators, diffraction, and interference effects are clearly determined from analyses of the active intensity, reactive intensity, potential energy, kinetic energy, phase speed, and complex specific acoustic impedance.

UnclassifiedSECURITY CLASSIFICATION OF THIS PAGE

ABSTRACT

This study explores the physical interpretations of the instantaneous intensity, active intensity, and reactive intensity vectors in terms of energy transfer and wave properties in the nearfield of a general monochromatic sound field. The time dependent energy transfer is described by the instantaneous intensity, which contains contributions by the active intensity and the reactive intensity. The time independent intensity vectors are directly related to wave form properties. The active intensity vector is shown to be perpendicular to the resultant wave fronts and the reactive intensity is shown to point in the direction of decreasing pressure amplitude. Time dependent instantaneous intensity flux lines are drawn to show that in general the energy does not propagate with the resultant wave fronts.

The speed of wave front propagation and the complex specific acoustic impedance are calculated from the nearfield measurements of the time independent intensity vectors and energy densities. Five measured examples are presented which show that the location of energy sources, resonators, diffraction, and interference effects are clearly determined from analyses of the active intensity, reactive intensity, potential energy, kinetic energy, phase speed, and complex specific acoustic impedance.

Accession For		
NTIS GRA&I	<input checked="" type="checkbox"/>	
DTIC TAB	<input type="checkbox"/>	
Unannounced	<input type="checkbox"/>	
Justification		
By		
Distribution/		
Availability Codes		
Avail and/or		
Dist	Special	
A-1		

TABLE OF CONTENTS

	<u>Page</u>
ABSTRACT	iii
LIST OF FIGURES	viii
LIST OF TABLES	xvii
LIST OF SYMBOLS	xviii
ACKNOWLEDGEMENTS	xxi
 <u>Chapter</u>	
1 INTRODUCTION AND OUTLINE	1
1.1. Introduction	1
1.2. Goals and Outline of Thesis	2
2 ACOUSTIC INTENSITY AS A DESCRIPTION OF ENERGY TRANSFER	5
2.1. Introduction	5
2.2. Basic Equation of Pressure, Velocity, and Instantaneous Intensity	5
2.2.1. Focus on One Infinitesimal Volume of Fluid	7
2.3. Time Independent Intensity Vectors	11
2.3.1. Development of Equations	12
2.3.2. Energy Transfer Considerations	13
2.4. Sources of Acoustic Energy	15
2.4.1. Sources of Active Intensity	15
2.4.2. Sources of Reactive Intensity	20
2.5. Instantaneous Intensity Flux Lines	22
2.5.1. Instantaneous Intensity Flux Lines for Three Point Sources	25

Table of Contents (continued)

<u>Chapter</u>		<u>Page</u>
3	WAVE PROPERTIES DESCRIBED BY INTENSITY..	31
3.1.	Introduction.....	31
3.2.	General Functional Form of Acoustic Pressure	31
3.3.	Differential Equations for $P(r)$ and $\phi(r)$	32
3.4.	Wave Characteristics for \bar{I} and \bar{Q}	33
3.5.	Generalized Phase Speed	34
3.6.	Differential Equations for $P(r)$ and $\phi(r)$ in Terms of the Wave Form Properties	37
3.7.	Example: Plane Waves Incident on a Rigid Boundary ...	38
4	CONCEPTS INCORPORATING ENERGY TRANSFER AND WAVE PROPERTIES	43
4.1.	Introduction.....	43
4.2.	A Simplified Comparison of Wave Front and Energy Propagation	43
	4.2.1. Group Velocity	47
4.3.	Reactive Intensity: A Practical Viewpoint	48
4.4.	Active Intensity Vortex.....	49
	4.4.1. The Conditions for the Vortex Formation	50
	4.4.2. Energy Flux in the Vortex	58

Table of Contents (continued)

<u>Chapter</u>	<u>Page</u>
5 EXPERIMENTAL PROCEDURE AND DATA PROCESSING	63
5.1. Introduction.....	63
5.2. Experimental Facilities	63
5.3. Plotting Symbols.....	66
5.4. Data Processing.....	67
5.4.1. Calculation of the Pressure Phase	67
5.4.2. Specific Acoustic Impedance	70
6 EXPERIMENTAL ANALYSIS OF SOURCE- RESONATOR INTERACTIONS AND A SIMPLE SOURCE.....	71
6.1. Introduction.....	71
6.2. Two In Phase Piston Sources Surrounding a Resonating Tube	71
6.2.1. Fundamental Resonance of the Tube	74
6.2.2. Anti-Resonance of the Tube	82
6.2.3. Second Resonance of the Tube	88
6.2.4. Comparison of the Impedance Above the Tube	92
6.3. Variations in the Radiation Impedance and Output Power.....	93
6.3.1. Measurement Setup.....	95
6.3.2. Analysis of the Results	97

Table of Contents (continued)

<u>Chapter</u>		<u>Page</u>
7	EXPERIMENTAL ANALYSIS OF DIFFRACTION	105
7.1.	Introduction.....	105
7.2.	Diffraction in a Loudspeaker Nearfield	105
	7.2.1. Diffraction Effects at 1500Hz	107
	7.2.2. Diffraction Effects at 2500Hz	114
7.3.	The Nearfield of a Circular Disc	119
	7.3.1. Rigid Disc.....	122
	7.3.2. Fiberglass Disc in an Anechoic Room	130
	7.3.3. Fiberglass Disc in a Reverberant Room	135
4.2.	Distinguishing Between Radiation and Diffraction	135
8	SUMMARY, CONCLUSIONS, AND RECOMMENDATIONS.....	146
8.1.	Summary and Conclusions.....	146
8.2.	Recommendations for Further Work	151
	REFERENCES.....	155

LIST OF FIGURES

<u>Figure</u>	<u>Page</u>
2.1 The path of an incremental volume during one period ($\vec{U}_a = \hat{i}$, $\vec{U}_r = \hat{j}$). The dashed circle represents the initial volume, the solid circle represents the instantaneous volume, and the arrow represents the instantaneous intensity.....	9
2.2 The path of an incremental volume during one period [$\vec{U}_a = \hat{i}(.5) + \hat{j}(.25)$, $\vec{U}_r = \hat{i}(.3) + \hat{j}(.6)$]. The dashed circle represents the initial volume, the solid circle represents the instantaneous volume, and the arrow represents the instantaneous intensity.....	9
2.3 A closed volume, surrounding a source, in which the intensity is defined.....	17
2.4 The ratio of the power radiated by three sources to the power radiated by one source. The sources are separated by 18cm with the center source out of phase.....	21
2.5 Schematic of the construction of instantaneous intensity flux lines. The instantaneous intensity vectors are represented at six points at times t_0 and $t_0 + \Delta t$, and the resulting flux line (dashed) is drawn.....	24
2.6 The calculated active intensity and reactive intensity around three point sources separated by 18cm with the center source out of phase. The frequency is 2070Hz.....	24
2.7 The calculated active intensity and reactive intensity around three point sources separated by 18cm with the center source out of phase. The frequency is 200Hz.....	27
2.8 Instantaneous intensity flux lines at 2070Hz. (Three point sources with the center source out of phase.) The circles represent the starting positions of the lines. Two lines leave each starting position one at times t_0 and $t_0 + \frac{T}{6}$	28

LIST OF FIGURES(continued)

<u>Figure</u>	<u>Page</u>
2.9 Instantaneous intensity flux lines at 200Hz. (Three point sources with the center source out of phase.) The circles represent the starting positions of the lines. Two lines leave each starting position one at times t_o and $t_o + \frac{T}{6}$	29
3.1 A sketch of the configuration for a plane wave incident on a rigid boundary. The phase speed, c_p , and the group velocity, $c \sin(\theta)$, are clearly marked.	39
3.2 A sketch of the resultant wave fronts for the example of the plane wave incident on a rigid boundary. The resultant wave vector, \vec{k}_p , the resultant wave length, λ_p , and the active intensity, \vec{I} , are clearly marked.	41
4.1 The magnitude of the pressure and velocity as a function of distance in the direction of a propagating plane wave at times t and $t + \Delta t$. ($\Delta t = \frac{T}{8}$) The wave packets I, II, III, and IV are labeled so that their progress can be followed.	45
4.2 The magnitude of the pressure and the velocities \vec{U}_a and \vec{U}_r as a function of distance in the direction of a propagating wave, where the pressure amplitude decreases in the propagation direction and $c_p \neq c$, at times t and $t + \Delta t$. ($\Delta t = \frac{T}{8}$) The wave packets I, II, and III are labeled so that their progress can be followed.	46
4.3 The calculated active intensity and wave fronts above three point sources separated by 18cm at 2070Hz with the center source out of phase. The vortex center is circled.	51
4.4 The calculated active intensity and reactive intensity in a vortex region for the three point sources separated by 18cm at 2070Hz with the center source out of phase.	52
4.5 The scaled magnitude of active intensity, reactive intensity, potential energy, kinetic energy, and curl of the active intensity along a line through the saddle point and vortex center.	53

LIST OF FIGURES(continued)

<u>Figure</u>	<u>Page</u>
4.6 The scaled magnitude of \vec{U}_a and \vec{U}_r at the vortex center.....	55
4.7 The magnitude of the pressure phase gradient, $ \nabla\phi $, in the vortex region.....	55
4.8 The phase speed, c_p , around the vortex center.....	57
4.9 The contribution of the active intensity to the instantaneous intensity during the vortex buildup. The time increment is $0.038T$	59
4.10 Snapshots of the instantaneous intensity in the vortex region for one complete cycle of the energy ($\frac{T}{2}$). The time increment is $\frac{T}{12}$	61
4.11 Instantaneous intensity flux lines beginning in the vortex region. Two lines start at each point at times t_o and $t_o + .3T$. The top plot is in the vortex region and the bottom plot is an expanded view of the same lines leaving the vortex region.....	62
5.1 An example of a calibration spectrum for a microphone pair phase matching. The free field modified switching technique is used.....	65
5.2 A schematic of the integration paths used to reconstruct the pressure phase from the measured data.....	69
5.3 A schematic of the segmentation (labeled 1,2,3), origin relocation (circled), and connection paths (arrows) for the reconstruction of the pressure phase around an obstacle in a measurement plane.....	69
6.1 The measurement configuration of two baffled pistons with a resonating tube tuned to a one-quarter wavelength resonance of 200Hz.....	72

LIST OF FIGURES(continued)

<u>Figure</u>		<u>Page</u>
6.2	The measured active intensity and wave fronts and reactive intensity at 200Hz in a plane perpendicular to the baffled containing two in phase piston sources and a tube with a 200Hz fundamental resonance.	75
6.3	The measured potential energy and calculated phase speed at 200Hz in a plane perpendicular to the baffled containing two in phase piston sources and a tube with a 200Hz fundamental resonance.	76
6.4	The measured kinetic energy, due to the velocity normal to the baffle, at 200Hz in a plane perpendicular to the baffled containing two in phase piston sources and a tube with a 200Hz fundamental resonance.	77
6.5	The real and imaginary parts of the impedance normal to the baffle at 200Hz. The measurement plane is parallel to and 3cm above the baffle containing two in phase piston sources and a tube with a 200Hz fundamental resonance.	78
6.6	The numerical values of the real and imaginary parts of the impedance normal to the baffle at 200Hz. The measurement plane is parallel to and 3cm above the baffle containing two in phase piston sources and a tube with a 200Hz fundamental resonance.	79
6.7	The measured active intensity and wave fronts and and reactive intensity at 400Hz in a plane perpendicular to the baffled containing two in phase piston sources and a tube with a 200Hz fundamental resonance.	83
6.8	The measured kinetic energy, due to the velocity normal to the baffle, at 400Hz in a plane perpendicular to the baffled containing two in phase piston sources and a tube with a 200Hz fundamental resonance.	85

LIST OF FIGURES(continued)

<u>Figure</u>	<u>Page</u>
6.9 The real and imaginary parts of the impedance normal to the baffle at 400Hz. The measurement plane is parallel to and 3cm above the baffle containing two in phase piston sources and a tube with a 200Hz fundamental resonance.....	86
6.10 The numerical values of the real and imaginary parts of the impedance normal to the baffle at 400Hz. The measurement plane is parallel to and 3cm above the baffle containing two in phase piston sources and a tube with a 200Hz fundamental resonance.....	87
6.11 The measured active intensity and wave fronts and reactive intensity at 600Hz (the second resonance of the tube) in a plane perpendicular to the baffled containing two in phase piston sources and a tube with a 200Hz fundamental resonance.....	89
6.12 The measured kinetic energy, due to the velocity normal to the baffle, at 600Hz (the second resonance of the tube) in a plane perpendicular to the baffled containing two in phase piston sources and a tube with a 200Hz fundamental resonance.....	90
6.13 The real and imaginary parts of the impedance normal to the baffle at 600Hz (the second resonance of the tube). The measurement plane is parallel to and 3cm above the baffle containing two in phase piston sources and a tube with a 200Hz fundamental resonance.....	91
6.14 The numerical values of the real and imaginary parts of the impedance normal to the baffle at 600Hz (the second resonance of the tube). The measurement plane is parallel to and 3cm above the baffle containing two in phase piston sources and a tube with a 200Hz fundamental resonance.....	93
6.15 A sketch of the B&K reference sound source and the position of the measurement point.....	98

LIST OF FIGURES(continued)

<u>Figure</u>	<u>Page</u>
6.16 The impedance measured above the B&K reference sound source: the real part, imaginary part and the total magnitude.	99
6.17 The difference in dB between the real part of the impedance measured with the source raised 20cm, 40cm, and 80cm above the floor and the source on the floor.	101
6.18 The difference in dB between the radiated power measured with the source raised 20cm, 40cm, and 80cm above the floor and the source on the floor.	101
6.19 A schematic of the signal processing in a real-time analyzer which calculates the time-averaged sound intensity level.	103
7.1 A sketch of the loudspeaker used for diffraction measurements.	106
7.2 The active intensity and wave fronts and the reactive intensity measured at 1500Hz on a plane perpendicular to the loudspeaker surface.	108
7.3 The potential energy measured at 1500Hz on a plane perpendicular to the loudspeaker surface.	109
7.4 The kinetic energy due to the particle velocity normal to the loudspeaker surface, measured at 1500Hz on a plane perpendicular to the loudspeaker surface.	109
7.5 The active intensity and wave fronts and the reactive intensity measured at 1500Hz on a plane parallel to and 3.5cm above the loudspeaker surface.	110

LIST OF FIGURES(continued)

<u>Figure</u>		<u>Page</u>
7.6	The kinetic energy due to the particle velocity normal to the loudspeaker surface, measured at 1500Hz on a plane parallel to and 3.5cm above the loudspeaker surface.	112
7.7	The real and imaginary parts of the impedance normal to the loudspeaker surface, measured at 1500Hz on a plane parallel to and 3.5cm above the loudspeaker surface.	113
7.8	The active intensity and wave fronts and the reactive intensity measured at 2500Hz on a plane perpendicular to the loudspeaker surface.....	115
7.9	The potential energy measured at 2500Hz on a plane perpendicular to the loudspeaker surface.	116
7.10	The active intensity and wave fronts and the reactive intensity measured at 2500Hz on a plane parallel to and 3.5cm above the loudspeaker surface.....	117
7.11	The kinetic energy due to the particle velocity normal to the loudspeaker surface, measured at 2500Hz on a plane parallel to and 3.5cm above the loudspeaker surface.	118
7.12	The real and imaginary parts of the impedance normal to the loudspeaker surface, measured at 2500Hz on a plane parallel to and 3.5cm above the loudspeaker surface.	120
7.13	Sketches of the configurations for the disc diffraction measurements. The measurements were made at 1000Hz on a plane perpendicular to the disc and intersecting the source and disc symmetrically.	121
7.14	The active intensity and wave fronts and the reactive intensity measured at 1000Hz on a plane perpendicular to the rigid disc. The source is 1.5λ to the left, positioned symmetrically with respect to the disc center.....	123

LIST OF FIGURES(continued)

<u>Figure</u>	<u>Page</u>
7.15 The potential energy and resultant phase speed measured at 1000Hz on a plane perpendicular to the rigid disc. The source is 1.5λ to the left, positioned symmetrically with respect to the disc center.....	124
7.16 The active intensity and wave fronts and the reactive intensity measured at 1000Hz on a plane perpendicular to the rigid disc. The source is 1.5λ to the left, along a line extending from the disc top.....	126
7.17 The potential energy and resultant phase speed measured at 1000Hz on a plane perpendicular to the rigid disc. The source is 1.5λ to the left, along a line extending from the disc top.....	127
7.18 The real and imaginary parts of the total impedance around the disc. The top figures, Z^s , are for the rigid disc with the symmetric source position and the bottom figures, Z^r , are for the rigid disc with the raised source position. The numbers represent the dB level below the maximum level labeled above each plot.....	128
7.19 The active intensity and wave fronts and the reactive intensity measured at 1000Hz on a plane perpendicular to the 8cm thick fiberglass disc. The source is 1.5λ to the left, along a line extending from the disc top.....	131
7.20 The potential energy and resultant phase speed measured at 1000Hz on a plane perpendicular to the 8cm thick fiberglass disc. The source is 1.5λ to the left, along a line extending from the disc top.....	132
7.21 The real and imaginary part of the total impedance around the fiberglass disc with the raised source position. The numbers represent the dB level below the maximum level labeled above each plot.....	134

LIST OF FIGURES(continued)

<u>Figure</u>	<u>Page</u>
7.22 The active intensity and wave fronts and the reactive intensity measured at 1000Hz on a plane perpendicular to the 8cm thick fiberglass disc. The source is 1.5λ to the left, along a line extending from the disc top. The measurements were made in reverberant conditions.....	136
7.23 The potential energy and resultant phase speed measured at 1000Hz on a plane perpendicular to the 8cm thick fiberglass disc. The source is 1.5λ to the left, along a line extending from the disc top. The measurements were made in reverberant conditions.....	137
7.24 A sketch of the truncated sphere.....	138
7.25 The response of the truncated sphere surface vibration when excited by pink noise from a loudspeaker 25cm from the truncated sphere.....	140
7.26 An expanded view of the measurement over the truncated sphere top plate in the shadow zone of a rigid disc. The frequency is 1930Hz and the source is 53cm to the left of the disc top.....	141
7.27 An expanded view of the measurement over the truncated sphere top plate in the shadow zone of a rigid disc. The frequency is 2570Hz and the source is 53cm to the left of the disc top.....	142
7.28 A schematic for interference of a direct wave over the disc top and a wave reflected from the truncated sphere top plate.....	144

LIST OF TABLES

<u>Table</u>		<u>Page</u>
6.1	The real and imaginary parts of the impedance normal to the baffle, averaged over the tube opening. The frequencies of 200Hz and 600Hz are at resonances of the tube and 400Hz is at the tube anti-resonance.....	94
8.1	A summary of the distinguishing characteristics of the active intensity, reactive intensity, potential energy, kinetic energy, and the real and imaginary parts of the specific acoustic impedance near vibration sources, resonators, and diffraction.....	150

LIST OF SYMBOLS

A_i	amplitude of the i^{th} point source
c	speed of sound
c_p	resultant phase speed
d	separation of the point sources
\underline{g}	general source term (complex function)
H	Heaviside step function
\bar{I}	active intensity vector
\bar{I}_c	complex intensity vector (complex function)
\bar{I}_i	instantaneous intensity vector
I_{ix}	instantaneous intensity: x-component
I_{iy}	instantaneous intensity: y-component
\hat{i}	unit vector in the x-direction
\hat{j}	unit vector in the y-direction
j	square root of -1
k	free field wavenumber ($\frac{\omega}{c}$)
\bar{k}	free field wave vector in the direction of wave propagation
k_p	resultant wavenumber ($\frac{\omega}{c_p}$)
\bar{k}_p	resultant wave vector perpendicular to the resultant wave fronts
L	Lagrangian
\hat{n}	unit vector
p	acoustic pressure
\underline{p}	acoustic pressure (complex function)
P	pressure amplitude
\underline{p}_i	pressure due to the i^{th} point source
\bar{Q}	reactive intensity vector

r	general spatial coordinate
r_i	distance from the i^{th} point source to the observation point
\vec{r}_i	vector from the i^{th} point source to the observation point
S	surface area enclosing the volume V
SIL	should intensity level in dB
SPL	sound pressure level in dB
SQL	reactive intensity level in dB
t	time
T	kinetic energy density or one period of oscillation
T_n	kinetic energy due to the particle velocity in the direction \hat{n}
\vec{u}	particle velocity
$\underline{\vec{u}}$	particle velocity (complex function)
\vec{U}_a	particle velocity in phase with pressure
U_{ax}	particle velocity in phase with pressure: x-component
U_{ay}	particle velocity in phase with pressure: y-component
$\underline{\vec{u}}_i$	particle velocity due to the i^{th} point source
\vec{U}_r	particle velocity in phase quadrature with pressure
U_{rx}	particle velocity in phase quadrature with pressure: x-component
U_{ry}	particle velocity in phase quadrature with pressure: y-component
V	potential energy density or volume
x_i	spatial coordinate of the i^{th} point source
y_i	spatial coordinate of the i^{th} point source
z_i	spatial coordinate of the i^{th} point source
\underline{z}_n	specific acoustic impedance in the direction \hat{n} (complex function)

Greek and other symbols

α_i	relative phase of the i^{th} point source
β	scalar component of the Helmholtz decomposition of the active intensity vector
η_{nm}	phase term for the n^{th} and m^{th} point sources
θ	angle of incidence relative to the normal to a surface
κ	constant
μ_n	coordinate (x,y, or z) of the n^{th} point source
ν_n	coordinate (x,y, or z) of the n^{th} point source
Π_1	power radiated by one point source
Π_3	power radiated by three acoustically coupled point sources
ρ	air mass density
ϕ	pressure phase: a function of space
$\vec{\psi}$	vector component of the Helmholtz decomposition of the active intensity vector
ω	radial frequency
$()^*$	complex conjugate
$(\underline{\quad})$	signifies a complex function

ACKNOWLEDGEMENTS

I sincerely thank the following people for their guidance and friendship: Professor Jiri Tichy, thesis advisor, and Dr. Courtney Burroughs, member of the committee, who provided invaluable advice, insights, and support; Dr. Sabih Hayek and Dr. Carter L. Ackerman, members of the committee, for their constructive criticism; Dr. Anthony Romano, Dr. Michel Josserand, Dr. Gary Elko, Karl Grosh, Jean-Francois Degeorges, and Eugene Taschuk who were always willing to give constructive comments and encouragement; and Barbara Crocken, administrative aide for the Graduate Program in Acoustics, and Carolyn Smith, department secretary, for their invaluable assistance. Above all I thank my parents, Dr. J. Adin Mann, Jr., and Arlene E. Mann and sisters, Elizabeth and Jennifer, for their loving guidance and support.

This work, excluding section 6.3, was supported by the Naval Sea Systems Command.

I also sincerely thank Dir. u. Prof. Dr. R. Martin and Prof. Dr.-Ing. J. Meyer who invited me to be a guest at the Physicalisch-Technische Bundesanstalt (PTB) in Braunschweig, Federal Republic of Germany, during the fall of 1987, also Dr.-Ing. Hans-O Finke and the others in the laboratory whose skill, patience, and great hospitality made the visit invaluable. The work presented in section 6.3 was supported by the PTB.

Chapter 1

INTRODUCTION AND OUTLINE

1.1. Introduction

Energy transfer between a vibrating body and the surrounding fluid can only be thoroughly understood by studying the nearfield where the energy transfer takes place. Likewise, the energy propagation where diffraction occurs must be examined in the nearfield. These and other acoustic phenomena can be carefully investigated using acoustic intensity analysis. Therefore, the principle aspiration of this thesis is to present a physical interpretation of acoustic intensity and to demonstrate the application of the understanding of the physical interpretations of acoustic intensity to enhance the use of the acoustic intensity technique as an analysis tool of the acoustic nearfield.

The fundamental issues of intensity have not been fully developed in the open literature because convenient measurement equipment has been developed only in the last ten years. By 1975 the two microphone technique was being used with analog real-time signal processing. The inclusion of digital signal processing using the fast Fourier transform (FFT), first shown by Fahy (1977), greatly aided in the convenience and accuracy of acoustic intensity measurements. Elko (1984) further developed the technique showing that the complex intensity vector, energy density, and instrument and field dependent bias errors are easily calculated from the FFT of the pressure signal from two closely spaced pressure microphones.

Acoustic intensity was first introduced as a tool to measure the time averaged power. Limiting acoustic intensity analysis to time averaged power incorporates

only a small fraction of the available information. In fact contemporary interpretations of the time averaged intensity vector are sometimes in error.

Beyond the time averaged sound power, the complex acoustic intensity and related analysis provide the total energy propagation and wave properties in a sound field. Many of these issues are imbedded in articles and books published before 1965. However, these classical concepts of sound fields have not been directly linked to acoustic intensity. Researchers are only now beginning to employ fundamental acoustic intensity concepts necessary to understand basic phenomena that occur in the nearfield of vibrating bodies such as sources, sinks, diffraction, and reflection.

The process of interpreting the active intensity vortex played an important role in the development of this thesis when it became obvious that the conventional interpretation of the active intensity lead to an incorrect understanding of energy flux in the vortex. Work on this thesis began by exploring the physical interpretation of the intensity vectors.

1.2. Goals and Outline of Thesis

A great deal of initial emphasis is placed on basic interpretations of the acoustic intensity vectors. The ultimate goals of this work are to demonstrate that acoustic intensity is a powerful analysis tool for investigating the acoustic nearfield of sources and scatterers and interpreting energy transfer between sources and pressure fields in surrounding fluids, and also to expand the applications of the intensity analysis. Based on fundamental theories of sound fields, the acoustic intensity and energy density and flux patterns are linked to fundamental concepts of acoustics. The measurements which are presented are chosen to demonstrate basic phenomena. Only aspects of each measurement relevant to fundamental concepts of acoustic intensity and energy flux are

discussed so that the logic of the analysis can be followed. With these ends in mind the thesis is organized as follows.

Chapter 2 investigates the energy flux described by acoustic intensity. The time dependent intensity is compared with the time independent active and reactive intensity. The comparison focuses on the description of time dependent energy flux and its uniqueness.

Chapter 3 links fundamental wave properties to the vector characteristics of the active and reactive intensity. This shows that the active intensity represents the propagating wave fronts and the reactive intensity characterizes the pressure distribution. The phase speed, a basic description of a wave, is calculated from the active intensity and potential energy.

Chapter 4 contains three topics which are understood by combining the energy and wave properties discussed in Chapters 2 and 3. These topics are the group velocity, the reactive intensity, and the active intensity vortex formation.

Chapter 5 briefly describes the measurement equipment and the method for measuring acoustic intensity and calculating the pressure phase from the time independent active intensity and potential energy.

Chapters 6 and 7 detail measurements which illustrate the intensity analysis methods discussed in the preceding chapters. Simple configurations are investigated which model some basic aspects of more complicated configurations. The phenomena which are focused on are acoustic sources, absorbers, diffraction, and resonators.

Chapter 6 concentrates on sources and passive absorbers. Measurements are described for a configuration of two piston sources with a tube between the pistons. Measurements were performed at the one quarter wavelength resonance, the half wavelength anti-resonance, and three quarter wavelength resonance of the tube. The second example compares the change in the radiation impedance

and output power for a standard calibration source as a function of the distance of the source from a rigid surface. The impedance and power were measured with the intensity technique.

Chapter 7 contains three examples of diffraction. The diffraction at impedance discontinuities is shown around a loudspeaker and a circular disc. The circular disc measurements compare the diffraction for two incident wave configurations and are made with a rigid and an absorptive disc. The final example is measurements made above a truncated sphere in the shadow zone of a rigid disc. The analysis includes diagnostics of the structural vibrations of the truncated sphere induced by the incident sound.

Chapter 8 contains the conclusions and recommendations for further work. A summary of the analysis capabilities of the complete intensity measurements is included so that this powerful analysis technique can be applied to a great variety of fundamental and applied situations.

Chapter 2

ACOUSTIC INTENSITY AS A DESCRIPTION
OF ENERGY TRANSFER

2.1. Introduction

The fundamental intent of acoustic intensity is to describe the transfer of energy in an acoustic field. To this end extensive literature has been developed on understanding the energy transfer process. The majority of work done with acoustic intensity focuses on the time averaged intensity, which is commonly called the active intensity. The intent of this chapter is to derive the intensity quantities in terms of a general expression for the acoustic pressure. The focus will be placed on a comparison and interpretation of the energy flux as described by the instantaneous intensity, active intensity, and reactive intensity.

2.2. Equations for Pressure, Velocity, and Instantaneous Intensity

There are many examples in the literature for the development of the formalism for acoustic intensity (Schultz, Smith, and Malme 1964; Pierce 1981; Elko 1984). A nice introductory summary of the literature is given by Elko (1984) who develops Equation (2.1) from the linear acoustic equations in the form of a corollary of the conservation of energy.

$$\begin{aligned} \frac{\partial}{\partial t} \iiint_V \left[\frac{1}{2} \rho u^2 + \frac{1}{2 \rho c^2} p^2 \right] dV &= - \iiint_V \nabla \cdot (p \cdot \vec{u}) dV \\ &= - \iint_S p \vec{u} \cdot \hat{n} dS = - \iint_S \vec{I}_i \cdot \hat{n} dS, \end{aligned} \quad (2.1)$$

where ρ is the density, p is the acoustic pressure, u is the magnitude of the particle velocity, \vec{u} is the particle velocity vector, $\vec{I}_i(\vec{r}, t) \stackrel{\text{def}}{=} p(\vec{r}, t) \vec{u}(\vec{r}, t)$ is the instantaneous intensity, and \hat{n} is a unit vector normal to the surface S enclosing the volume V . This equation signifies that the time rate of change of the total

internal energy of a volume is equal to the energy flux (instantaneous intensity) through the volume surface. (Contributions from any body forces, e.g. gravity, and viscous dissipation are ignored.)

Before proceeding, we must introduce a general functional form to be used in this thesis as a basis to study a general three-dimensional pressure field. The formula is given and discussed in Morse and Feshbach (1953, p. 145):

$$\underline{p}(r, t) = P(r) \underline{f}[\phi(r) - ct] , \quad (2.2)$$

where r is a general spatial variable and $P(r)$ and $\phi(r)$ are real. (The complex variables are underlined throughout, to clearly distinguish them from the real functions.) This form will be discussed in greater detail in Chapter 3. For a mono-chromatic pressure field Equation (2.2) can be written as

$$\underline{p}(r, t) = P(r) e^{j(\omega t - \phi(r))} . \quad (2.3)$$

In this form the spatial amplitude and spatial phase distribution are explicitly described, from which all linear acoustic quantities can be derived (Pascal and Lu 1984; Mann, Tichy, and Romano 1987).

The particle velocity is calculated using Euler's equation and Equation (2.3):

$$\begin{aligned} \underline{\vec{u}}(r, t) &= \frac{-1}{j\omega\rho} \nabla \underline{p}(r, t) \\ &= \frac{1}{\omega\rho} (P(r) \nabla \phi(r) + j \nabla P(r)) e^{j(\omega t - \phi(r))} . \end{aligned} \quad (2.4)$$

Comparing the particle velocity with pressure explicitly shows that there are two components of the particle velocity (Kurtze 1968). The component $P \nabla \phi$ is in phase with pressure and ∇P is ninety degrees out of phase with pressure. Consequently, the particle velocity can be written in a form to emphasize this fact:

$$\underline{\vec{u}}(r, t) = [\vec{U}_a(r) + j \vec{U}_r(r)] e^{j(\omega t - \phi(r))} , \quad (2.5)$$

where

$$\begin{aligned}\vec{U}_a(\mathbf{r}) &= \frac{1}{\omega\rho}P\nabla\phi, \\ \vec{U}_r(\mathbf{r}) &= \frac{1}{\omega\rho}\nabla P.\end{aligned}\tag{2.6}$$

The instantaneous intensity, \vec{I}_i , is calculated from Equation (2.1), where the form of the particle velocity expressed in Equation (2.4) will be used. One must also note that Equation (2.1) is defined for real quantities thus only the real parts of the pressure and particle velocity in equations (2.3) and (2.4) are used:

$$\begin{aligned}\vec{I}_i(\mathbf{r},t) &= \text{Re}\{\underline{p}(\mathbf{r},t)\} \cdot \text{Re}\{\underline{\vec{u}}(\mathbf{r},t)\} \\ &= \frac{1}{\omega\rho}P^2(\mathbf{r})(\nabla\phi(\mathbf{r}))\cos^2(\omega t - \phi) \\ &\quad - \frac{1}{2\omega\rho}P(\mathbf{r})(\nabla P(\mathbf{r}))\sin 2(\omega t - \phi).\end{aligned}\tag{2.7}$$

The time dependence has purposely been maintained by using the instantaneous intensity so that the energy transfer process can be discussed explicitly in its true nature. The pressure and particle velocity are phase shifted in time, but their product at every instant is the energy flux from the point in space where these two quantities are described.

2.2.1. Focus on One Infinitesimal Volume of Fluid

A short detour is taken from the formalism to focus on the behavior of the fluid described in the previous section. We consider an infinitesimal mass of fluid as it undergoes acoustic motion.

Morse and Ingard (1968, p. 227) formulate a derivation of the internal energy in an acoustic field where a one-dimensional duct is used to view the forces and reactions of a small volume of the fluid. The extension to three dimensions is very useful. Let us observe an element of fluid with three-dimensional motion and emphasize cases where the pressure and velocity are not in phase. Since the velocity is represented by two vectors in space, \vec{U}_a and \vec{U}_r , there is a plane

which contains both the vectors. Thus the general three-dimensional motion at a single element of fluid is locally two dimensional.

The element of fluid is regarded as an infinitesimal mass such that the particles which make up the mass move together. We will examine the pressure, volume, velocity, displacement, and acceleration of the mass.

The discussion will not be confined to any specific source configuration. We are only interested in representing a situation where the pressure and velocity are phase shifted in time. The following equations are used:

$$\begin{aligned}
 v &= v_0 - v_0 \cos(t) \quad , \\
 I_{ix}(t) &= \cos(t)(U_{ax} \cos(t) - U_{rx} \sin(t)) \quad , \\
 I_{iy}(t) &= \cos(t)(U_{ay} \cos(t) - U_{ry} \sin(t)) \quad .
 \end{aligned}
 \tag{2.8}$$

where v is the instantaneous volume of the infinitesimal mass, v_0 is the initial volume, U_a and U_r are the two quadrature components of the particle velocity, and t varies from 0 to 2π to represent one cycle of the motion. The quantities $I_{ix}(t)$ and $I_{iy}(t)$ are the two perpendicular components of the instantaneous intensity vector.

It should be noted that the motion is indeed very small, a result emphasized by the acoustic velocity c being much greater than the particle velocity. Thus the position of the surrounding masses relative to the mass we are observing remains essentially constant during the motion of the mass.

Time histories of the incremental mass for two different values of U_a and U_r , are plotted in Figures 2.1 and 2.2 for one complete cycle of its motion around the equilibrium position. The initial volume is represented by dashed circles and the instantaneous volume is represented by solid circles. The path is represented by a thin elliptical line with the instantaneous volume represented at one-twelfth period increments along the path. At each position the instantaneous intensity

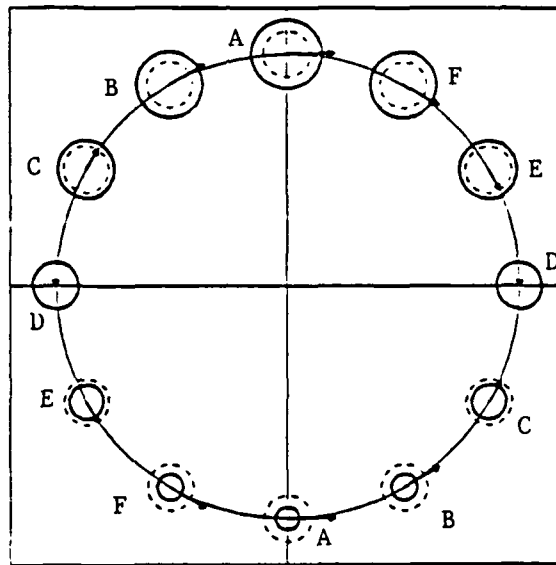


Figure 2.1 The path of an infinitesimal volume during one period ($\vec{U}_a = \hat{i}$, $\vec{U}_r = \hat{j}$). The dashed circle represents the initial volume, the solid circle represents the instantaneous volume, and the arrow represents the instantaneous intensity.

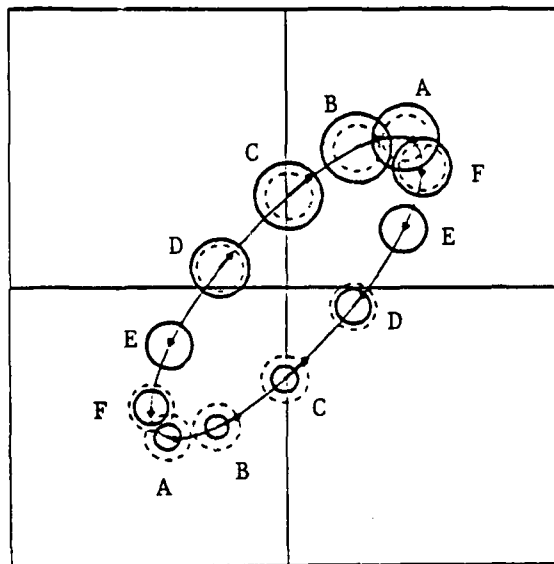


Figure 2.2 The path of an infinitesimal volume during one period [$\vec{U}_a = \hat{i}(.5) + \hat{j}(.25)$, $\vec{U}_r = \hat{i}(.3) + \hat{j}(.6)$]. The dashed circle represents the initial volume, the solid circle represents the instantaneous volume, and the arrow represents the instantaneous intensity.

direction is represented by an arrow whose length is proportional to the relative instantaneous intensity magnitude.

In Figure 2.1 U_a and U_r are the same magnitude but perpendicular. The resulting particle motion is a circle. In Figure 2.2 $\vec{U}_a = \hat{i}(0.5) + \hat{j}(0.25)$ and $\vec{U}_r = \hat{i}(0.3) + \hat{j}(0.6)$ which results in an ellipse. In these two figures there are instants labeled A to F. Each letter labels two instants where the instantaneous intensity points in a given direction with the same magnitude.

Consider the times labeled by A in Figure 2.1. The motion of the mass at the top position is to the left. The instantaneous volume is greater than the equilibrium volume so the acoustic pressure is negative. The instantaneous intensity, the product of the acoustic pressure and particle velocity, points to the right which at this instant is opposite the direction of motion. When the mass is at the bottom position the velocity is to the right and the volume is compressed so that the acoustic pressure is positive. Thus the instantaneous intensity points to the right, as it did with the mass in the top position. With the mass at the bottom the direction of the instantaneous intensity and the particle velocity are the same. Despite the difference in the direction of motion for these two instances, the instantaneous intensity indicates that the mass is doing work on the same neighboring mass to the right at both times.

As seen in Equation (2.7) the instantaneous intensity is a function of $2\omega t$ thus oscillating at twice the mass motion frequency, so that there are only two instants where the instantaneous intensity points in a given direction. The variation of the direction of the instantaneous intensity vector is also clearly seen in Figures 2.1 and 2.2. This observation is central to arguments against conventional views that the energy propagates with the time averaged intensity, \vec{I} .

Consider a case where \vec{U}_a and \vec{U}_r are in the same direction or one of these is zero, the path of the mass would be a straight line. Consequently, the

infinitesimal mass we are viewing would only transfer energy to or from the two adjacent masses along the motion path. This corresponds to conventional views. However, counter examples are easily constructed. For if \vec{U}_a and \vec{U}_r are both non-zero and not parallel, there are only two instances during the motion cycle when the infinitesimal mass we are observing transfers energy to specific adjacent masses. In other words, over one period, the mass we are observing is having some work done on it and in turn is doing work on all the surrounding masses, not just the two masses along the direction of the time averaged instantaneous intensity.

The view that the time averaged intensity sufficiently describes the energy transfer ignores this fact and says that the mass we are observing only transfers energy to one neighboring mass which is oriented in the direction of the time averaged intensity. This issue can be more thoroughly addressed when considering a large region of an acoustic field and looking at some specific cases, which will be done in section 2.5.

2.3. Time Independent Intensity Vectors

The development of the time averaged quantities has been the subject of numerous papers, so the equations are only briefly developed here. In this discussion the time independent intensity vectors will be derived emphasizing their relationship to the general form of the acoustic pressure, which is expressed by Equation (2.2) in terms of the pressure amplitude and phase spatial distributions. These intensity vectors will be linked to the instantaneous intensity and the energy transfer associated with the intensity vectors will be discussed.

The interpretation of the intensity vectors is not limited to energy considerations, and often the wave interpretations are more significant when investigating an acoustic field. The wave interpretations will be discussed in detail in Chapter

3. Here the discussion will be confined to energy interpretations because of the distinction which must be made between the time dependent instantaneous intensity and time independent active and reactive intensity.

2.3.1. Development of Equations

The complex intensity vector is defined as (Pascal 1981; Elko 1984):

$$\underline{\bar{I}}_c(\mathbf{r}) \stackrel{\text{def}}{=} \frac{1}{2} \underline{p}(\mathbf{r}) \underline{\bar{u}}^*(\mathbf{r}) \stackrel{\text{def}}{=} \bar{I}(\mathbf{r}) + j\bar{Q}(\mathbf{r}) . \quad (2.9)$$

The spatial components of the pressure and particle velocity defined in Equations (2.3) and (2.4) are

$$\underline{p}(\mathbf{r}) = P(\mathbf{r})e^{-j\phi(\mathbf{r})} , \quad (2.10)$$

$$\underline{\bar{u}}(\mathbf{r}) = \frac{1}{\omega\rho} [P(\mathbf{r})\nabla\phi(\mathbf{r}) + j\nabla P(\mathbf{r})]e^{-j\phi(\mathbf{r})} . \quad (2.11)$$

Substituting Equations (2.10) and (2.11) into Equation (2.9) results in the following equation for the complex intensity:

$$\underline{\bar{I}}_c(\mathbf{r}) = \frac{1}{2\omega\rho} [P^2(\mathbf{r})\nabla\phi(\mathbf{r}) - jP(\mathbf{r})\nabla P(\mathbf{r})] . \quad (2.12)$$

The real and imaginary parts of Equation (2.12) define the two vectors which make up the complex intensity vector. The vector \bar{I} , defined as the real part of Equation (2.12), will be called the active intensity, which is

$$\bar{I}(\mathbf{r}) \stackrel{\text{def}}{=} \frac{1}{2\omega\rho} P^2(\mathbf{r})\nabla\phi(\mathbf{r}) . \quad (2.13)$$

The imaginary part of $\underline{\bar{I}}_c$ is called the reactive intensity:

$$\bar{Q}(\mathbf{r}) \stackrel{\text{def}}{=} \frac{-1}{2\omega\rho} P(\mathbf{r})\nabla P(\mathbf{r}) . \quad (2.14)$$

The origins of the equation for the complex intensity is based in the fact that the real part of $\underline{\bar{I}}_c$ is the time average of the instantaneous intensity. The instantaneous intensity is defined by the power balance equation as the pressure

at an instant of time times the particle velocity at that same instant; however, the time average of this quantity can be calculated using the mathematical complex forms of pressure and velocity. This mathematical manipulation also allows the reactive intensity, \bar{Q} , to be calculated.

2.3.2. Energy Transfer Considerations

Comparing the equations for the active and reactive intensity, Equations (2.13) and (2.14), and the instantaneous intensity, Equation (2.7), the vectors \bar{I} and \bar{Q} can be substituted into the instantaneous intensity. Thus the instantaneous intensity can be written explicitly in terms of the time independent vectors \bar{I} and \bar{Q} as follows:

$$\bar{I}_i(r, t) = 2\bar{I}(r)\cos^2(\omega t - \phi) + \bar{Q}(r)\sin 2(\omega t - \phi) . \quad (2.15)$$

Expanding $\cos^2(\omega t - \phi) = \frac{1}{2} + \frac{1}{2}\cos 2(\omega t - \phi)$ gives a more useful form of Equation (2.15):

$$\bar{I}_i(r, t) = \bar{I}(r) + \bar{I}(r)\cos 2(\omega t - \phi) + \bar{Q}(r)\sin 2(\omega t - \phi) . \quad (2.16)$$

This form of the instantaneous intensity clearly shows the contribution of the active and reactive intensity to the energy transfer process. The instantaneous intensity is composed of the term $\bar{I}(r)$ which is independent of time. The two additional terms containing the active and reactive intensity oscillate in quadrature at twice the frequency, as illustrated in Section 2.2.1.

Conventionally, the instantaneous intensity is time averaged, which Equation (2.16) clearly shows leaves the active intensity. However, the instantaneous propagation of energy, described by the instantaneous intensity, also includes the reactive intensity. This is evident in Figures 2.1 and 2.2 where at only two instances in one cycle does the instantaneous intensity point in a given direction. These two figures show that the direction of the energy flux is biased in one

direction by the active intensity term, but in general, the energy flux oscillates around the direction of the active intensity. The active intensity does describe the average direction and magnitude of the instantaneous intensity. But due to the averaging process, the active intensity does not describe the total energy transfer, because of the two terms in Equation (2.16) which are ignored. Quite simply, the average direction of a vector does not necessarily indicate the direction of the vector at all times. The active intensity in general only describes the energy flux at two instances in one cycle, not the time dependent process of energy transfer.

Justifications that the time independent active intensity adequately describes energy flow often involve the rationalization that the reactive intensity although present, is of no consequence because its contribution time averages to zero. Equation (2.16) contains a term of the active intensity which likewise time averages to zero. Consequently, if the active intensity alone is used to describe the energy flux over all time then there is a contribution of the active intensity, $\bar{I}(\mathbf{r})\cos 2(\omega t - \phi(\mathbf{r}))$ which is likewise being ignored along with the reactive intensity.

Interpretations of Equation (2.16) is the basis of the argument against the conventional view of active intensity as a total description of energy transfer. The active intensity has great significance, but \bar{I} only describes the net flux of energy at a point, \bar{I} does not indicate in general where the energy goes or how it arrives at the point.

Take the example of a pure standing wave, where the active intensity is zero. Conventional viewpoints would indicate that there is no energy flux in the standing wave. However, the reactive intensity is non-zero. Therefore, from Equation (2.16), the instantaneous intensity is non-zero, indicating that there is energy propagating in the standing wave. At every point the energy flux

will time average to zero, but the existence of the acoustic field requires energy propagation.

These arguments go beyond semantics. It is important that the proper physical meanings are given to the instantaneous intensity, active intensity, and reactive intensity vectors, in terms of energy propagation. These views do not diminish the significance of the vectors, but try to specify the insight the vectors provide for the energy propagation in an acoustic field.

2.4. Sources of Acoustic Energy

The net outflow of a vector is the divergence of the vector. Since derivations of the divergence of \vec{I} and \vec{Q} are well documented, (Schultz, Smith and Malme 1964; Elko 1984) only the results will be stated here:

$$\nabla \cdot \vec{I} = 0 \quad , \quad (2.17)$$

$$\nabla \cdot \vec{Q} = -2\omega(T - V) = -2\omega L \quad , \quad (2.18)$$

where L , the Lagrangian, is the difference of the potential and kinetic energy.

2.4.1. Sources of Active Intensity

Equation (2.17) is of great interest because it states that the divergence of the active intensity is zero everywhere it is defined. However, this term is contained in the conservation of energy corollary stated in Equation (2.1), which in time averaged form is

$$\iiint_V \left[\frac{1}{2} \rho u^2 + \frac{1}{2\rho c^2} p^2 \right] dV = - \iiint_V \nabla \cdot \vec{I} dV \quad . \quad (2.19)$$

This equation is the basis of power measurements which relate the power radiated from a source in volume V to the active intensity. However, substituting Equation (2.17) into Equation (2.19) the time averaged change in energy in the volume V is zero. Consequently, if the source which causes the acoustic field in volume V

does radiate power, the source is not in the volume V . Therefore we must be careful in constructing the volume in which the intensity is defined.

The conservation of energy corollary, Equation (2.1), is derived for a source free region. Thus the intensity vector, for our use, is only defined in regions of no sources. If the acoustic field around a source is of interest then the volume sketched in Figure 2.3 can be constructed. The volume integral can subsequently be converted to a surface integral using Green's Theorem. However, the surface integral is not only over S_4 , which is conventionally used, but also includes S_1 , S_2 , and S_3 . These added surfaces allow the construction of the volume around but not including the sources. The surface integral will be

$$\begin{aligned} \iiint_V \nabla \cdot \vec{I} dV = & \iint_{S_1} \vec{I} \cdot d\vec{S}_1 + \iint_{S_2} \vec{I} \cdot d\vec{S}_2 + \iint_{S_3} \vec{I} \cdot d\vec{S}_3 \\ & - \iint_{S_4} \vec{I} \cdot d\vec{S}_4 . \end{aligned} \quad (2.20)$$

The paths S_2 and S_3 will give the same result but opposite in sign, therefore cancel. The integral over S_1 and S_4 are left and must cancel, which means that the energy entering V through S_1 leaves through S_4 , and that the power output by the source is quantified by the integral over S_1 or S_4 .

This observation produces the same result which has always been used for power measurements, but it is important to realize the formality of this argument which is based on the fact that the intensity vectors are only defined in source free regions.

Pascal (1985) derived a Helmholtz decomposition of the vector \vec{I} which split it into a part defined from a gradient of a scalar and another part from the curl of a vector:

$$\vec{I} = \nabla\beta + \nabla \times \vec{\psi} . \quad (2.21)$$

The divergence of the term $\nabla \times \vec{\psi}$ is zero by definition of the divergence and curl operators. However, the divergence of the term $\nabla\beta$ is in general not

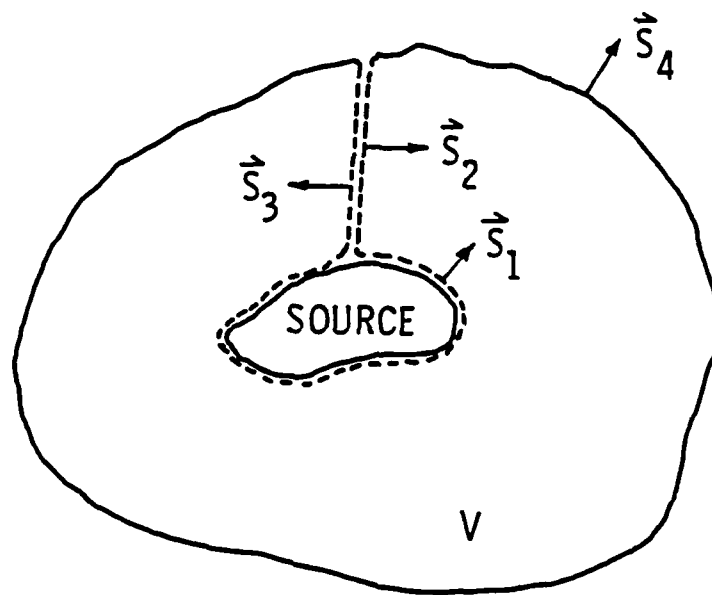


Figure 2.3 A closed volume, surrounding a source, in which the intensity is defined.

zero. Consequently, Pascal concluded from Equation (2.19) that $\nabla\beta$ accounts for radiated power. But, as already stated, $\nabla \cdot \vec{I} = 0$, thus $\nabla \cdot \nabla\beta$ must be zero. In light of the previous discussion of the volume in which intensity is considered, the conclusion that $\nabla\beta$ does not account for the time averaged output power of a source is valid.

This same conclusion can be reached by considering the case of the radiation of N point sources, where the total pressure and particle velocity are

$$\underline{p}(\underline{r}) = \sum_{i=1}^N \underline{p}_i(\underline{r}) \quad , \quad (2.22)$$

$$\underline{u}(\underline{r}) = \sum_{i=1}^N \underline{u}_i(\underline{r}) \quad , \quad (2.23)$$

where

$$\underline{p}_i(\underline{r}) = \frac{A_i}{r_i} e^{-j(kr_i - \alpha_i)} \quad , \quad (2.24)$$

$$\underline{u}_i(\underline{r}) = \frac{A_i}{j\omega\rho} \frac{(1 + jkr_i)\vec{r}_i}{r_i^3} e^{-j(kr_i - \alpha_i)} \quad . \quad (2.25)$$

The constants A_i and α_i are the relative amplitude and phase of the i -th source, and r_i and \vec{r}_i are the distance and direction vector from the i -th source to the measurement point \underline{r} :

$$r_i^2 = (x - x_i)^2 + (y - y_i)^2 + (z - z_i)^2 \quad , \quad (2.26)$$

$$\vec{r}_i = (x - x_i, y - y_i, z - z_i) \quad . \quad (2.27)$$

The complex intensity vector \vec{I}_c can be calculated from equations (2.22) and

(2.23):

$$\begin{aligned}
\vec{I}_c(\mathbf{r}) &= \frac{1}{2} p \vec{u}^* \\
&= \frac{-1}{2j\omega\rho} \left[\sum_{i=1}^N A_i \frac{e^{-j(kr_i - \alpha_i)}}{r_i} \right] \left[\sum_{i=1}^N A_i \frac{(1 - jkr_i)}{r_i^3} \vec{r}_i e^{j(kr_i - \alpha_i)} \right] \\
&= j \sum_{i=1}^N A_i^2 \frac{(1 - jkr_i)}{2\omega\rho r_i^4} \vec{r}_i \\
&\quad + j \sum_{n=1}^N \sum_{\substack{m=1 \\ m \neq n}}^N \frac{A_m A_n}{2\omega\rho} \frac{(1 - jkr_i)}{r_n r_m^3} \vec{r}_m e^{-j[k(r_n - r_m) - (\alpha_n - \alpha_m)]} .
\end{aligned} \tag{2.28}$$

Since $\vec{I}_c = \vec{I} + j\vec{Q}$ and defining $\eta_{nm} = k(r_n - r_m) - (\alpha_n - \alpha_m)$ Equation (2.28) can be separated, such that

$$\vec{I}(\mathbf{r}) = \frac{1}{2\rho c} \sum_{i=1}^N A_i^2 \frac{\vec{r}_i}{r_i^3} + \frac{1}{2\rho c} \sum_{n=1}^N \sum_{\substack{m=1 \\ m \neq n}}^N A_m A_n \frac{\vec{r}_m}{r_n r_m^2} (kr_m \cos\eta_{nm} - \sin\eta_{nm}) , \tag{2.29}$$

$$\vec{Q}(\mathbf{r}) = \frac{1}{2\omega\rho} \sum_{i=1}^N A_i^2 \frac{\vec{r}_i}{r_i^4} + \frac{1}{2\omega\rho} \sum_{n=1}^N \sum_{\substack{m=1 \\ m \neq n}}^N A_m A_n \frac{\vec{r}_m}{r_n r_m^3} (\cos\eta_{nm} - kr_m \sin\eta_{nm}) . \tag{2.30}$$

Now calculate the curl of the intensity defined in Equation (2.29):

$$\begin{aligned}
\nabla \times \vec{I}(\mathbf{r}) &= \frac{1}{\omega\rho} \sum_{n=1}^N \sum_{m=n+1}^N \frac{A_m A_n}{r_n^3 r_m^3} \left\{ \left[(k^2 r_n r_m + 1) \sin\eta_{nm} \right. \right. \\
&\quad \left. \left. + k(r_m - r_n) \cos\eta_{nm} \right] \langle \epsilon_{nm}^{yz}, \epsilon_{nm}^{zz}, \epsilon_{nm}^{zy} \rangle \right\} , \tag{2.31}
\end{aligned}$$

where $\langle \epsilon_{nm}^{yz}, \epsilon_{nm}^{zz}, \epsilon_{nm}^{zy} \rangle$ is a vector which has the components $\epsilon_{nm}^{\mu\nu} = \mu(\nu_m - \nu_n) + \nu(\mu_n - \mu_m)$; $\mu = x, y, \text{ or } z$, $\nu = x, y, \text{ or } z$. Equation (2.31) shows that the part of the equation for the active intensity with the cross terms proportional to $A_m A_n (n \neq m)$ is the part of \vec{I} which has a non-zero curl. Consequently, for a distribution of point sources the active intensity can be split as Equation (2.21) in the following manner:

$$\nabla \beta = k \sum_{i=1}^N A_i^2 \frac{\vec{r}_i}{r_i^3} , \tag{2.32}$$

$$\nabla \times \vec{\psi} = k \sum_{n=1}^N \sum_{\substack{m=1 \\ m \neq n}}^N A_m A_n \frac{\vec{r}_m}{r_n r_m^2} (k r_m \cos \eta_{nm} + \sin \eta_{nm}) . \quad (2.33)$$

Equation (2.32) means that $\nabla \beta$ is the vector sum of the active intensity from each point source ignoring the coupling of the sources. Further, $\nabla \times \psi$ defined in Equation (2.33) represents the effect of coupling between the point sources.

As an example we will calculate the total power Π_3 radiated by three point sources compared to the power Π_1 radiated by one point source. The three point sources are in a line separated by distance d with relative amplitudes $+1, -1, +1$. Using the expressions in Skudrzyk (1971),

$$\frac{\Pi_3}{\Pi_1} = 3 - 4 \frac{\sin kd}{kd} + \frac{\sin 2kd}{kd} . \quad (2.34)$$

Figure 2.4 represents Equation (2.34) as a function of kd , clearly shows the effect of mutual coupling of the sources especially at low kd . To identify the terms in Equation (2.34) the power can be calculated from the intensity by integrating \vec{I} over a surface enclosing the sources. Without performing the integration explicitly, the power associated with $\nabla \beta$ is clearly $3\Pi_1$. Consequently, the power associated with $\nabla \times \psi$ is $-4 \frac{\sin kd}{kd} + \frac{\sin 2kd}{kd}$. Therefore, in the region excluding the sources, $\nabla \beta$ does not totally account for the energy propagating to the farfield, because the mentioned terms due to the source coupling are not negligible.

2.4.2. Sources of Reactive Intensity

A very nice development of the sources of reactive intensity is presented by Elko (1985). He derives an expression from the complex power and the divergence of the complex intensity vector, which is much the same as the power balance for the active intensity:

$$\iint_S \vec{Q} \cdot \vec{n} dS = \Pi_I + \iiint_V 2\pi L dV , \quad (2.35)$$

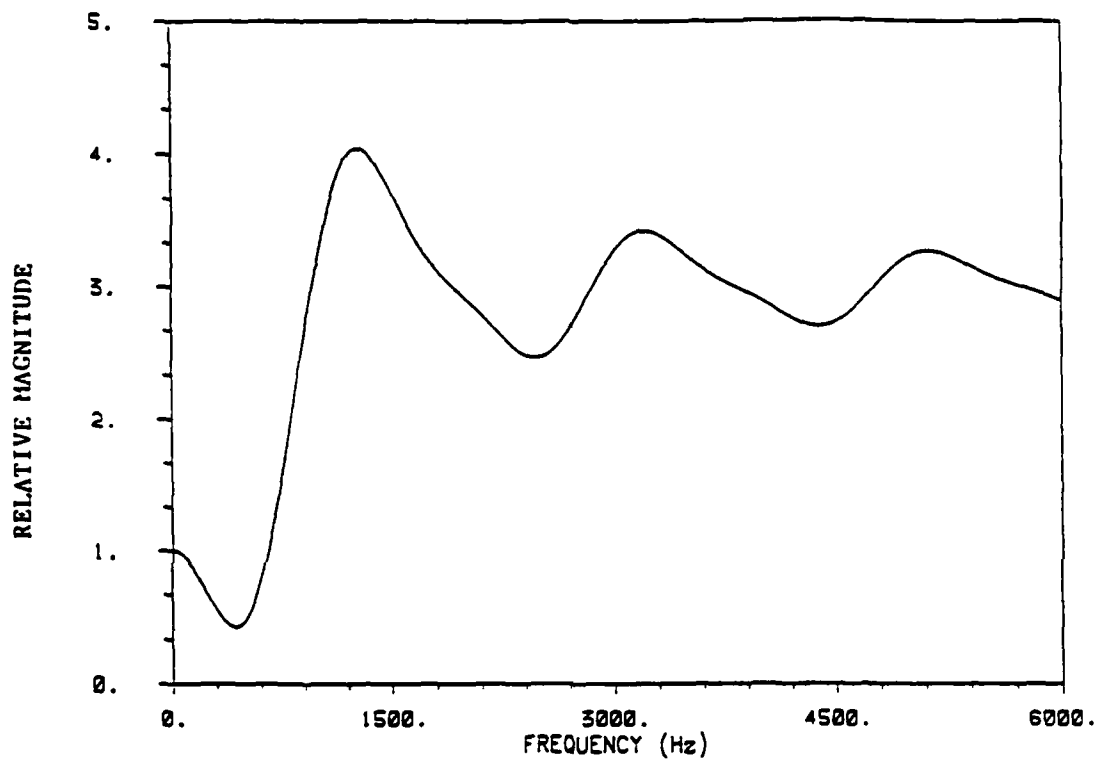


Figure 2.4 The ratio of the power radiated by three sources to the power radiated by one source. The sources are separated by 18cm with the center source out of phase.

where Π_I is the imaginary part of the complex power radiated by a source, L is the Lagrangian, which enters from the divergence of the reactive intensity, V is the volume enclosing a source, and S is the surface area of the volume.

Equation (2.35) shows that the reactive energy enters the volume through its boundaries (sources) as signified by the term Π_I , but there is also the energy which is originating in the volume, represented by the term including the Lagrangian. The integral of the Lagrangian signifies that the reactive energy is present because of a difference of the kinetic and potential energy. It is interesting that it includes the difference of the total kinetic energy which has a component associated with the particle velocity accounting for the active intensity.

The reactive intensity exists if there is a nonvanishing pressure gradient. With a nonvanishing pressure gradient there is an imbalance in the potential and kinetic energies. Thus, there is energy which is removed from the potential energy density which is needed for maintaining the pressure gradient. This is energy which is input to a region during one-half of a cycle then work exerted back by the region during the other one-half of a cycle. Consequently, energy is removed from that energy which is radiated to infinity by a source to maintain a nonvanishing pressure gradient associated with the imbalance in the potential and kinetic energies.

2.5. Instantaneous Energy Flux Lines

As discussed in Section 2.3.2., the instantaneous intensity describes energy propagation through a point. To follow energy through space, lines must be drawn parallel to the instantaneous intensity vector. The resulting instantaneous intensity flux lines will create a complicated picture because they are a function of space and time. These lines clearly show the distinction between the time

dependent description of energy transfer (instantaneous intensity) and the time independent description of power flux (active intensity).

The scheme to construct the instantaneous intensity flux lines is represented in Figure 2.5 for a hypothetical example. The instantaneous intensity vectors at six points are drawn for two times, t_0 and $t_0 + \Delta t$. The resulting flux line is drawn with a dashed line. The variation of the instantaneous intensity vectors with the increment of time is greatly exaggerated in Figure 2.5, as is the distance between the points between which the flux line is drawn.

The instantaneous intensity flux line begins in Figure 2.5a at point 1 at time t_0 . The flux line is drawn in the direction of the instantaneous intensity at time t_0 at point 1, which is toward point 5. Thus the energy propagates through point 1 toward point 5 at speed c . The propagation distance is Δr , so that this propagation takes time $\Delta t = \frac{\Delta r}{c}$. At time $t_0 + \Delta t$ the instantaneous intensity vectors at the six points are different, as represented in Figure 2.5b. The energy now propagates through point 5 toward point 3 in time Δt .

The instantaneous intensity flux line for this example is drawn from point 1 to point 5 to point 3 and continues through space as time increases. The resulting line represents the energy propagation as a function of space and time, although only the spatial dependence can be shown. The direction of the instantaneous intensity at point 1, the initial point, varies over one half of a cycle. When the line begins at some other time at point 1 the path will begin in another direction and continue on another path. Only at times separated by one half of a period does the line beginning at point 1 trace the same path. Consequently, there is no one line which describes the energy propagation at all times.

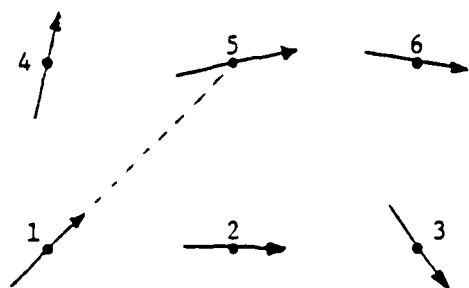
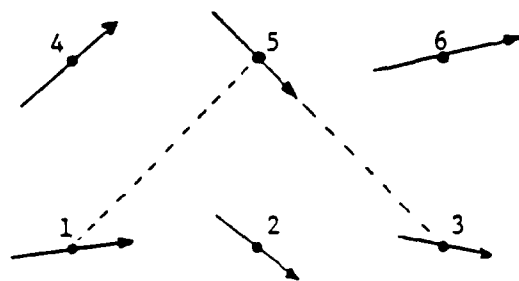
a) time t_0 b) time $t_0 + \Delta t$

Figure 2.5 Schematic of constructing instantaneous intensity flux lines. The instantaneous intensity vectors are represented at six points at times t_0 and $t_0 + \Delta t$, and the resulting flux line (dashed) is drawn.

2.5.1. Instantaneous Intensity Flux Lines for Three Point Sources

Consider the field radiated by point sources arranged on a line with 18cm center to center spacing. The two outer sources are in phase and the center source vibrates in opposite phase. This source configuration is used because it provides examples of high mutual coupling and low mutual coupling. Two frequencies will consequently be discussed: (1) 2070 Hz (low mutual coupling, the sources are separated by 1.1λ) and (2) 200 Hz (high mutual coupling, the sources are separated by 0.1λ). The active and reactive intensity for these frequencies are plotted in Figures 2.6 and 2.7. These are commonly discussed examples so the analysis will be limited.

At 2070 Hz, with the low mutual coupling, the active and reactive intensity point out of the three sources. Thus one can conclude that all the energy in the region propagates away from the sources. At 200 Hz, high mutual coupling, the active intensity points into the center source, leading to the conclusion that the center source absorbs power. However, the reactive intensity points out of each source since the pressure is a local maximum above the sources, independent of the direction of the active intensity.

Now look at the instantaneous intensity flux lines; Figure 2.8 and 2.9. The energy is followed from four initial points marked by circles. Two initial times are chosen so there are two paths which leave each point. The direction of the energy propagation is indicated by an arrow. There is an infinite set of paths leaving each point at different instances during one period; however, for the purposes here two initial times adequately demonstrate an important point.

Figure 2.8 is intuitively very easy to understand. Each path shows propagation away from the three sources. This would be expected because the sources have low coupling and the active and reactive intensity vectors point

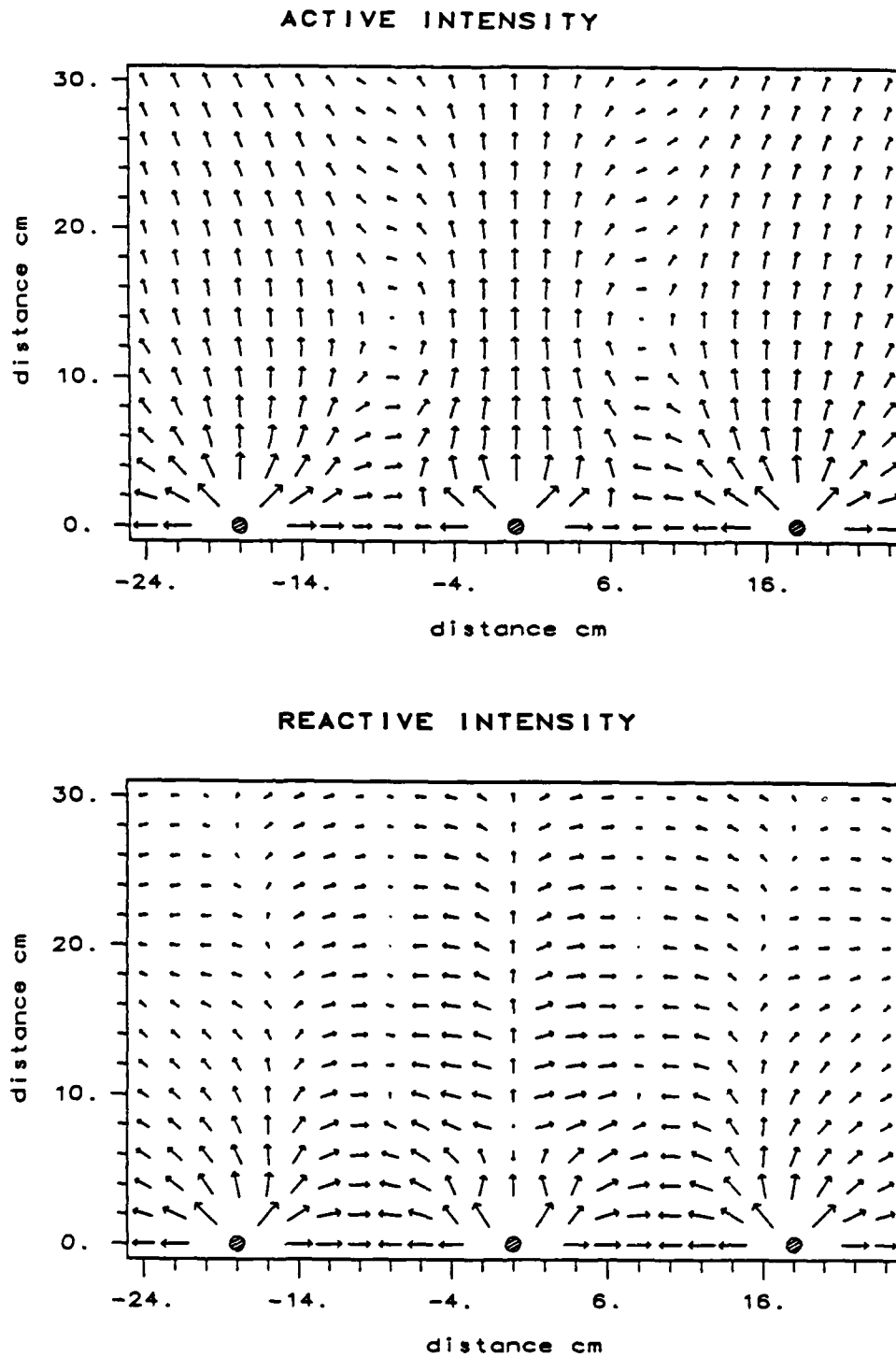


Figure 2.6 The calculated active intensity and reactive intensity around three point sources separated by 18cm with the center source out of phase. The frequency is 2070Hz.

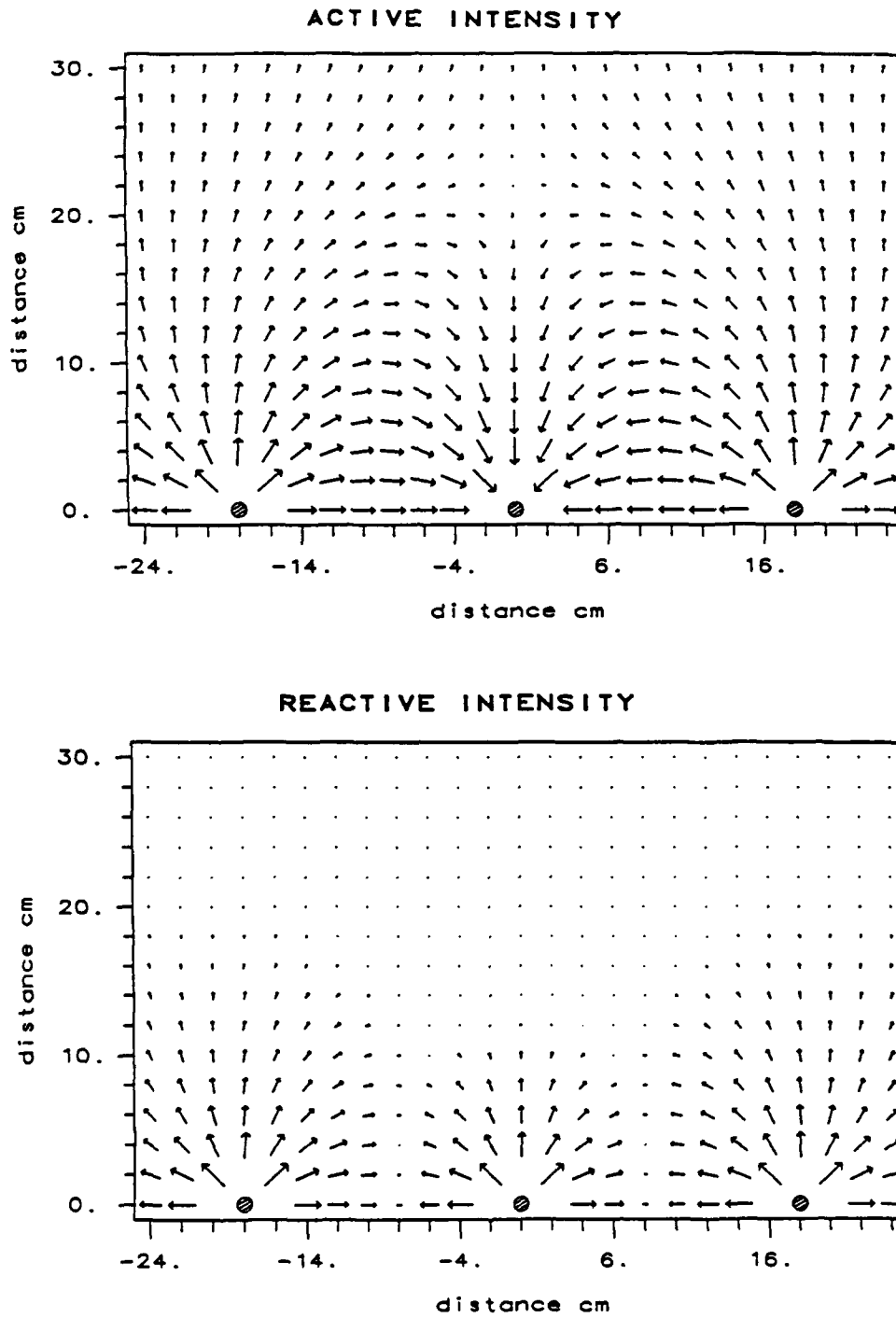


Figure 2.7 The calculated active intensity and reactive intensity around three point sources separated by 18cm with the center source out of phase. The frequency is 200Hz.

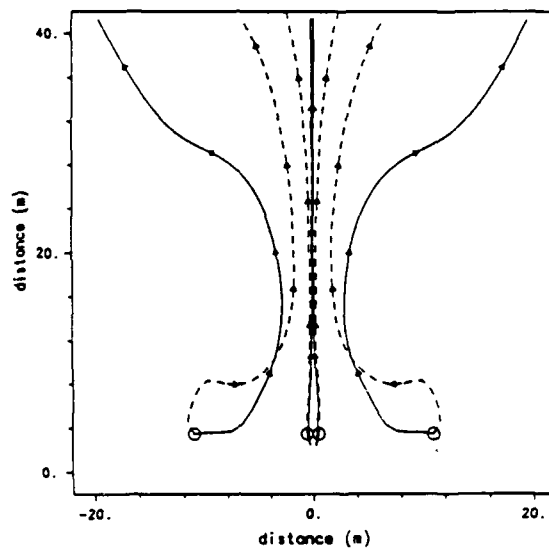


Figure 2.8 Instantaneous intensity flux lines at 2070Hz. (Three point sources with the center source out of phase.) The circles represent the starting positions of the lines. Two lines leave each starting position one at times t_0 and $t_0 + \frac{T}{6}$.

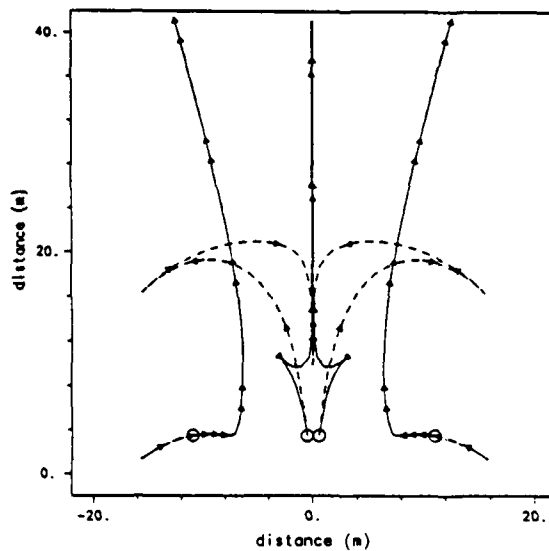


Figure 2.9 Instantaneous intensity flux lines at 200Hz. (Three point sources with the center source out of phase.) The circles represent the starting positions of the lines. Two lines leave each starting position one at times t_0 and $t_0 + \frac{T}{6}$.

out of the sources. Thus the present views that the active intensity show energy propagation are essentially true since it would conclude that the energy propagates from the sources.

However, Figure 2.9 shows a rather surprising result, because each path, although erratic, does go to the farfield. Thus energy at each of the four starting positions does get to the farfield. This directly contradicts present views that the active intensity shows the path of energy propagation, since for this frequency, Figure 2.7, the active intensity would say that all energy in the four starting positions, shown in Figure 2.9, goes into the center source. Consequently it is invalid to say that the active intensity shows the path of energy propagation, because it is a time averaged quantity which does not include the contribution of the reactive intensity to the energy transfer.

It was stated that in each period of the acoustic motion an infinite set of different paths from each point can be constructed. Consequently an important issue is the practicality of studying simultaneously the time and spatial dependence energy propagation. It is obvious that a proper description of energy propagation must include the reactive intensity along with the active intensity; however, this is an impractical view because there is not one path along which the energy propagates at all time. Thus one must turn to the time independent vectors, \vec{I} and \vec{Q} , and remember that the active intensity vector quantifies in magnitude and direction the time averaged power flux, not the path of energy propagation. It should also be understood that the energy in the reactive intensity does not simply oscillate back and forth but is indeed transferred to the farfield in the form of the energy propagation described by the instantaneous intensity.

A few authors have published papers about constructing lines which they call energy streamlines that are drawn tangent to the active intensity vector (Waterhouse, Yates, Feit, and Liu 1985; Skelton and Waterhouse 1986; Waterhouse and Feit 1986; Waterhouse 1987). The claim is that these lines show the flow of energy through space. However, as already discussed, the instantaneous intensity is the description of energy flow. Consequently, to follow energy through space, energy flux lines must be drawn parallel to the instantaneous intensity. The resulting instantaneous intensity flux lines show the distinction between the time dependent process of energy transfer and the time averaged power flux.

Chapter 3

WAVE PROPERTIES DESCRIBED BY INTENSITY

3.1. Introduction

Intensity is used primarily to describe the transfer of energy in an acoustic field. However, the vector properties of the active and reactive intensity are linked directly to properties of wave forms. These interpretations begin from the general description of acoustic pressure which was used to develop the energy transfer characteristics in the previous chapter. The result of this analysis is a method of representing the wave structure. This proves especially useful in the nearfield where the acoustic field is normally viewed as very complicated. The visualization of the nearfield which is provided by the active and reactive intensity is a valuable use of the acoustic intensity analysis along with the energy interpretations.

There have been many authors who have addressed the issues of wave propagation. Commonly the wave structure is discussed in terms of the energy density, wave shape, phase speed and group velocity. The new contribution of this chapter is to link these well established ideas to the intensity analysis.

3.2. General Functional Form of Acoustic Pressure

The essence of this chapter is the interpretation of the general functional form for the acoustic pressure which was briefly introduced in the previous chapter. The pressure is described in three dimensions by the following equation:

$$\underline{p}(\underline{r}, t) = P(\underline{r}) \underline{f}[\phi(\underline{r}) - ct] , \quad (3.1)$$

where \underline{r} is a general coordinate, $P(\underline{r})$ is a positive real function of the general coordinate, and $\phi(\underline{r})$ is a real function of the general coordinate. This form

clearly separates the pressure into two parts: (1) the pressure amplitude spatial distribution specified by $P(r)$ and (2) the phase spatial distribution specified by $f[\phi(r) - ct]$.

An important aspect of this description is the wave shape and wave propagation described by $f[\phi(r) - ct]$. Contained in this function is the wave front which is inherent in our concepts of acoustic fields. For this thesis the function will be studied for monochromatic fields, so that the pressure is written as

$$\underline{p}(r, t) = P(r)e^{j(\omega t - \phi(r))} . \quad (3.2)$$

In classical theories waves are defined as surfaces of constant phase, thus this functional form, although specifying the time dependence as harmonic, maintains a general wave front shape defined by surfaces where $\phi(r) = \text{constant}$.

This functional form is not the most general representation of wave propagation. Whitham (1960; 1961) discusses the notion of a wave form from its transient development to the steady state; consequently, addressing the time and spatial variation of an acoustic wave form. However, for the purpose of this thesis it is sufficient to investigate a steady state field. These fields can be decomposed into frequency components, so it is also valid to discuss monochromatic fields. Consequently the developments can be focused on the consequence of a general wave shape $\phi(r)$ with a pressure distribution $P(r)$ recognizing this as a step to extending the understanding toward broad band and transient phenomena.

3.3. Differential Equations for $P(r)$ and $\phi(r)$

A constraint on the generalized form of the pressure is that it satisfies the wave equation. The function $P(r)$ and $\phi(r)$ can not be chosen arbitrarily. But differential equations can be developed which relate the two functions so that

$\underline{p}(r, t)$ satisfies the wave equation. This interdependence is derived by substituting the pressure into the Helmholtz equation:

$$\nabla^2 \underline{p}(r, t) - \frac{1}{c^2} \frac{\partial^2 \underline{p}(r, t)}{\partial t^2} = \underline{g}(r, t) , \quad (3.3)$$

where $\underline{g}(r, t)$ is a source term. However, the intensity is developed for a source free region so the source term $\underline{g}(r, t)$ is zero. Substituting Equation (3.2) into Equation (3.3) gives

$$[\nabla^2 P - P \nabla \phi \cdot \nabla \phi - j(2 \nabla P \cdot \nabla \phi + p \nabla^2 \phi) + k^2 P] e^{j(\omega t - \phi)} = 0 . \quad (3.4)$$

The real and imaginary parts of this equation can be separated so that the following differential equations can be written:

$$\nabla^2 P + [k^2 - \nabla \phi \cdot \nabla \phi] P = 0 , \quad (3.5)$$

$$P \nabla^2 \phi + 2 \nabla \phi \cdot \nabla P = 0 , \quad (3.6)$$

where $k = \frac{\omega}{c}$, which is independent of position. Equations (3.5) and (3.6) are non-linear partial differential which couple the phase characteristics of the pressure to the pressure amplitude variation.

3.4. Vector Characteristics of \vec{I} and \vec{Q}

Before going any further we need to attach a physical meaning to the vector characteristics of the active and reactive intensity. From the functional form of the acoustic pressure, Equation (3.2), the following equations were developed in the previous chapter for \vec{I} and \vec{Q} :

$$\vec{I}(r) \stackrel{\text{def}}{=} \frac{1}{2\omega\rho} P^2(r) \nabla \phi(r) , \quad (3.7)$$

$$\vec{Q}(r) \stackrel{\text{def}}{=} \frac{-1}{2\omega\rho} P(r) \nabla P(r) . \quad (3.8)$$

The active intensity has the direction of the spatial gradient of the pressure phase, consequently \vec{I} is perpendicular to surfaces of constant phase. By definition, the surfaces of constant phase are wave fronts; so the active intensity is perpendicular to the resultant wave fronts in an acoustic field. The term "resultant" is used because these wave fronts are a result of the interference of many waves. For instance, with a plane wave incident on a reflecting boundary, the acoustic field can be considered as the interference of the direct plane wave and the reflected plane wave. This interference produces the resultant waves to which the active intensity is perpendicular.

As noted by numerous authors the reactive intensity is proportional to the negative of the spatial gradient of the pressure amplitude (Elko 1984; Tichy 1984). Consequently, \vec{Q} points normal to surfaces of constant pressure. More specifically, \vec{Q} points out of pressure maxima and into pressure minima. This proves very useful for visualizing the fine structure of the pressure distribution.

With the interpretations of the active and reactive intensity the acoustic field can be organized into resultant wave fronts and a pressure distribution. The idea of organizing the acoustic field is central to the powerful insight the acoustic intensity analysis provides for visualizing and interpreting the nearfield of sources and scatterers. This will become evident with several examples in Chapters 6 and 7 where these two simple ideas are applied to otherwise complicated acoustic nearfields.

3.5. Generalized Phase Speed

The active intensity has been shown to visualize the resultant wave fronts. Implicit to the concept of a wave front is the speed of propagation. Conventionally, the speed of sound c , is associated with the propagation speed of simple waves such as plane waves and spherical waves. However, in general the speed of

sound, c , is different than the speed of wave front propagation, c_p . For instance, this is recognized in a waveguide where the phase speed is not c . The extension to the general acoustic field has been done in the historic literature (Rayleigh 1877, Lamb 1904), but is included here to link the phase speed with the active intensity.

The general phase speed for the surfaces of constant phase is calculated by setting the pressure phase equal to a constant for a change in time and position normal to the surfaces of constant phase. Thus,

$$(\omega t_o - \phi(r_o)) = [\omega(t_o + \Delta t) - \phi(r_o + \Delta r)] . \quad (3.9)$$

This is equivalent to setting the total derivative of the pressure phase with respect to time and distance normal to the lines of constant phase, equal to zero:

$$d[\omega t - \phi(r)] = 0 . \quad (3.10)$$

The spatial derivative will be taken with respect to the distance ξ in the direction \hat{n} , which is normal to the wave front. (The direction \hat{n} varies with the position of the wave front.) Equation (3.10) can then be expanded using the chain rule:

$$\begin{aligned} \frac{\partial}{\partial t}(\omega t - \phi(\xi))dt + \frac{\partial}{\partial \xi}(\omega t - \phi(\xi))d\xi = \\ \omega dt + \frac{\partial \phi}{\partial \xi}d\xi = 0 . \end{aligned} \quad (3.11)$$

The propagation speed of the constant phase surface, normal to the surface, is defined as $c_p \stackrel{\text{def}}{=} \frac{d\xi}{dt}$. The derivative of the phase with respect to the distance normal to the constant phase, $\frac{\partial \phi}{\partial \xi}$, is the amplitude of the phase gradient, $|\nabla \phi|$. Thus the phase speed c_p can be calculated from Equation (3.11) to be

$$c_p \stackrel{\text{def}}{=} \frac{d\xi}{dt} = \frac{\omega}{|\nabla \phi|} . \quad (3.12)$$

Using the equation for the active intensity and potential energy $|\nabla\phi|$ can be expressed as

$$|\nabla\phi| = 2\omega\rho\frac{|\vec{I}|}{P^2} = \frac{\omega}{2c^2}\frac{|\vec{I}|}{V}, \quad (3.13)$$

where $V = \frac{1}{4\rho c^2}P^2$ is the potential energy. Thus, a more convenient form for c_p is

$$c_p = 2c^2\frac{V}{|\vec{I}|}, \quad (3.14)$$

which expresses c_p in terms of two measurable quantities.

It should be noted that c_p is dependent on position. Consequently, at each point in space and along any wave front the phase speed may vary. Further, the phase speed is called resultant to make a clear distinction between two view points of an acoustic field. Huygen's principle concludes that an acoustic field can be represented as a result of the interference of waves which travel at speed c . Thus the resultant wave propagates at the resultant phase speed not at the speed c at which the interfering waves travel.

A quantity often referred to is a wave number. For plane and spherical waves the wave number is $\frac{\omega}{c}$. In general we can discuss a resultant wave number $k_p = \frac{\omega}{c_p}$, which varies in space. The concept of a spatially dependent wave number is not easily accepted because of a common mathematical tool of transforming real space into wave number space. The transform spaces have a one to one mapping. But the wave number, one of the transform variables, is independent of real space, the other transform variable.

From the viewpoint of a wave number decomposition of an acoustic field, where the wave number and space is a transform pair such that a quantity with the units of wave number is an independent variable, the variation of the pressure phase is a result of the superposition of wave numbers. The amplitude of the contribution from each wave number, k , is independent of space; where as the

resultant wave number $k_p = \frac{\omega}{c_p}$, which results from a superposition of all the wave numbers in the field and is a directly measurable quantity which varies in space. Thus, k_p defines a local wave number in contrast to k which is a global wave number that is averaged over all space.

It is often convenient to split a field into a superposition of waves, wave numbers, point sources, or some other simplified form. However, the Helmholtz-Huygen integral states that for a given pressure and velocity distribution there is not a unique source distribution which creates the field. Thus, there is an infinite set of realizable decompositions of an acoustic field. The viewpoint of this thesis is to visualize an acoustic field in its resultant form, without decomposing it into different forms.

3.6. Differential Equations for $P(r)$ and $\phi(r)$ in Terms of the Wave Properties

The resultant wave number can be used to simplify the differential Equations (3.5) and (3.6), which contains the term $\nabla\phi \cdot \nabla\phi$. The resultant wave number in terms of the phase gradient is

$$k_p = \frac{\omega}{c_p} = \frac{\omega}{\frac{\omega}{|\nabla\phi|}} = |\nabla\phi| . \quad (3.15)$$

In vector form this is

$$\vec{k}_p = \nabla\phi . \quad (3.16)$$

Substituting this into Equation (3.5) and using the fact that $\vec{k}_p \cdot \vec{k}_p = k_p^2$ results in the following differential equation for the pressure amplitude.

$$\nabla^2 P + (k^2 - k_p^2)P = 0 , \quad (3.17)$$

$$P\nabla^2\phi + 2\vec{k}_p \cdot \nabla P = 0 . \quad (3.18)$$

Equations (3.17) and (3.18) are interesting because the pressure amplitude at every point in space is a simple function of the wave number, k , and the resultant wave number, k_p , at that point. Consequently, any field, even a complicated nearfield, can be viewed microscopically on a very simple basis.

Using Equation (3.17) and (3.18), let us investigate the example of a plane wave where the phase distribution can be specified as $\phi(x) = kx$ which are waves propagating at speed c . Consequently, $k_p = k$. Equation (3.17) and (3.18) become

$$\frac{\partial^2}{\partial x^2} P = 0 \quad , \quad (3.19)$$

$$2k \frac{\partial}{\partial x} P = 0 \quad . \quad (3.20)$$

The only solution to both equations is $P = \text{constant}$, which is the form for a plane wave.

The significance of Equation (3.17) and (3.18) is that for a specific phase distribution the pressure amplitude is specified by these equations; likewise, for a specific pressure amplitude distribution the equations specify the phase distribution. Consequently, if the potential energy is known as a function of space the active and reactive intensity can be calculated using the two differential equations.

3.7. Example: Plane Wave Incident on a Rigid Boundary

Let us tie together some of the ideas on the wave form by the example of a plane wave incident on a rigid boundary, Figure 3.1. The incident pressure is

$$p_i(x, y, t) = A_i e^{j(\omega t - k(x \sin \theta + y \sin \theta))} \quad . \quad (3.21)$$

The total pressure is the sum of the incident wave and a wave reflected from the boundary. The velocity can be calculated from the pressure, so the total pressure

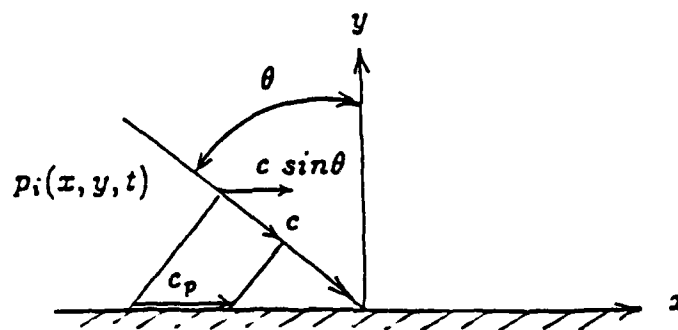


Figure 3.1 A sketch of the configuration for a plane wave incident on a rigid boundary. The phase speed, c_p , and the group velocity, $c \sin(\theta)$, are clearly marked.

and particle velocity are

$$\underline{p}(x, y, t) = 2A \cos(ky \cos \theta) e^{j(\omega t - kz \sin \theta)} , \quad (3.22)$$

$$\begin{aligned} \underline{u}(x, y, t) = \hat{i} \left[\frac{2A \sin \theta}{\rho c} \cos(ky \cos \theta) e^{j(\omega t - kz \sin \theta)} \right] \\ + \hat{j} \left[\frac{2A \cos \theta}{\rho c} \sin(ky \cos \theta) e^{j(\omega t - \frac{\pi}{2} - kz \sin \theta)} \right] . \end{aligned} \quad (3.23)$$

Using these two equations the intensity and energy densities are

$$\bar{I}(x, y) = \hat{i} \frac{2A^2}{\rho c} \sin \theta \cos^2(2ky \cos \theta) , \quad (3.24)$$

$$\bar{Q}(x, y) = \hat{j} \frac{A^2}{\rho c} \cos \theta \sin(2ky \cos \theta) , \quad (3.25)$$

$$V(x, y) = \frac{A^2}{\rho c^2} \cos^2(2ky \cos \theta) , \quad (3.26)$$

$$T(x, y) = \frac{A^2}{\rho c^2} \left[\frac{1}{2} - \cos 2\theta \cos(2ky \cos \theta) \right] . \quad (3.27)$$

There are some features of these equations which should be noted and are sketched in Figure 3.2. The active intensity is parallel to the rigid boundary; consequently, the wave fronts are surfaces perpendicular to the boundary propagating in the positive x direction. The reactive intensity only has a component perpendicular to the boundary, so the pressure fluctuates only as a function of the distance above the boundary. This can also be visualized as a vertical standing wave.

The phase speed is calculated from Equation (3.14):

$$c_p(x) = 2c^2 \frac{V}{|\bar{I}|} = \frac{c}{\sin \theta} . \quad (3.28)$$

As stated, the direction of the resultant wave propagation is parallel to the boundary, which is marked Figure 3.2. Two extremes can be looked at. First the case of $\theta = \frac{\pi}{2}$ which is the grazing angle of the incident wave so there is no reflected wave. The wave speed for $\theta = \frac{\pi}{2}$ is c since there are no interference

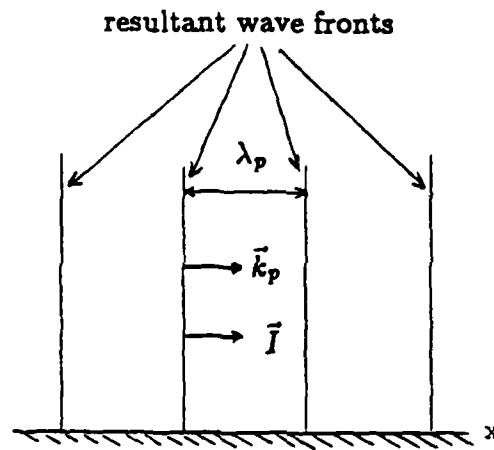


Figure 3.2 A sketch of the resultant wave fronts for the example of the plane wave incident on a rigid boundary. The resultant wave vector, \vec{k}_p , the resultant wave length, λ_p , and the active intensity, \vec{I} , are marked.

affects. However for the case of $\theta = 0$, $c_p = \infty$ which is the case of the incident wave being normal to the boundary so there is no component horizontal to the boundary.

For this example the wave vector is

$$\vec{k}_p = i \frac{\omega}{c} \sin \theta \quad , \quad (3.29)$$

which is independent of space. This brings up an interesting point. Going back to Equation (3.18) if \vec{I} is independent of space $\nabla^2 \phi = 0$, then Equation (3.18) becomes

$$2\vec{k}_p \cdot \nabla P = 0 \quad . \quad (3.30)$$

Consequently, the active intensity and reactive intensity are perpendicular everywhere when the resultant wave speed is independent of space.

Another issue which needs to be addressed is the speed of energy propagation. Conventional views are that the active intensity represents the energy flow; however, this example clearly shows a problem with this interpretation. With the incident angle θ the component of the incident wave which propagates parallel to the rigid boundary is $c \sin \theta$. The implication of the conventional view is that the energy would propagate with the wave fronts. In this example the wave fronts propagate faster than the speed of sound. However, the acoustic energy cannot travel faster than the energy which creates the acoustic field which propagates at the speed of sound. Therefore, in this example the group velocity, which is the average speed of the energy propagation, is the speed of the energy propagation parallel to the rigid boundary, which is less than the speed of sound.

Chapter 4

CONCEPTS INCORPORATING ENERGY TRANSFER AND WAVE PROPERTIES

4.1. Introduction

The previous two chapters addressed the implications of the intensity vectors in regard to energy transfer and to wave motion. Both of these interpretations must be used to take full advantage of the intensity analysis. This chapter will discuss an explanation of the reactive intensity contribution to energy propagation which is based on the ideas in both Chapters 2 and 3. The group velocity and practical aspects of the reactive intensity will also be discussed. Finally, the example of the active intensity vortex is explored, from the viewpoint of the wave properties and energy transfer.

4.2. A Comparison of Wave Front and Energy Propagation

Fundamental explanations of wave phenomena often use the special case of the plane wave to show that energy propagates with the wave fronts. However, combining the interpretations of Chapters 3 and 4, the energy travels with speed c in the direction of the instantaneous intensity which in a general wave is not in the direction of the wave fronts. It is difficult to conceptualize the idea that energy does not propagate with the waves, because intuitively, in a pressure wave, at a time or in a position with zero pressure, no acoustic energy is expected. However, the contribution of the reactive intensity is not considered in such an argument. With the wave properties linked to the active intensity in Chapter 3 a better physical understanding of the reactive intensity can now be introduced to clarify this.

The differential equations for $P(r)$ and $\phi(r)$, Equations 3.5 and 3.6, specify that if the resultant phase speed is different than the plane wave phase speed, then there is a pressure gradient. The pressure gradient means that there is a non-zero kinetic energy component due to U_r .

Keeping these ideas in mind let us consider a plane wave. The kinetic energy is in phase with pressure, because the pressure amplitude does not vary in space, $U_r = 0$. Figure 4.1 represents the time dependent potential energy and kinetic energy at times t and some small increment of time Δt later. The energy is contained in the regions marked (I), (II), (III), and (IV). At time $t + \Delta t$ the energy has progressed to the right at speed c in the packets (I), (II), (III), and (IV). This is one simple way to demonstrate that the energy propagates with the plane waves.

Now consider the case where the resultant waves do not travel at speed c ($c_p \neq c$), so that there is kinetic energy due to the components U_a and U_r . Figure 4.2 represents the time dependent energy densities as a function of distance for times t and $t + \Delta t$. The reference points which we call wave fronts, propagate the distance $c_p \Delta t$, thus the packets between pressure zeros labeled (I), (II), and (III) propagate a distance $c_p \Delta t$. The energy propagates at speed c which in this case is not with the packets thus there is more energy at point (1) in the kinetic energy associated with U_r than in the wave form. In order to maintain the shape of the propagating waves (I), (II), and (III), kinetic energy associated with U_r at point (2) is shifted into U_a and p .

To summarize this argument, it must be remembered that for the plane wave the energy travels with the waves because there is no energy associated with U_r . However, with a non-zero component of the kinetic energy due to U_r and with $c_p \neq c$, the energy propagates by shifting between the kinetic energy due to U_a and U_r so the wave fronts can propagate at a speed other than the speed of

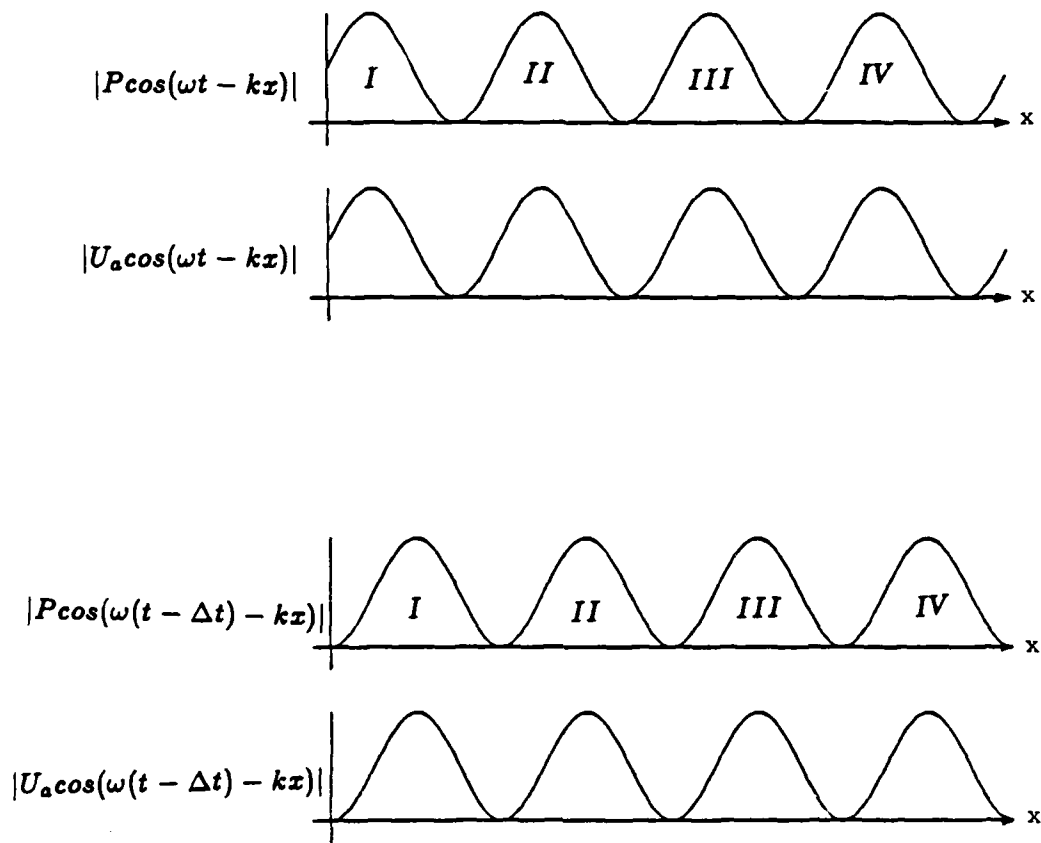


Figure 4.1 The magnitude of the pressure and velocity as a function of distance in the direction of a propagating plane wave at times t and $t + \Delta t$. ($\Delta t = \frac{T}{8}$) The wave packets I, II, III, and IV are labeled so that their progress can be followed.

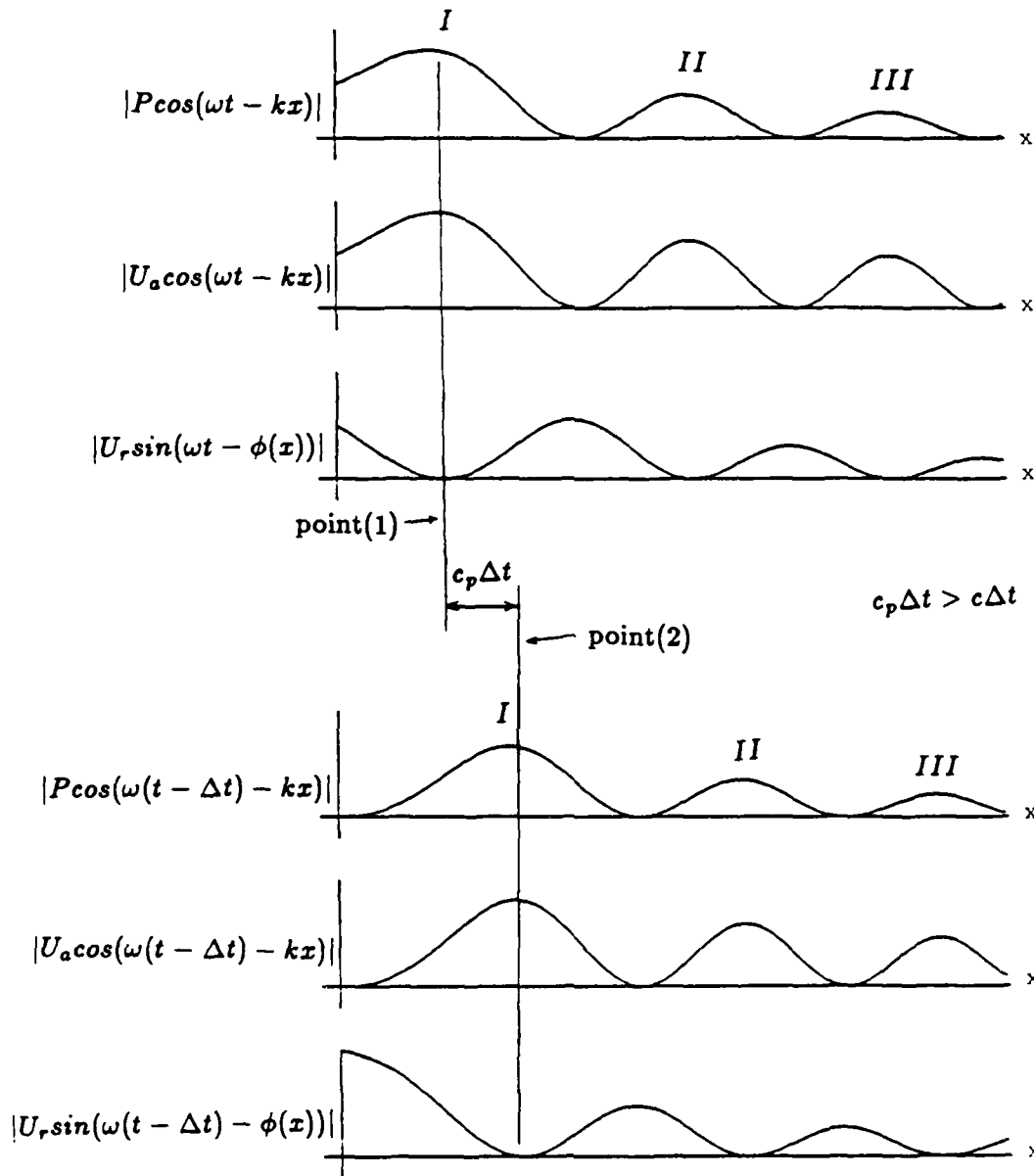


Figure 4.2 The magnitude of the pressure and the velocities \bar{U}_a and \bar{U}_r as a function of distance in the direction of a propagating wave, where the pressure amplitude decreases in the propagation direction and $c_p \neq c$, at times t and $t + \Delta t$. ($\Delta t = \frac{T}{8}$) The wave packets I, II, and III are labeled so that their progress can be followed.

energy propagation, c . The wave fronts are points of reference on a wave form. Only in special cases where $U_r = 0$ is the propagation characteristics of the wave front the same as the energy propagation.

4.2.1. Group Velocity

The group velocity was devised to quantify the speed of energy propagation through a region of space. This is a deceiving concept because it has already been stated that energy propagates at speed c in the direction of the instantaneous intensity. However, we have seen with the instantaneous energy paths that energy does not propagate over a single path for all times during one period. Thus a global description of energy propagation is in order.

The acoustic wave guide is the best example of the intent of group velocity. In an acoustic wave guide; i.e., a duct, the propagation speed of wave fronts, c_p , can be greater than the speed of sound. However, the active intensity does not include all of the energy flux in the duct since there is reactive intensity. Incorporating the energy propagation described by the reactive intensity results in the speed of energy propagation down the duct which is less than c . Thus the group velocity is defined in terms of the speed at which energy at one cross section of the duct propagates to another cross section down the duct.

There are several derivations of the group velocity (Lamb, 1904; Biot, 1957; Whitham, 1961; Jackson, 1975). However, a basic assumption of all the derivations specifies the farfield and time averages for mathematical ease. The conceptual issue is the validity of describing a time varying process of energy propagation with a time independent quantity. Presently, we are only able to quantify the effect of the time dependent process of energy propagation, but cannot conveniently or meaningfully describe the time dependent energy propagation itself.

The actual path of energy propagation are themselves open for interpretation and in fact there is not a single path, Section 2.5. Consequently, investigations of energy flow with the instantaneous intensity is not practical and may lack precise meaning. The group velocity is a compromise and is a means to quantify the idea of energy propagation; however, direction cannot be attached to the group velocity as we cannot attach direction of the energy propagation with the active intensity vector.

4.3. Reactive Intensity: A Practical Viewpoint

The reactive intensity has received little attention in the literature and is generally ignored since its contribution to the time average of the instantaneous intensity is zero at a given point. However, as emphasized in Chapters 3 and 4 the vector does have physical significance and thus helps characterize the acoustic field.

One refreshing article was published by Wolfgang Schmidt (1985), in which he used the intensity analysis in the nearfield of rotating machinery. The interesting aspect of his analysis was that he recognized that the component of the particle velocity in phase quadrature with the pressure is dominant in the nearfield of an acoustic source. Thus by electronically shifting the measured velocity signal 90 degrees Schmidt was able to measure the reactive intensity to characterize faulty equipment.

Indeed in the nearfield the reactive intensity dominates the active intensity, often by 10 to 15 dB. Thus a significant part of the acoustic energy in the nearfield is described by the reactive intensity. Let us revert for a minute to a pure standing wave with a maximum SPL= 140 dB. The active intensity will be zero so there is no net energy flux, which in a viewpoint of noise control is

a desirable result; however, a person in such an acoustic field will risk serious hearing loss if exposed for substantial periods of time.

Consequently, if we wish to take a noise control engineering approach to a noise source we can say that we are interested in the sound which a person is exposed to, which we need to somehow quantify. If the person is in the farfield of a source, then the power output of a source is a valid description of the acoustic energy to which the individual will be exposed. However, if an individual is situated in the nearfield of the acoustic source then the energy which is described by the reactive intensity can be significant if not dominant. Thus quantifying the source radiation by the active intensity alone is an inadequate characterization of the energy to which an individual is exposed in the nearfield of a source.

4.4. Active Intensity Vortex

The active intensity vortex has had a dubious rule in the development of intensity over the past 20 years. The active intensity vortex is a region where the active intensity vectors form a vortex pattern which is commonly seen in fluid flow. In 1964, Schultz, Smith and Malme made some measurements in which they concluded that the active intensity was forming circular paths. In a paper published in June 1975 where they revealed this conclusion, they frankly said that these were results they "did not have the nerve to present at that time, because they did not make sense." Since then there have been numerous authors who have presented evidence and explanations for the vortex (Kristiansen 1981; Elko 1984; Tichy and Mann 1985; Waterhouse, Crighton, and Ffowcs-Williams 1987; Waterhouse 1987; Mann, Tichy, and Romano, 1987).

Understanding the vortex has been a pivotal issue in much of the work presented in this thesis. The vortex developed into an interesting conversation piece because it presented a strong case against conventional views of the active

intensity representing total power flow. Such a perspective says that the energy in the vortex is circulating around the center point, thus representing energy which is locally trapped in a region of space. This concept was indeed puzzling and required an understanding of the intensity vector which was not readily available in the literature.

4.4.1. The Conditions for the Vortex Formation

The existence of the vortex pattern comes about because the curl of the active intensity vector is non-zero. This allows the pattern to be formed by the \vec{I} vector. Before addressing the issue of energy flux, let us use the wave structure interpretation detailed in Chapter 3 to explain the vortex.

The configuration of three point sources will be used for computational ease. The sources are in a straight line with 18 cm spacing and with relative amplitudes of +1, -1 and +1. The randomly chosen, frequency of 2070 Hz is used. Figure 4.3 is the active intensity superimposed with wave fronts of equal phase separation. There are two regions where the wave fronts intersect. The left region is enlarged in Figure 4.4 along with the reactive intensity. This region will be explored in detail.

There are two points in the vortex region that are of special significance: the vortex center and the saddle point. The reactive intensity points into the center of the vortex, meaning there is a pressure minimum at the center. In Figure 4.5 various quantities are plotted along a line passing through the saddle point and vortex center. The potential energy, active intensity, and reactive intensity are zero at the vortex center. However neither the curl of \vec{I} or the kinetic energy are zero or a maximum at the center.

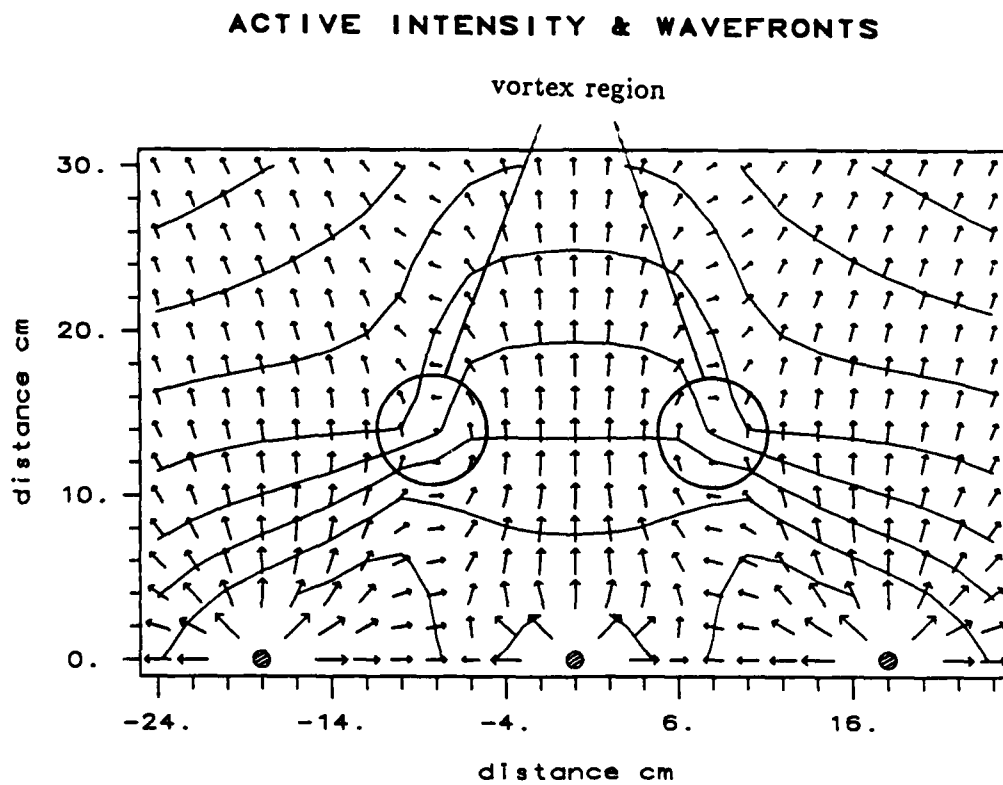


Figure 4.3 The calculated active intensity and wave fronts above three point sources separated by 18cm at 2070Hz with the center source out of phase. The vortex region is circled.

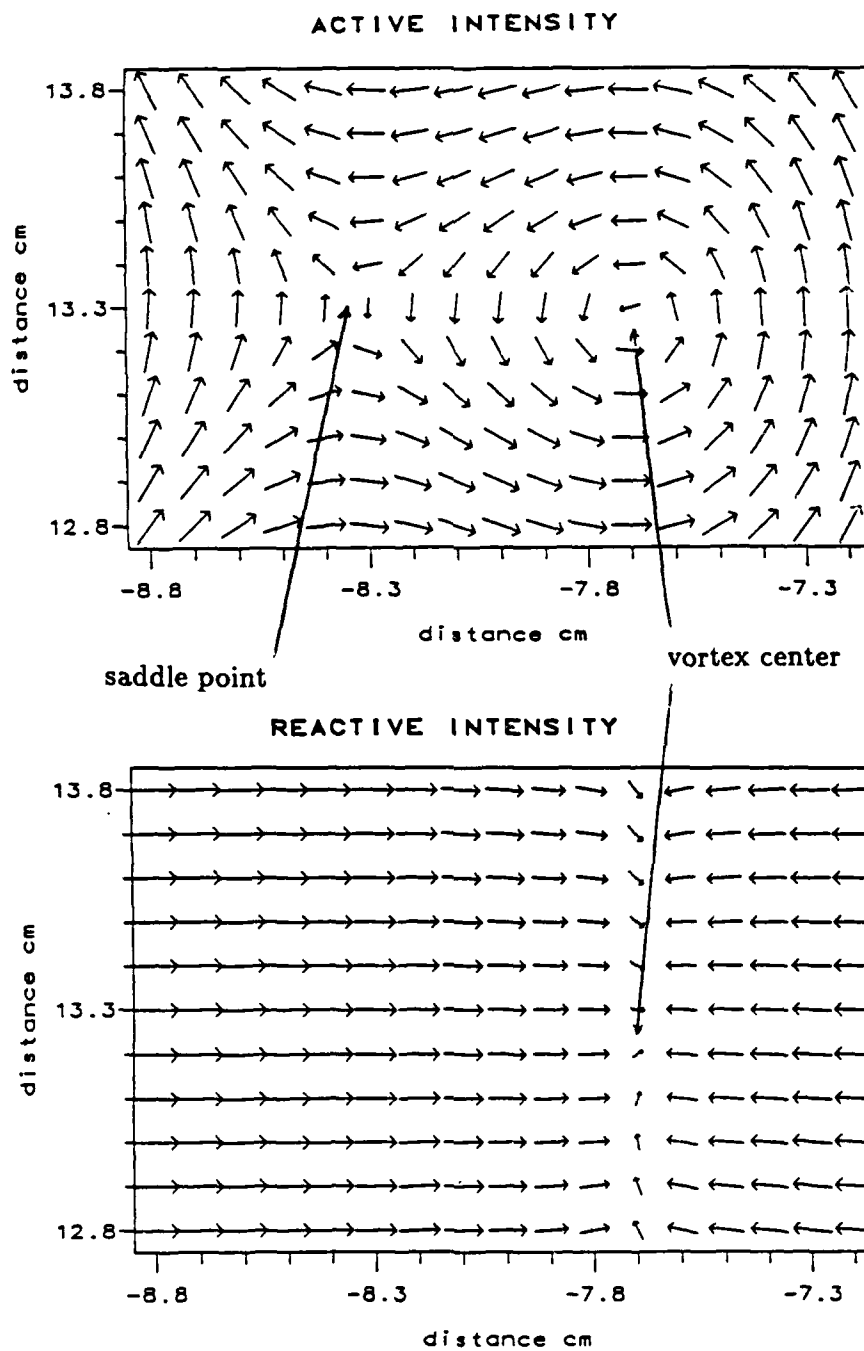


Figure 4.4 The calculated active intensity and reactive intensity in a vortex region for three point sources separated by 18cm at 2070Hz with the center source out of phase.

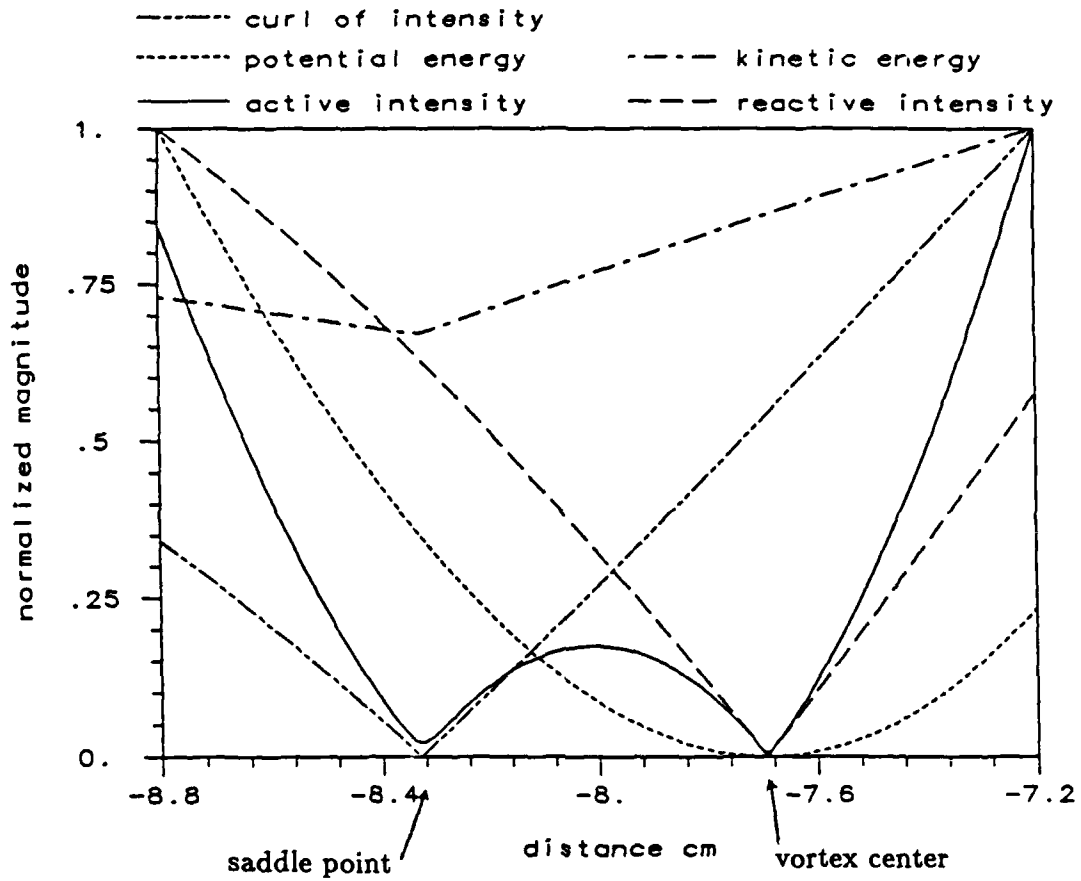


Figure 4.5 The scaled magnitude of active intensity, reactive intensity, potential energy, kinetic energy, and curl of the active intensity along a line through the saddle point and vortex center.

At the saddle point the curl of \vec{I} is zero. The saddle point is always present in a vortex region because it is the point where the circular pattern of the vortex is isolated from the rest of the acoustic field.

The most interesting quantities are the particle velocity and pressure phase. As already stated, the total kinetic energy has no significant properties in the vortex region; however, the two components U_a and U_r provide an interesting clue. At the saddle point $U_a = 0$ since $\vec{I} = 0$. Figure 4.6 is a close up of U_a and U_r around the vortex center. The relative magnitude normalized to the maximum of each quantity is plotted so that both quantities could be represented together. At the vortex center U_r has a relative minimum and U_a has a relative maximum. The peak in U_a has special significance. Since there cannot be an infinite amount of energy at a point, U_a has a finite limit at the center, call it κ . Now solve for $\nabla\phi$ in the equation for U_a , Equation (2.6):

$$|\nabla\phi| = \omega\rho\frac{|\vec{U}_a|}{P} = \omega\rho\frac{\kappa}{P} . \quad (4.1)$$

However at the vortex center $P = 0$; consequently at the vortex center

$$\nabla\phi \rightarrow \infty . \quad (4.2)$$

The spatial phase gradient is plotted in Figure 4.7. The resolution of the plot is sufficient to see that $\nabla\phi$ is going to infinity. This means that the pressure phase is discontinuous at the vortex center. However, it is true that $p(r, t)$ is smooth and continuous through the vortex center, goes to zero at the discontinuity; and is positive on one side of the zero and negative on the other. This is also observed in plane waves at nodal points where the physical quantities p and \vec{u} are continuous but the phase is discontinuous by $\frac{\pi}{2}$.

The phase discontinuity explains the vortex pattern and represents the condition for the formation of a vortex. In general, a phase discontinuity occurs

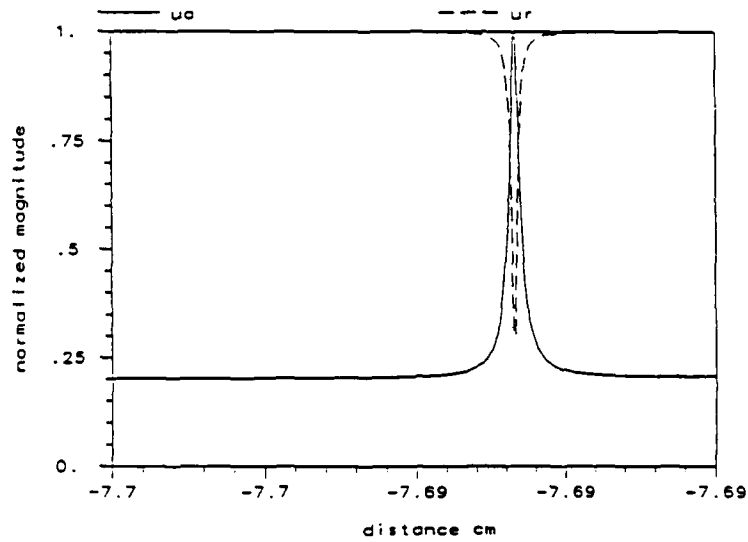


Figure 4.6 The scaled magnitude of \bar{U}_a and \bar{U}_r , at the vortex center.

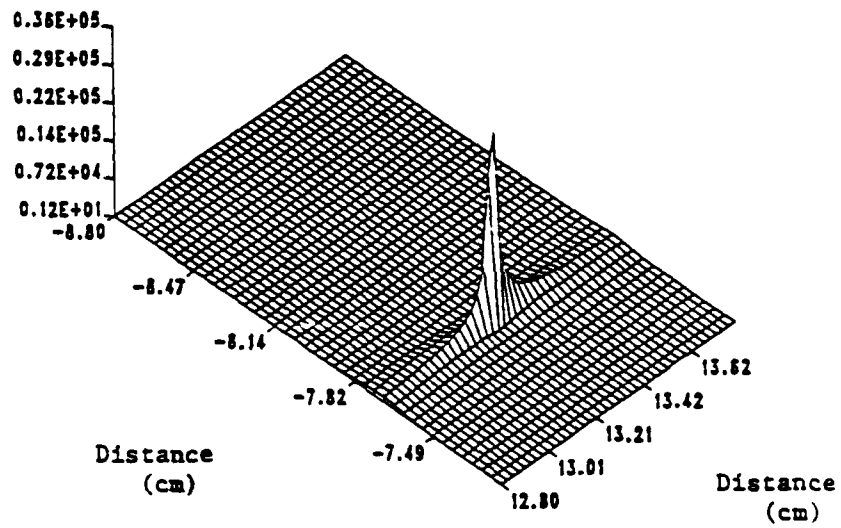


Figure 4.7 The magnitude of the pressure phase gradient, $|\nabla\phi|$, in the vortex region.

at the intersection of different surfaces of constant phase. Such intersections can occur along a line, or at a point, so that the phase discontinuities, and thereby the vorticities, must be on a line or at a point.

There are many examples of phase discontinuities. Let us first consider a dipole. On the plane between the two sources the pressure is zero and the phase is discontinuous. The surfaces of constant phase must be perpendicular to this plane of zero pressure which means that the active intensity must be parallel to the dividing plane. Consequently, a phase discontinuity which forms a plane will not produce a vortex pattern.

Now consider the case when the pressure phase is discontinuous on a line. (This is also a pressure null line.) The different surfaces of constant phase will extend radially from the pressure null line. The same will occur if the phase is discontinuous at a point. Since the active intensity is perpendicular to the wave fronts the active intensity will form a circular pattern, a vortex, around the line or point of phase discontinuity. Clearly, the vortex physically represents a resultant wave travelling around a phase discontinuity only when the phase discontinuity (also where the pressure is zero) is a line or a point.

This description of the vortex is consistent with the wave front interpretation in Chapter 3 and is in essence the observation made by Kristiansen (1981). The discontinuity could have been implied by constructing wave fronts from the active intensity. Connected with the wave fronts is the phase speed which is presented in Figure 4.8. This shows that the speed of the wave fronts increases with distance from the vortex center. Also there are regions where the waves progress slowly and others where they propagate very quickly.

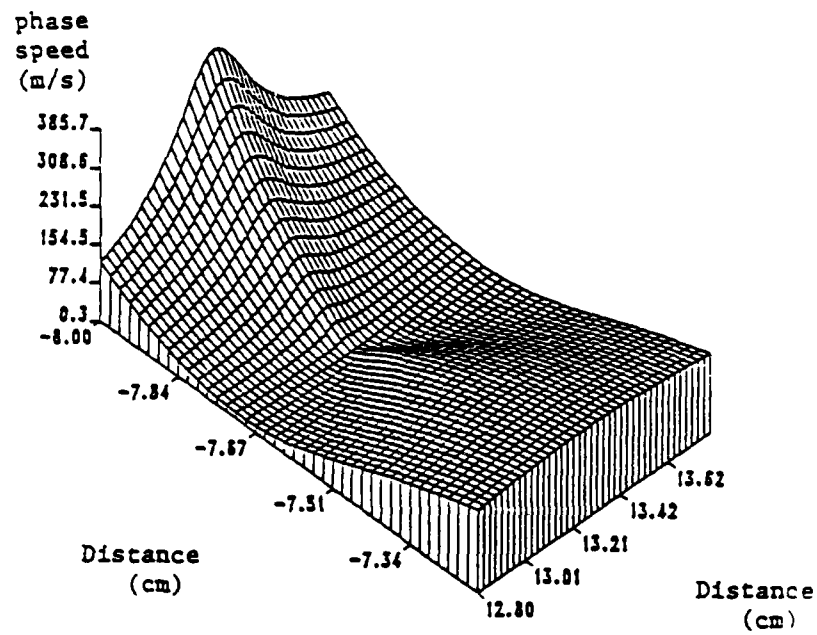


Figure 4.8 The phase speed, c_p , around the vortex center.

4.4.2. Energy Flux in the Vortex

Having resolved the meaning of the vortex formation, the more significant issue is the energy flux in the vortex. Statements have been made that the energy in the vortex arrives during the transient build up of the vortex, and thus flows in closed paths until the sound sources are turned off and the field decays (Kristiansen 1981; Waterhouse, Crighton, and Ffowcs-Williams 1987; Waterhouse 1987). Such interpretations are in direct conflict with the concepts of energy transfer presented in Chapter 2.

The transient build up of the vortex can be investigated by considering the time dependent pressure and particle velocity. The transient response is incorporated by considering the contribution of each point source only after the first wave front from each source has reached the point where the pressure and velocity are being calculated (Junger, 1966). This is expressed by including the unit step function in the summation such that from the time the sources are turned on until the wave traveling at speed c reaches a point the contribution to the pressure and velocity is zero:

$$\underline{p}(r, t) = \underline{p}_1(r, t)H(ct - r_1) + \underline{p}_2(r, t)H(ct - r_2) + \underline{p}_3(r, t)H(ct - r_3) \quad , \quad (4.3)$$

$$\underline{u}(r, t) = \underline{u}_1(r, t)H(ct - r_1) + \underline{u}_2(r, t)H(ct - r_2) + \underline{u}_3(r, t)H(ct - r_3) \quad . \quad (4.4)$$

The instantaneous intensity can subsequently be calculated. Let us look at the part of the instantaneous intensity containing the active intensity, $\vec{I}(r) \cos^2(\omega t - \phi)$. Figure 4.9 contains plots of this term for equal increments of time.

In Figure 4.9(a) the waves from the two closest sources have already arrived in the region of the vortex. At the lower right corner of Figure 4.9(b) the contribution from the third source is seen. The following plots show the progression of the wave through the region. It is important to notice that once

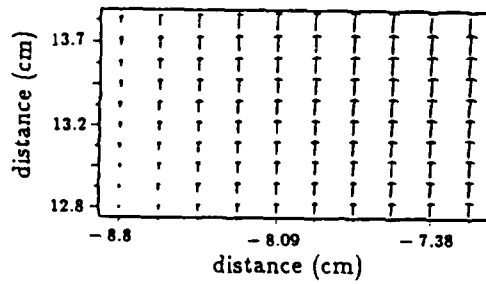
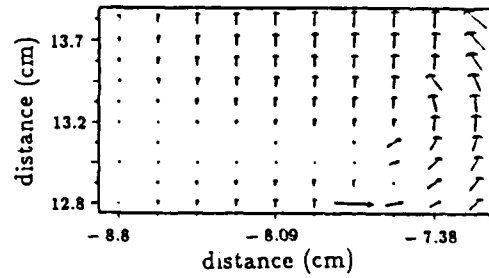
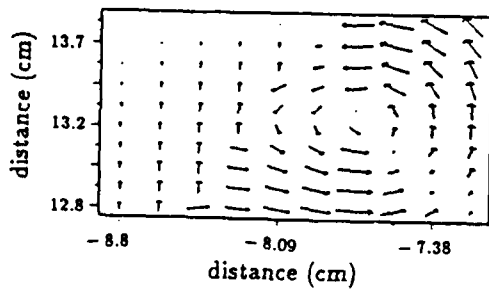
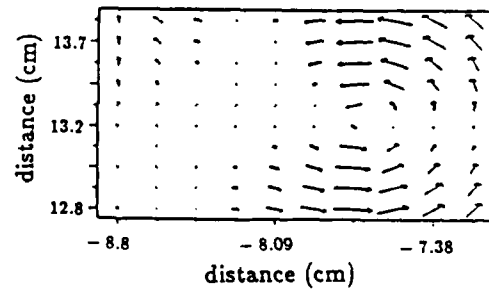
a) $t = t_0$ b) $t = t_0 + 0.038T$ c) $t = t_0 + 0.076T$ d) $t = t_0 + 0.114T$

Figure 4.9 The contribution of the active intensity to the instantaneous intensity during the vortex buildup. The time increment is $0.038T$.

the third wave arrives at a point the orientation of the active intensity vector is in the pattern of the vortex. There is no transient trapping of the energy in the vortex.

A more convincing argument is to view the instantaneous intensity in the steady state condition. Figure 4.10 is a sequence of snapshots over one cycle of the instantaneous intensity in the vortex region at equal time increments. These plots bear no resemblance to the vortex pattern, because the reactive intensity has a significant contribution to the energy transport.

The transfer of energy can also be described by the instantaneous flux paths which were described in Chapter 2. These are drawn in Figure 4.11. Figure 4.11(a) is the region of the vortex and Figure 4.11(b) is an expanded view which follows paths for more than one cycle. The seven starting positions are circled, and two times in one period are chosen to follow the energy. Figure 4.11(a) clearly shows paths which do not resemble the vortex, in fact all the paths leave the plotted region. Figure 4.11(b) shows that the paths leaving the vortex region continue and never return. Consequently energy is not trapped in the vortex.

Another argument against the belief of energy being trapped in the vortex was made by Romano (1986). Romano's argument is based on the interpretation of the acoustic field being the superposition of energy contribution from in this case the three sources. Following through this argument in turn concludes that energy is not trapped in the vortex.

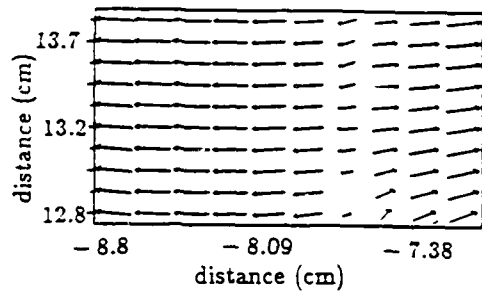
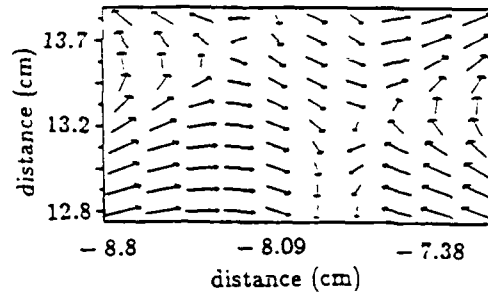
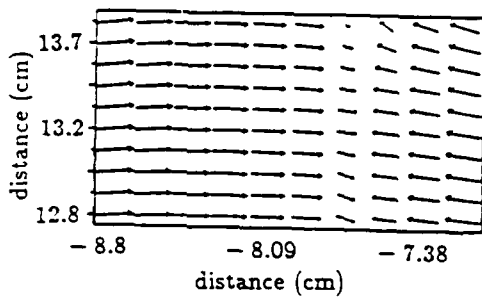
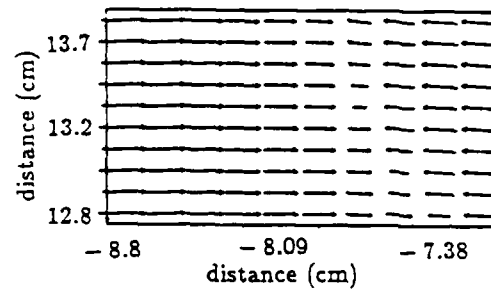
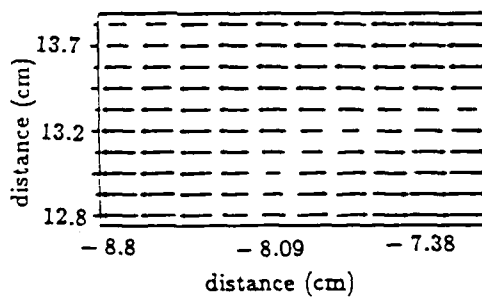
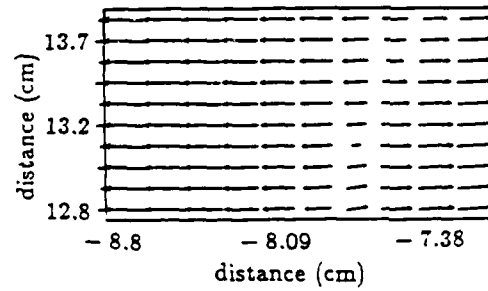
a) $t = t_0$ b) $t = t_0 + \frac{T}{12}$ c) $t = t_0 + \frac{T}{6}$ d) $t = t_0 + \frac{3T}{12}$ e) $t = t_0 + \frac{T}{3}$ f) $t = t_0 + \frac{5T}{12}$

Figure 4.10 Snapshots of the instantaneous intensity in the vortex region for one complete cycle of the energy ($\frac{T}{2}$). The time increment is $\frac{T}{12}$.

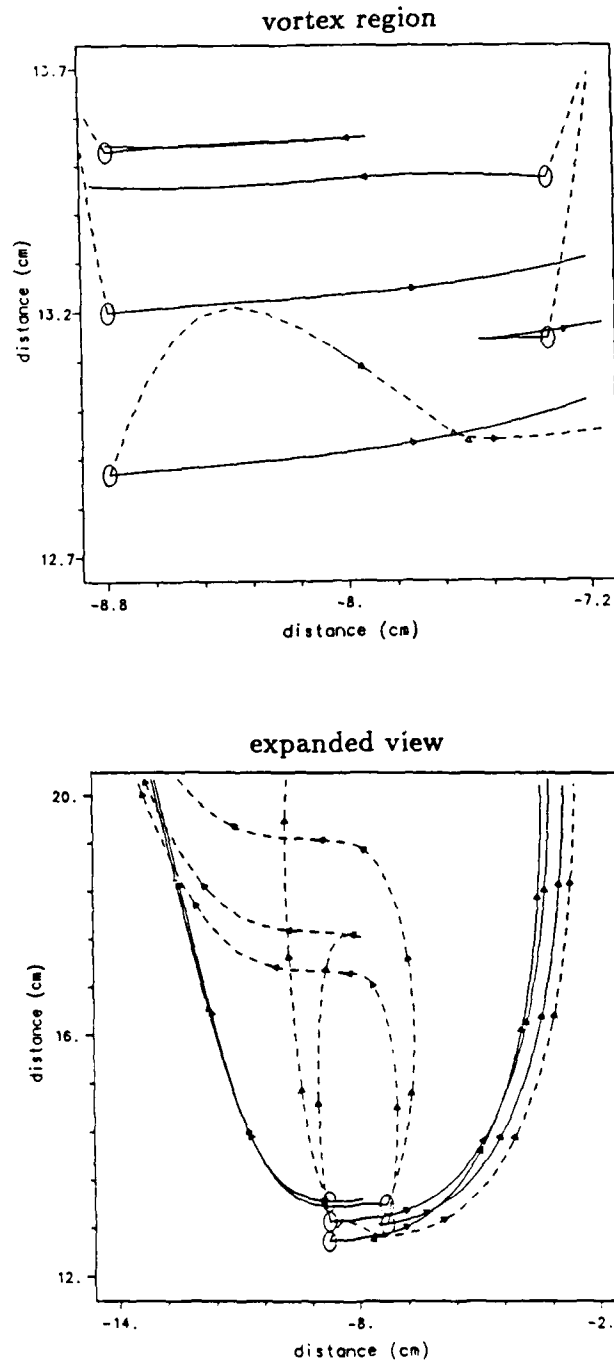


Figure 4.11 Instantaneous intensity flux lines beginning in the vortex region. Two lines start at each point at times t_0 and $t_0 + .3T$. The top plot is in the vortex region and the bottom plot is an expanded view of the same lines leaving the vortex region.

Chapter 5

EXPERIMENTAL PROCEDURE AND DATA PROCESSING

5.1. Introduction

This chapter discusses the experimental facilities and the processing of the measured data. The emphasis of this thesis is understanding and interpreting acoustic intensity; consequently, there was little development of the measurement procedures beyond the available instrumentation.

5.2. Experimental Facilities

The experimental facilities used were developed by Gary Elko and described in his dissertation (1984). The system is controlled by a PDP11/34 computer, fully automating the measurement procedure. The data are transferred to a VAX 780 computer for phase and impedance calculations, plotting, and permanent storage on magnetic tape.

The measurements are performed in a 2.36m by 1.51m by 1.89m room with hard walls. After installing foam wedges to make the room anechoic the available uninterrupted interior space is 1.4m by 0.85m by 1.6m. The wedges provide an anechoic environment to the lowest frequency of 300Hz, which establishes the lower limit for measurements requiring an anechoic environment. A three-dimensional motion system installed in the room moves the intensity probe to any position within the room. The motion system is controlled by the PDP11/34 computer through a RS232 serial communication line.

The intensity probe consisted of four B&K $\frac{1}{4}$ inch pressure microphones. The four microphones are grouped in two pairs. Each pair of microphones measure the velocity in a given direction. The two pairs are orientated so that they

measure perpendicular components of the particle velocity. The minimum center to center spacing of the microphones is 17mm. This establishes the upper limit of the measurement system at 4500Hz for the microphone spacing to be within about 2 percent of the acoustic wavelength.

The two microphone pairs were phase calibrated using the modified switching technique in a free field as outlined by Elko (1984). This gave a corrected phase with the accuracy less than 0.1 degrees, which is a conservative estimate. The phase shift introduced by the microphone cartridge was compensated for in the calculation of the cross-spectrum. The shift was a constant time delay so the frequency shift was linear. The calibration curves were fitted with a least squares algorithm to the form $Af + B$, making it easy in the data processing to calculate the phase mismatch at each frequency. An example of the phase calibration is given in Figure 5.1.

The microphone signals are amplified 50dB to 70dB so that the signals are well within the dynamic range of the A/D converter. The four pressure signals are then passed through anti-aliasing filters with a 48dB per octave roll off. The amplified and filtered signals are input to the A/D converter in the PDP11/34 computer. The PDP digitally sample the four signals and using an array processor calculates the 1024 point FFT's and the 512 point auto-spectra and cross-spectra. The intensity vectors, energy densities, and the bias errors are calculated from the spectra of the two microphone pairs. The spectrum analysis is detailed in Elko's dissertation.

The PDP fully automates the measurement process by moving the microphone probe to specified positions in the chamber and acquiring data. The process takes about three and a half hours for 300 data points when a single frequency is being used. Often measurements were made around an obstacle in the scanning plane. For such cases the measurement was performed in separate

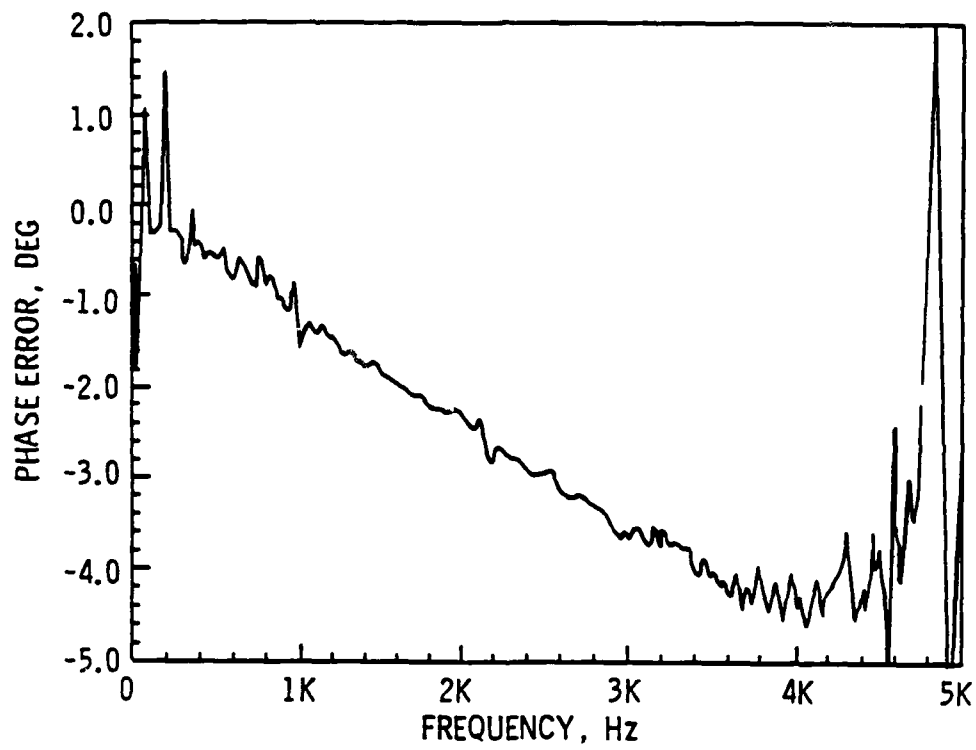


Figure 5.1 An example of a calibration spectrum for the phase mismatch of a microphone pair. The free field modified switching technique is used.

segments which followed the contour of the obstacle. The data files from the segments were subsequently combined so that the the entire field around the obstacle was represented.

Measurements were performed at single frequencies. To speed up some measurements multiple frequencies were input to the source; however, at frequencies far apart. Broad band signals were avoided because of the long averaging time needed for adequate accuracy. Broad band signals also produce difficulties because there are low signal levels at desired frequencies bands since the energy is spread over a large frequency range.

Many measurements can be performed on a symmetric plane so that the intensity components are only within the plane. For these cases the two dimensional four microphone probe is ideal. When the intensity is three dimensional the measurements are made with the probe in one orientation, first measuring, for instance, the x and y components, then the probe is rotated 90 degrees, now measuring, for instance, the y and z components. The data are then combined and the common measured component is compared to monitor the accuracy of the measurement. The two probe orientations are measured in separate scans, so it is crucial to guarantee that the measurement positions are accurately repeated. There have been some probe configurations developed to measure three components simultaneously; however, these are prone to diffraction errors and for mechanical reasons the scan cannot be made close to surfaces. The method of two probe orientations has been accurate and measurements can be made within 2.5cm of a surface.

5.3. Plotting Symbols

The representation of the intensity and energy quantities is consistent with conventional representations. The active and reactive intensity are represented

by arrows pointing in the direction of the intensity vector. The potential energy is represented by circles. The kinetic energy is represented by parallelograms which display the two spatial components of the kinetic energy by varying the height and width of the parallelogram. The center of each symbol is centered at the measurement points. The intensity vectors are often drawn with the base at the measurement point, but we have found centering the vector at the measurement point provides the best graphic dynamic range. The symbols are scaled in dB to the maximum value in the plotted area with a 30dB dynamic plotting range. The maximum value is indicated on the top of the plot. The dB value of each quantity is given as a numeric value representing the dB level below the maximum value.

Measurements are also presented for three-dimensional regions. In these plots, the in plane components of the intensity vector are represented by the direction of the arrow, and the out-of-plane component is represented by the thickness of each arrow. The thickness is scaled to $\frac{1}{2}$ the actual out of plane value. The arrow is solid when pointing out of the paper and empty when pointing into the paper.

5.4. Data Processing

During the measurements the active intensity, reactive intensity, potential energy, kinetic energy and bias errors are calculated. The phase distribution, resultant phase speed, and specific acoustic impedance are calculated once the data are transferred to the VAX. The calculation of the resultant phase speed and specific acoustic impedance is straight forward; however, the pressure phase calculation will be explained here.

5.4.1. Calculation of the Pressure Phase

As shown in Chapter 2 the active intensity is proportional to the pressure squared times the gradient of the pressure phase. Thus the gradient of the

pressure phase can be calculated as follows from the active intensity and potential energy:

$$\nabla\phi = \frac{\omega}{2c^2} \frac{\bar{I}}{V} \quad (5.1)$$

From the gradient over a grid of points numerical integration can be used to calculate the pressure phase (Imaich and Ohmi 1983). Surfaces of constant phase can then be plotted at equal phase increments so the wave front shapes and propagation characteristics can be effectively visualized.

The gradient is spatially integrated using the trapezoidal rule. A schematic of the procedure is presented in Figure 5.2. The integration begins at the center to minimize accumulative errors. Lines extending vertically and horizontally from the center, labeled I, II, III, and IV, are the first integration paths. From these four lines the other points are approached along two paths, as indicated by two arrows pointing to each point. The two values obtained from each path are averaged for the phase at that point. The procedure continues for all the points resulting in a phase distribution referenced to zero at the center of the grid.

Measurement areas containing obstacles, require segmentation of the integration region. The areas must be segmented such that no point is reached by integrating through an unmeasured area. This also means shifting the origin of integration. The sections are then integrated separately, but referenced to one section so the phase is continuous through the entire plot. Figure 5.3 gives an example of the segmentation, origin relocation, and connection scheme.

The phase resulting from this process is in radians referenced to some arbitrary zero phase, which is unrelated to the source phase. However, if desired the data can be referenced to the source by a quick measurement of the phase between the pressure at the source and one point in the measurement region. Since the data is in radians, the wave fronts, lines of constant phase, can be

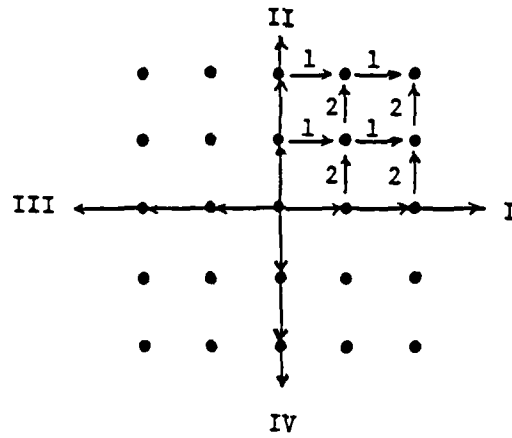


Figure 5.2 A schematic of the integration paths used to reconstruct the pressure phase from the measured data.

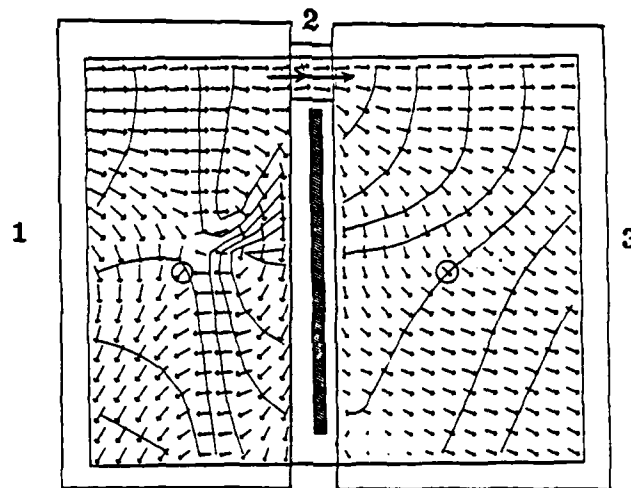


Figure 5.3 A schematic of the segmentation (labeled 1,2,3), origin relocation (circled), and connection paths (arrows) for the reconstruction of the pressure phase around an obstacle in a measurement plane.

drawn a fraction of cycle apart. This is convenient since the resultant local wavelength can be visually related to the free field wavelength ($\lambda = \frac{c}{f}$)

5.4.2. Specific Acoustic Impedance

The specific acoustic impedance is intrinsic in concepts of acoustic fields. It is a complex function defined by the ratio of the pressure and particle velocity. Lahti (1985) develops the impedance directly in terms of the auto-spectra and cross-spectrum of two microphone signals. However, it is convenient to express the impedance in terms of the active and reactive intensity since the spectra may not be directly available. The impedance is a scalar, but it can be calculated from the particle velocity in a given direction. For instance, it is usually desired to calculate the impedance normal to a particular radiating surface. Consequently, the complex specific acoustic impedance, Z_n , in the direction of the unit vector \hat{n} is

$$\begin{aligned} Z_n &= \frac{p}{\hat{n} \cdot \vec{u}} = \frac{P e^{-j\phi}}{\hat{n} \cdot (\vec{U}_a + j\vec{U}_r) e^{-j\phi}} = \frac{\rho}{4} \frac{\hat{n} \cdot (P\vec{U}_a - jP\vec{U}_r)}{T_n} \\ &= \frac{\rho}{2} \frac{\hat{n} \cdot \vec{I} + j\hat{n} \cdot \vec{Q}}{T_n}, \end{aligned} \quad (5.2)$$

where T_n is the kinetic energy due to the velocity in the direction \hat{n} . The specific acoustic impedance can be measured at any point; however, the impedance has significant meaning at boundaries, because of sources and sinks of energy. Thus measuring the impedance around acoustic sources and diffraction boundaries is a useful analysis tool. The measurements presented in Chapters 6 and 7 will clearly show some examples of the specific impedance measured at boundaries.

There are some examples in the literature of using the specific acoustic impedance. They are geared toward general absorption characteristics of materials. However in this thesis a point by point analysis of the specific acoustic impedance will be made.

Chapter 6

EXPERIMENTAL ANALYSIS OF SOURCE-RESONATOR INTERACTIONS AND A SIMPLE SOURCE

6.1. Introduction

This chapter focuses on analysis of source and resonator interactions using the acoustic intensity measurement technique. Machines, other noise producing mechanisms, and transducers which are designed to radiate sound can be classified as a combination of sources with significant structural vibration and cavities which resonate and absorb energy. For much of the analysis, the active and reactive intensity is qualitatively used to visualize the wave front propagation and pressure amplitude distribution. The real and imaginary parts of the specific impedance show in detail the sources and absorbers and distinguishes between them.

This chapter also compares the measured radiation impedance and radiated power of a simple source as a function of the source height above a rigid boundary. These measurements show that measurement errors are introduced by signal processing equipment inaccuracies besides phase the mismatch of the signal processing channels.

6.2. Two In Phase Piston Sources Surrounding a Resonating Tube

The first example is a configuration sketched in Figure 6.1. There are two in phase piston sources in a baffle with a closed ended tube between them. The tube is tuned to a one quarter wavelength resonance of 200 Hz. The outer sources are separated by 36cm, center to center.

This configuration was devised to be compared with the case of three point sources with the center source driven out of phase of the outer sources, which was discussed in Section 2.5.1. At 200Hz, Figure 2.4, the active intensity is pointing

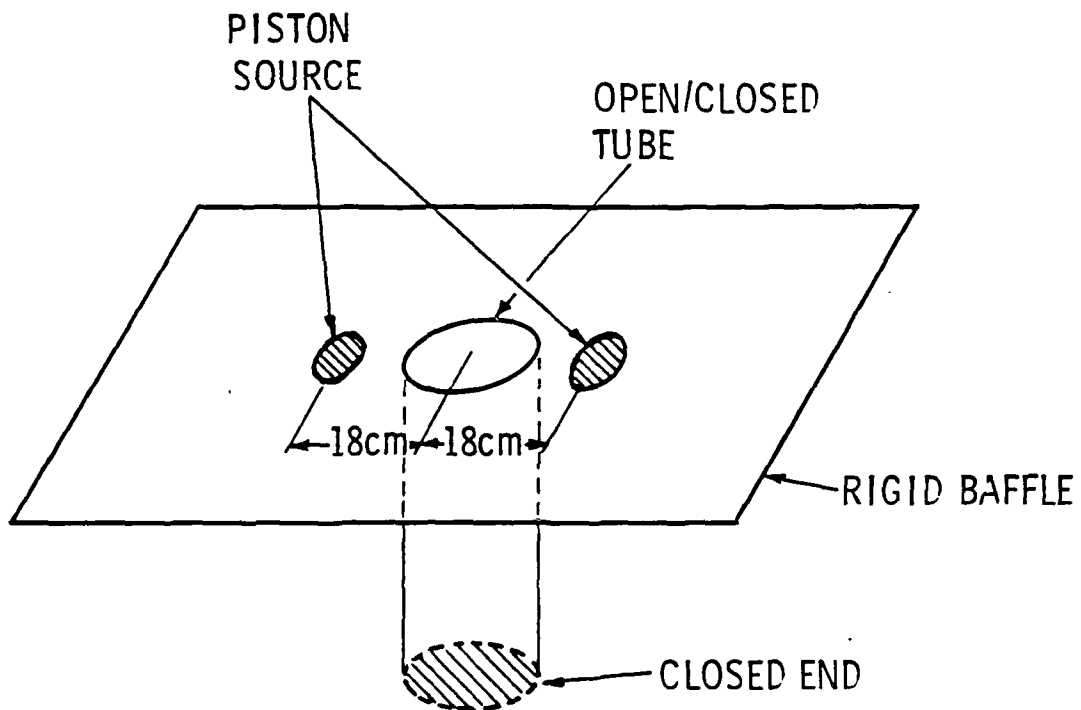


Figure 6.1 The measurement configuration of two baffled pistons with a resonating tube tuned to a one-quarter wavelength resonance of 200Hz.

into the center source, indicating that it is absorbing power. However, the reactive intensity is pointing out of all three sources because there is a pressure maximum above each point of vibration. Consequently, to locate these three sources the reactive intensity must be used. The source localization capabilities of the reactive intensity are shown very clearly by Degeorges and Tichy (1986).

The two source and tuned resonator configuration was intended to mirror the situation with the three sources when the center source appeared to be absorbing power. In this case, we have a resonator playing the role of a power absorber. Intuitively we can say that at the resonant frequency of the tube, the impedance of the tube will be very low so the tube will absorb energy. However, at an anti-resonant frequency the impedance will be very high at the tube opening, so that the energy will propagate to the farfield. Consequently, the analysis is confined to the first two resonant frequencies, 200Hz and 600Hz, and to an anti-resonance, 400Hz.

The measurements were made over two planes for each frequency. Measurements were conducted in a vertical plane along the symmetric cross section of the sources and perpendicular to the baffle. Since this plane is symmetric with respect to the sources only the two components of the intensity within the plane needed to be measured. Additional measurements were conducted in a second plane parallel to the baffle and 3cm above the sources. Measurements were made in the vertical plane to investigate the radiation to the farfield and the source interaction, and in the horizontal plane to investigate the characteristics of the sources and the tube and their boundaries with the baffle.

A quick overview of the measured data reveals that the data are acceptably symmetric, as would be expected with the configuration. Looking at the wave fronts we can see that the right source lags the left source by about 3 degrees. The same signal was input into each piston source, but it is within reason for them

not to respond identically. Three degrees is 1% of a cycle which is acceptable. This minor delay accounts for the non symmetry in the active intensity data. A similar bias is seen at all frequencies.

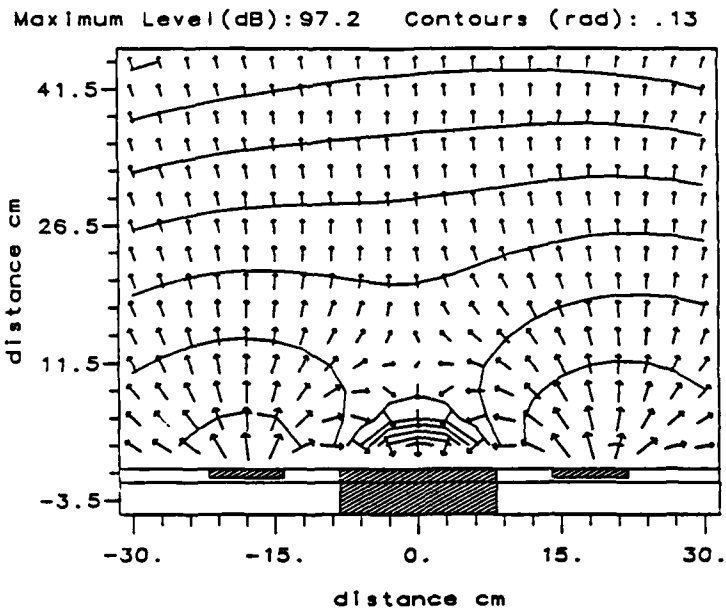
6.2.1. Fundamental Resonance of the Tube

Let us first look in detail at the measurements at 200Hz, Figures 6.2 to 6.6. The active intensity in Figure 6.2 is pointing out of the two sources and into the resonator. The resonator is absorbing power because it effectively dissipates energy. This energy comes from the two sources. At 200Hz the sources are strongly coupled, so a large part of the energy is consumed by the resonant tube. The wave front propagation shows that the waves combine from the two sources and at the point marked by a peak in the phase speed, Figure 6.3 , is split into waves that enter the tube and waves which propagate to the farfield.

The reactive intensity plot shows some fascinating results. These are sensible results, and demonstrate the powerful analysis capabilities of the intensity analysis. The reactive intensity points out of the sources since there is a pressure maximum over each source. However, the reactive intensity points into the resonating tube. Consequently all the energy, even that associated with the reactive intensity is being input to the tube to drive it at resonance.

These results provide a good comparison between power absorbed by a passive source and an active source. In Figure 2.6 the active intensity is directed into the center source, which is driven out of phase of the two outer sources. However, the reactive intensity in Figure 2.6 points out of the active center source because the pressure is a local maximum directly over the source, even though there is a time averaged net flux of energy into the center source. In the case of the resonating tube, Figure 6.2, the pressure at the open end of the tube is a local minimum because of the boundary conditions at resonance, so that the

ACTIVE INTENSITY & WAVEFRONTS



REACTIVE INTENSITY

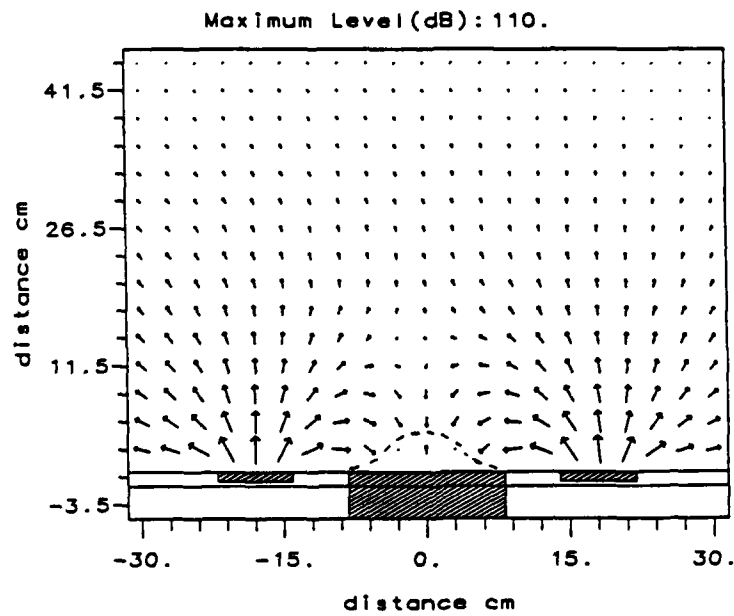
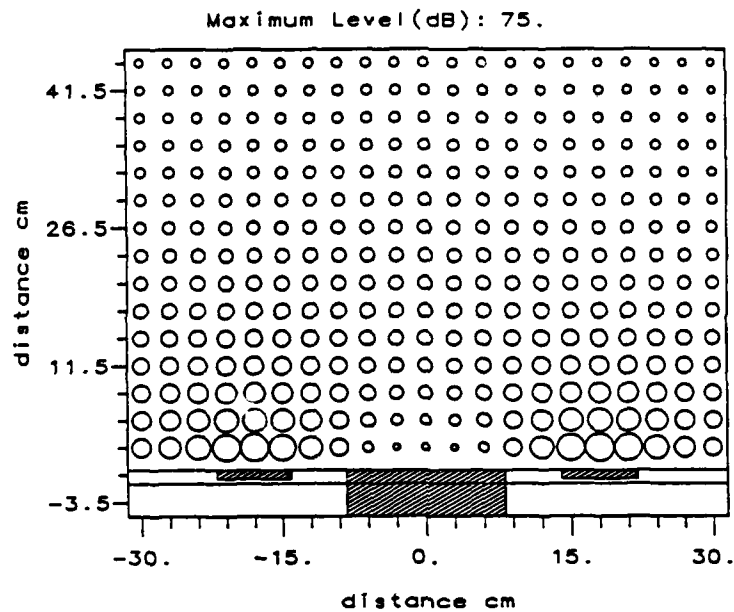


Figure 6.2 The measured active intensity and wave fronts and reactive intensity at 200Hz in a plane perpendicular to the baffled containing two in phase piston sources and a tube with a 200Hz fundamental resonance.

POTENTIAL ENERGY



RESULTANT PHASE SPEED

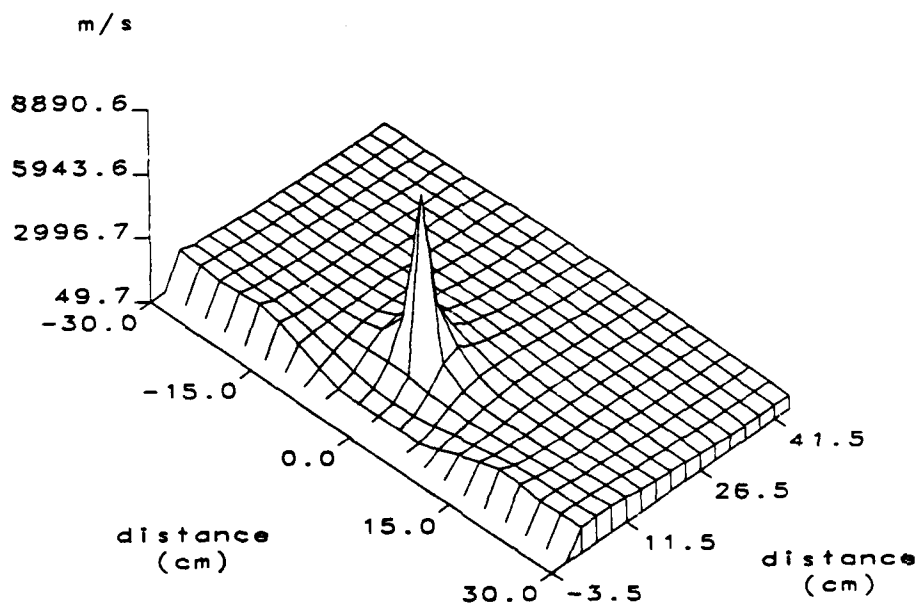
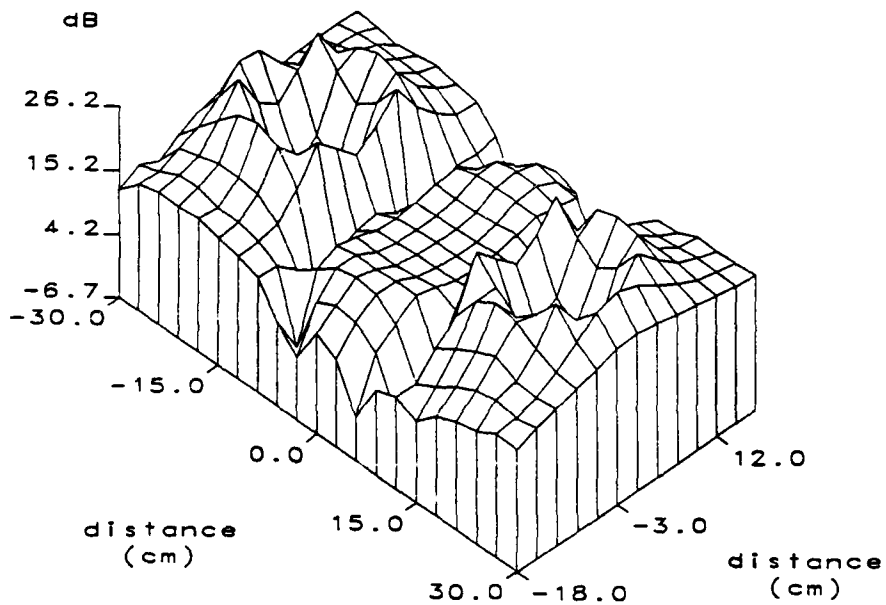


Figure 6.3 The measured potential energy and calculated phase speed at 200Hz in a plane perpendicular to the baffled containing two in phase piston sources and a tube with a 200Hz fundamental resonance.



IMAGINARY NORMAL IMPEDANCE

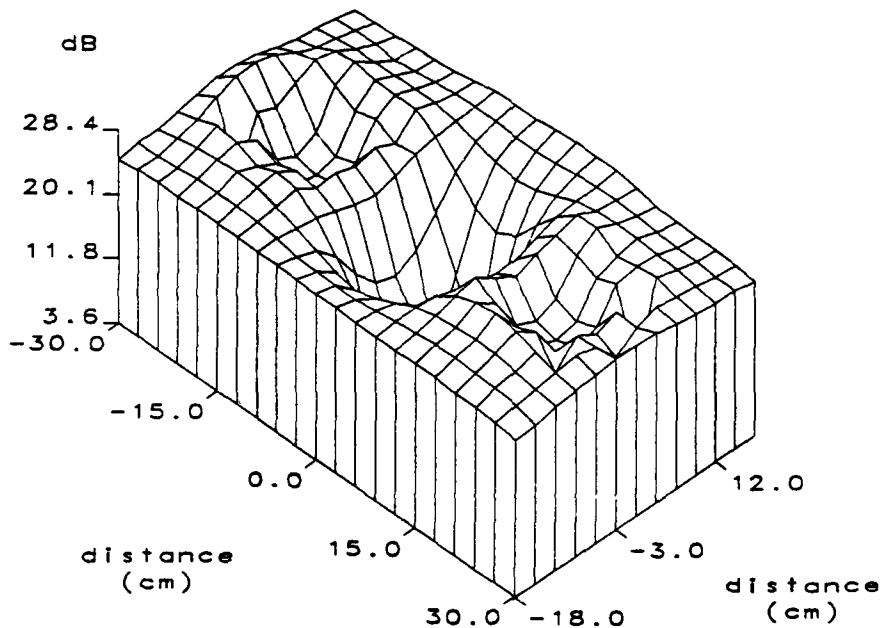


Figure 6.5 The real and imaginary parts of the impedance normal to the baffle at 200Hz. The measurement plane is parallel to and 3cm above the baffle containing two in phase piston sources and a tube with a 200Hz fundamental resonance.

reactive intensity points toward the tube opening. These two examples show that when the active intensity measurements indicate an absorption of power, as in Figures 2.6 and 6.2, the direction of the reactive intensity distinguishes between an active source coupled with other active sources, Figure 2.6, or a passive source absorbing energy to be driven, Figure 6.2.

For the resonance to occur in the tube the pressure is a maximum at the closed end of the tube and zero at the open end of the tube. There are two effects which should be emphasized. First the pressure is a minimum over the tube opening. The pressure is finite, not zero, because there are losses in the tube and the boundary conditions at the tube opening are not exactly pressure release, consequently, there is active intensity pointing into the tube. More interestingly, note that the pressure minimum forms an arc over the tube opening. The arc is best visualized by the reactive intensity. This pressure minimum is not directly at the tube opening, because of the end effects at the tube opening. Fundamental theories show that there is a mass of fluid attached with the air vibrating in the tube. This extends the effective length of the tube beyond its physical length. Consequently, the location of the pressure minimum marks the effective end of the tube.

It is interesting to note that the added mass is not a cylindrical extension of the tube, but has a hemispherical shape, Figure 6.3. Assuming symmetry, which the horizontal plane measurements show, the volume of fluid in this hemisphere is $\frac{2}{3}\pi(.05)^3 = 261\text{cm}^3$. This corresponds to an equivalent cylinder of fluid 1.5cm high. The theoretical end correction for an open tube is 0.84 times the tube radius if flanged and 0.6 times the radius if unflanged, which for this tube is 6.6cm and 4.8cm respectively. In both predictions an end correction much greater than the measurements are implied. Most likely, this is a consequence of the acoustic coupling between the two piston sources and the tube. The coupling alters the

boundary conditions at the tube opening from the ideal pressure release. The sources and tube are acoustically separated by 0.1λ so the tube opening is exposed to a large direct field from the sources, which alters the impedance of the tube opening and thereby reducing the extension of the tube length beyond the end of the tube.

Further support for the added oscillating mass is seen in the kinetic energy plots, Figure 6.4. There is a region above the tube where the kinetic energy is large. However, this is confined to a very close distance above the tube opening, compared to the region above sources which extends much further. The maximum velocity over the tube extends from the edge of the tube in a semi-circle to about 5cm above the tube opening. This is best visualized from the plot of the numeric values.

The next important feature of this measurement is the normal specific acoustic impedance: the real and imaginary parts, Figures 6.5 and 6.6. The measurements made on the plane parallel to the baffle cover the area over the entire surface of the piston sources and the tube opening. The real part of the complex normal impedance has significant minima over the piston sources, corresponding to power radiation. There is also a minimum above the tube because energy is being absorbed. Now looking at the imaginary part there are weak minima over the two piston sources because there is a reactive component associated with their radiation. However, there is a deep minimum directly over the tube. This is expected above a resonator and is graphically shown here. In a later section these results will be further analyzed by comparing them with the results at other frequencies.

A curious feature of the measurement is the large active intensity pointing into the tube opening, Figure 6.2. The kinetic energies associated with the particle velocities U_a and U_r are roughly of the same amplitude in this region.

Since the tube is a resonator one might expect to have a pure standing wave in the tube so that the kinetic energy is all contained in the component due to U_r . Consequently, it is expected that the kinetic energy just above the tube would be dominated by the component due to U_r . However, a more realistic analysis of the field in the tube must include damping from vibration of the tube walls and air gaps. The tube which is being driven at a resonance is an efficient hoarder of energy so there is a large response in the tube. Consequently, any small damping in the tube effectively absorbs energy because the tube easily accepts energy and is an efficient absorber resulting in a large power flux into the tube.

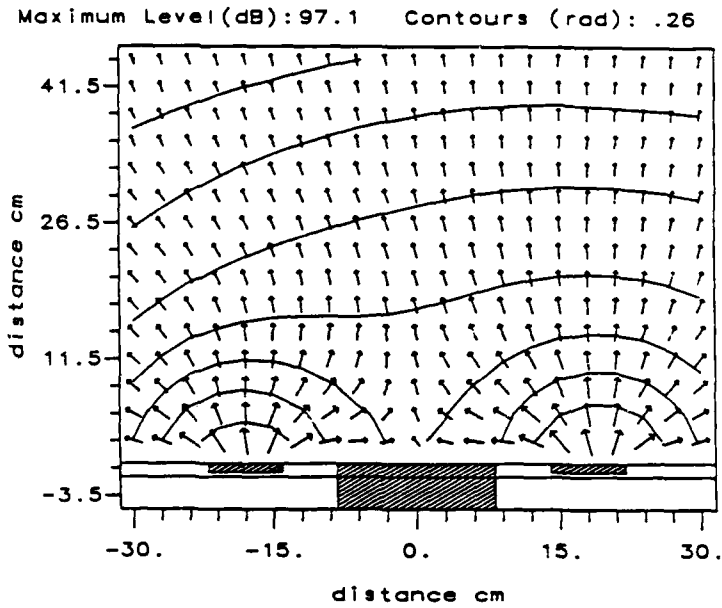
Another important aspect of the impedance above the tube shown in Figures 6.5 and 6.6 is that the real part does not go to zero because of the energy being absorbed by the tube. The fundamental equations which give the end correction of 0.84 times the tube radius also specify that the real part of the impedance at the tube opening is zero. Consequently, the losses in the tube and the coupling with the sources has shifted the predicted resonance of the tube with the extended length by decreasing the effective length of the tube. This is done by shifting kinetic energy associated with the added mass which would be U_r , into kinetic energy due to the component U_a which inputs power into the tube where it is dissipated.

6.2.2. Anti-Resonance of the Tube

Now let us compare the results at resonance with those at the first anti-resonance of the tube, 400Hz. At anti-resonance the closed tube has a very high input impedance, so that it is essentially not seen by the acoustic field. Therefore, the field should be much the same as that for two baffled pistons.

The active intensity, Figure 6.7, clearly shows that there is no power input to the tube and that the waves propagate over the tube unaltered. The reactive

ACTIVE INTENSITY & WAVEFRONTS



REACTIVE INTENSITY

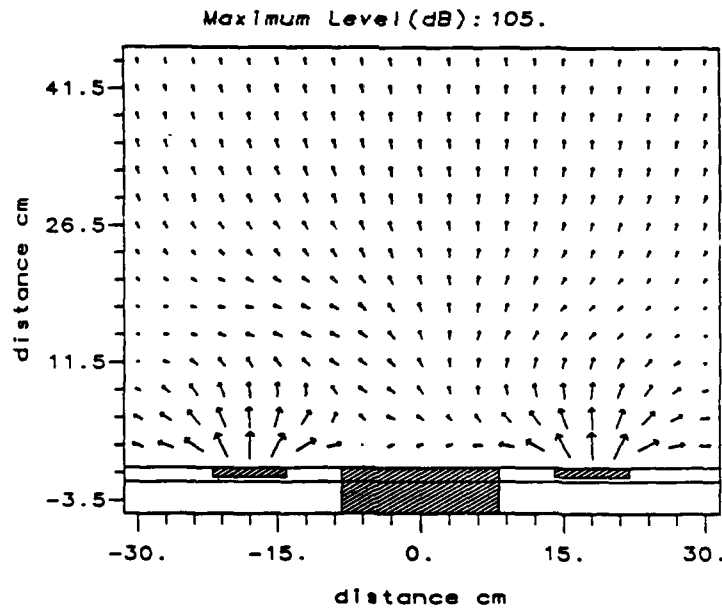


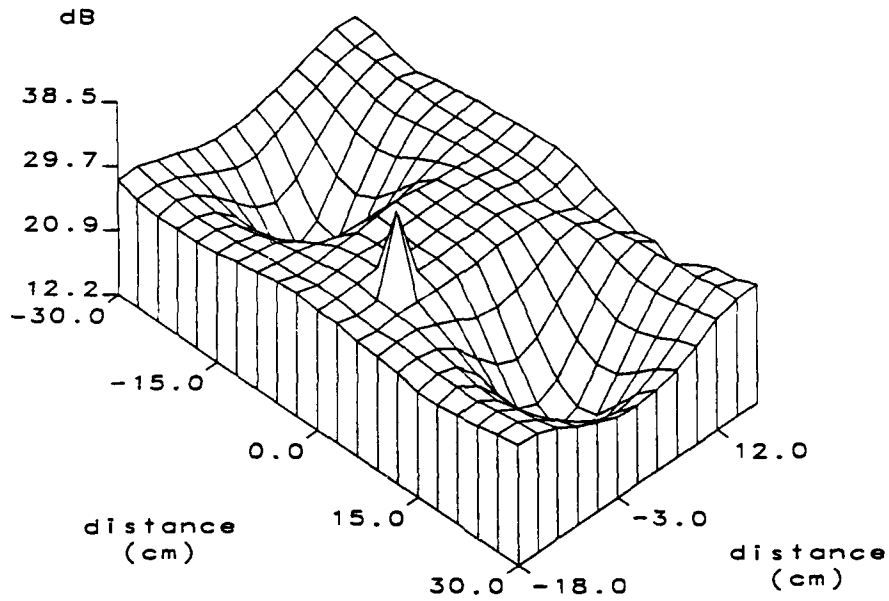
Figure 6.7 The measured active intensity and wave fronts and reactive intensity at 400Hz in a plane perpendicular to the baffled containing two in phase piston sources and a tube with a 200Hz fundamental resonance.

intensity around the tube opening is different than what would be expected than for two baffled pistons alone. The active and reactive intensity, with the tube having an infinite input impedance, should not be effected by the tube. The maximum level of the reactive intensity has decreased by 5dB compared to the maximum level of the reactive intensity at resonance (200Hz) This decrease is due to a smaller influence of the tube at anti-resonance and the lower mutual coupling between the pistons at this higher frequency.

The component of the kinetic energy normal to the baffle is plotted in Figure 6.8. The kinetic energy normal to the tube opening is very low. Thus the tube is acoustically a rigid boundary, as indicated in the previous paragraph.

The normal impedance, Figure 6.9 and 6.10, measured in the plane parallel to the baffle shows a sharp contrast between the anti-resonance and first resonance of the tube. The real part of the normal impedance at 400Hz has a significant dip at the sources. However, above the tube the real impedance has the same value as above the rigid baffle. The one peak is due to a measurement anomaly. These results show that the power radiated at this frequency is only a function of the coupling between the two sources and that the tube is the same as the rigid baffle.

The imaginary part of the normal impedance has slight dips over the piston sources, which is associated with the reactive component of their radiation. Above the center of the tube the imaginary part is the same level as over the baffle except for a ring where there is a local minimum. The high level of the imaginary part over the tube agrees with the high level of the real part, and the minimum ring is not as deep as the imaginary part measured at resonance. The plot of the numeric values shows that the dip in the imaginary part occurs at the edge of the tube. Consequently, we can conclude that there is some slight diffraction



IMAGINARY NORMAL IMPEDANCE

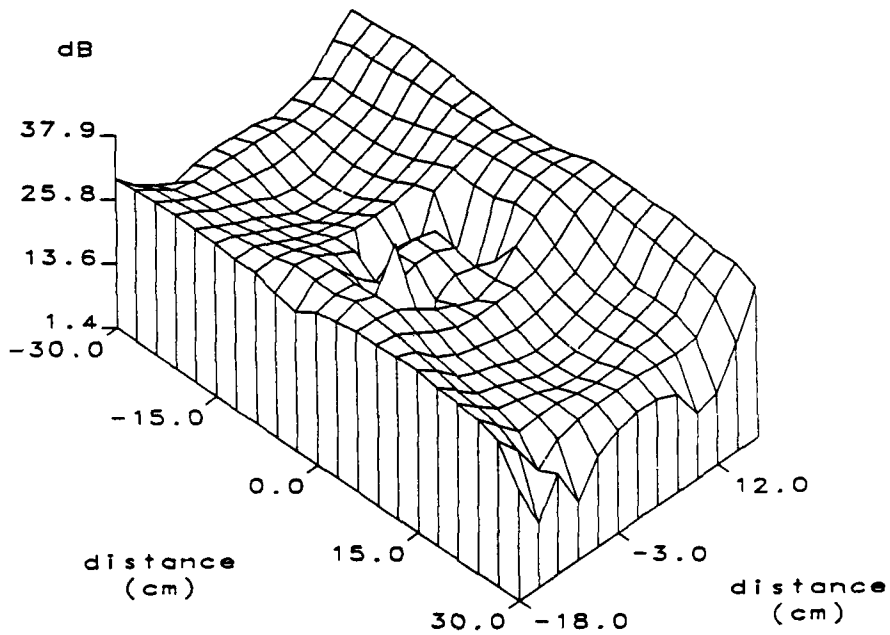
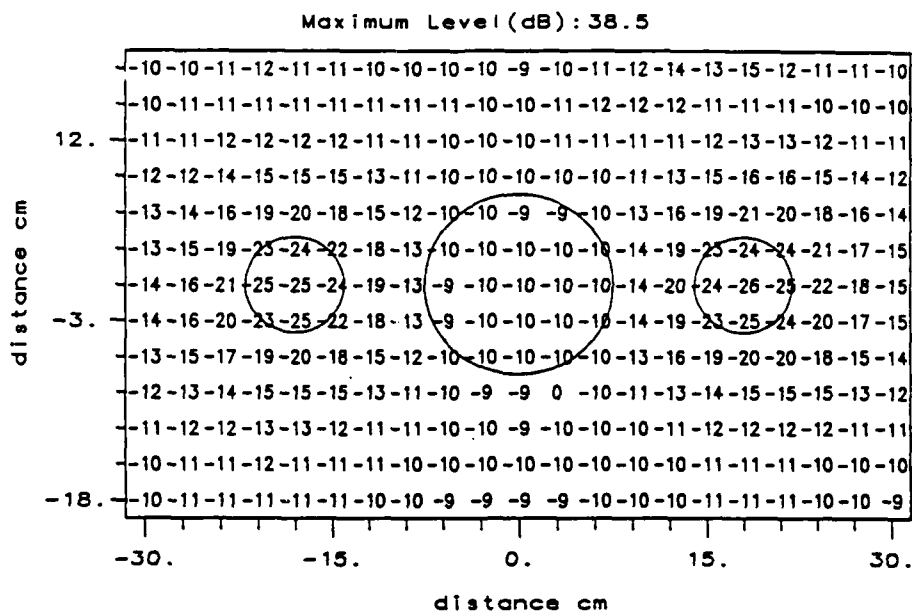


Figure 6.9 The real and imaginary parts of the impedance normal to the baffle at 400Hz. The measurement plane is parallel to and 3cm above the baffle containing two in phase piston sources and a tube with a 200Hz fundamental resonance.

REAL NORMAL IMPEDANCE



IMAGINARY NORMAL IMPEDANCE

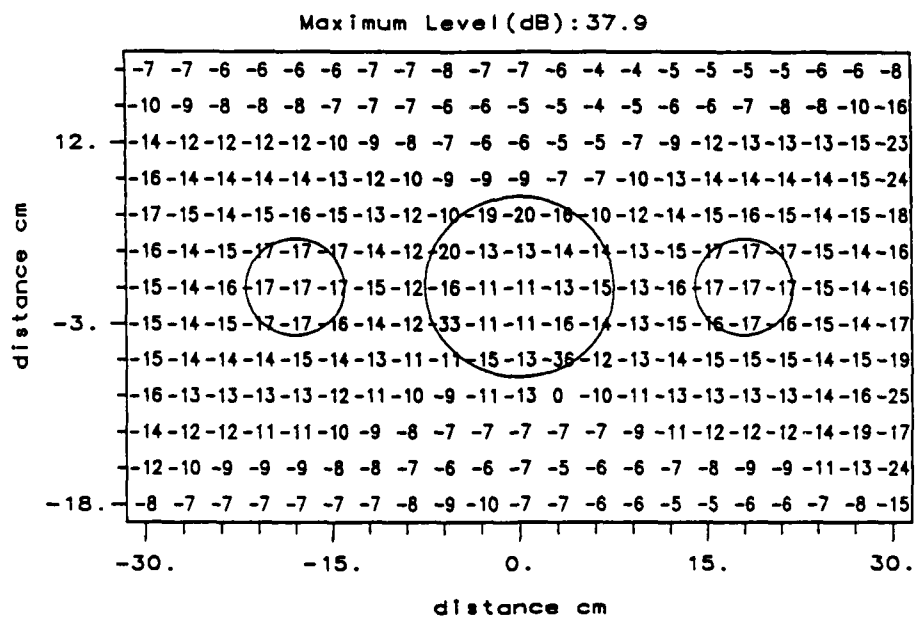


Figure 6.10 The numerical values of the real and imaginary parts of the impedance normal to the baffle at 400Hz. The measurement plane is parallel to and 3cm above the baffle containing two in phase piston sources and a tube with a 200Hz fundamental resonance.

occurring because of the sharp edge of the tube opening. This diffraction at the tube opening causes the variation in the reactive intensity seen in Figure 6.7.

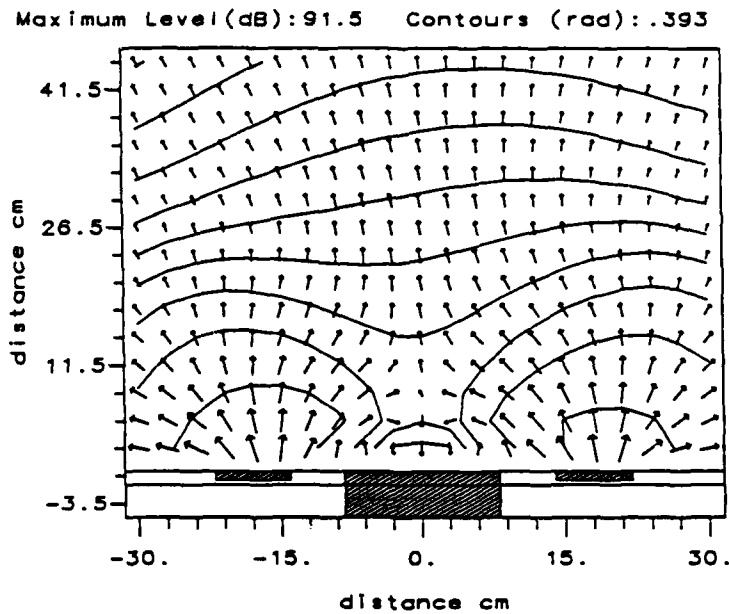
These results graphically show the well known effects of using resonators to absorb energy. At 400Hz the damping capabilities of the tube walls is no different than at 200Hz. However, at 400Hz the tube has a very high input impedance so that any energy in the vicinity of the tube would rather propagate toward the low impedance farfield than into the tube. Without any energy, the damping within the tube has nothing to dissipate. Therefore, an issue in absorbing energy is to first induce the energy to regions with damping.

6.2.3. Second Resonance of the Tube

The second resonance of the tube occurs at 600Hz. The field is much the same as at 200Hz, but some changes are very important to notice, Figure 6.11. Since the tube is operating at resonance the energy is once again being absorbed by the tube. At resonance there is sufficient energy in the tube for the damping to be effective. However, the distance where the energy being absorbed does not extend as far from the tube as at 200Hz.

Despite the small extent from the tube where the energy points in, the arc of pressure minima, seen clearly in the reactive intensity in Figure 6.11, has the same size as at 200Hz. This is expected because the tube length correction at the lower modes is independent of frequency. It is especially interesting to compare the normal kinetic energy at 600Hz, Figure 6.12, with 200Hz, Figure 6.4. The maximum amplitude is lower at 600Hz, but the relative distributions of the kinetic energy on the two lines of data above the baffle are the same at these two frequencies. This signifies that the pistons and tube are constant velocity sources, which are not altered by the mutual coupling of the sources and the tube.

ACTIVE INTENSITY & WAVEFRONTS



REACTIVE INTENSITY

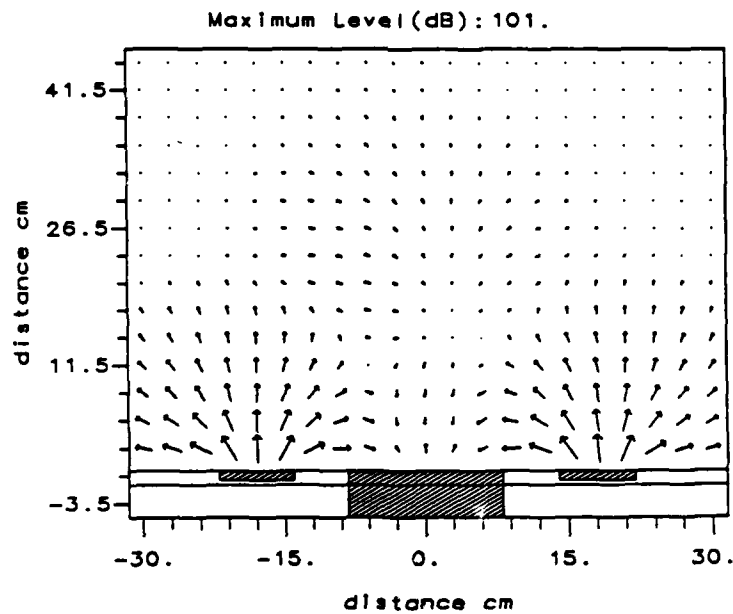


Figure 6.11 The measured active intensity and wave fronts and reactive intensity at 600Hz (the second resonance of the tube) in a plane perpendicular to the baffled containing two in phase piston sources and a tube with a 200Hz fundamental resonance.

The specific impedance shown in the plane parallel to the baffle, Figure 6.13, has the same characteristics at 600Hz as at 200Hz. The dips in the real part are confined much closer to the sources and tube opening because of the higher frequency, which results in the lower mutual coupling. In fact, this is apparent to a greater extent in the imaginary part. It is perhaps easier to compare the impedance at the two frequencies by using the numeric values, Figure 6.14. Many of the features of these plots are decreased geometrically in size by about 3 times, corresponding to the change in wavelength.

6.2.4. Comparison of the Impedance Above the Tube

The impedance measured above the tube is summarized in Table 6.1. Theoretically at the tube opening the impedance is purely imaginary and increases linearly with frequency at resonance, which would mean a 4.8 dB rise between 200 and 600 Hz. The imaginary part of the impedance follows this reasonably, increasing by 4 dB. The same theory predicts that the real part will increase with the square of the frequency or 9.5 dB. However, the measured change is negligible. One explanation of this is that at resonance the damping in the tube is dominating the power input to the tube, therefore the dominant influence on the impedance. Thus, the tube accepts energy much more readily than the resonant mechanism would predict. The other explanation is mutual coupling, which is frequency dependent.

6.3. Variations in Radiation Impedance and Output Power

The measurements which are reported in this section were performed at the Physikalisch-Technische Bundesanstalt (PTB) in Braunschweig, West Germany. The instrumentation was different from that which was used for all the other measurements in this thesis, so the description of the measurement setup is presented in Section 6.3.1.

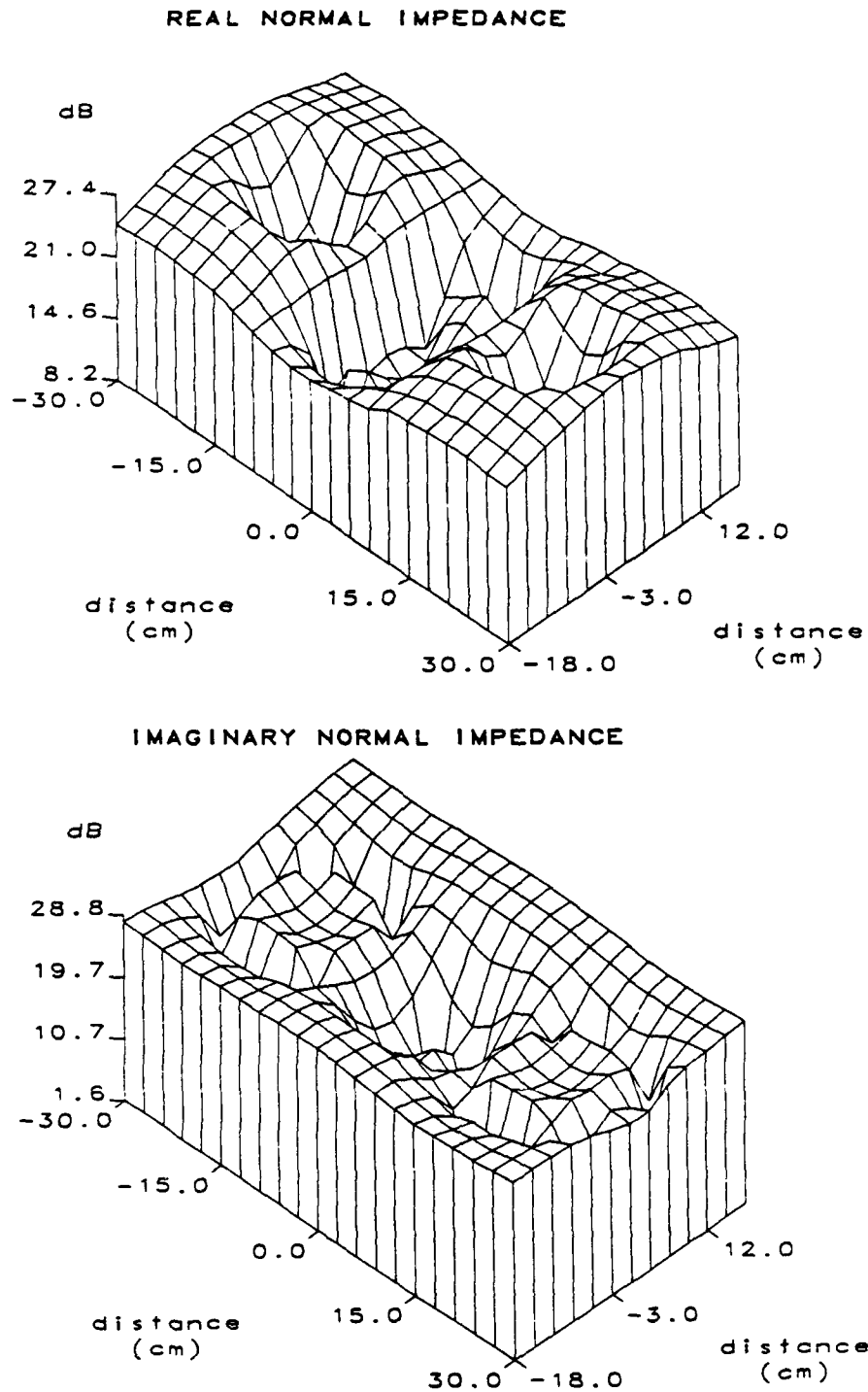


Figure 6.13 The real and imaginary parts of the impedance normal to the baffle at 600Hz (the second resonance of the tube). The measurement plane is parallel to and 3cm above the baffle containing two in phase piston sources and a tube with a 200Hz fundamental resonance.

Table 6.1 The real and imaginary parts of the impedance normal to the baffled, averaged over the tube opening. The frequencies 200Hz and 600Hz are at the tube resonance and 400Hz is at the tube anti-resonance.

Frequency (Hz)	$Re\{z\}$ (dB)	$Im\{z\}$ (dB)
200	13	11
400	28	16
600	14	15

The output power of a simple source can be calculated from the product of the source volume velocity and real part of the specific acoustic impedance at the surface of the source. Assuming that a source has a constant volume velocity, any change in the output power is equated to the variation of the radiation impedance. Variations of the output power and radiation impedance occur when the distance of a source above a reflecting plane changes. Such variations are confined to low frequencies and are of concern when determining the output power of a source. The height of the source during measurements may produce power estimates much different than the power which the source radiates in its normal environment. Therefore, the purpose of these measurements was to show that the intensity technique can measure the impedance at the surface of a source which can then be compared with the measurement of the output power.

An important result of these measurements was the observation that signal processing errors in the real-time analyzer were introduced. The error was due to a phase shift between the separate analog circuits which calculate the pressure and velocity. Thus, errors introduced by the two microphone intensity technique are not confined to the phase mismatch between the microphones and the two

channels of the signal processing. This is an important issue for institutes which are responsible for certifying the accuracy of equipment.

There is some notation which is only used in this section. The notation *SPL* will be used for the sound pressure level, *SVL* for the sound velocity level, *SIL* for the sound intensity level (active intensity), and *SQL* for the reactive intensity level. This is done to comply with the notation used at the PTB.

6.3.1. Measurement Setup

For these measurements a B&K $\frac{1}{4}$ inch phase matched, face-to-face intensity probe was used. The small size was needed to get close to the source surface while minimizing diffraction by the probe. For these two reasons larger devices such as the B&K $\frac{1}{2}$ inch probe and the Norwegian Electronics intensity probe (Bjor 1985) were not used. The Norwegian Electronics intensity probe measures the pressure with a single microphone and the velocity with four ultrasonic transducers. The ultrasonic transducers measure doppler shifts and are orientated on a line perpendicular to the axis of the microphone. In this application the Norwegian Electronics probe also has the disadvantage of being sensitive to air currents since the velocity is measured directly. Consequently, with a wind screen and the orientation of the ultrasonic transducers and the microphone, the probe was too bulky to be effective, for these measurements.

A Norwegian Electronics one-third octave real-time analyzer type 830 was used for the signal processing. This is a two-channel analyzer which measures in one-third octave bands the sound pressure level (*SPL*), sound velocity level (*SVL*), and sound intensity level (*SIL*). The reactive intensity was not measured directly by the analyzer, so it needed to be calculated after the measurement was completed. The active intensity (*SIL*) and reactive intensity (*SQL*) are

calculated from the amplitudes of the pressure and velocity and the phase angle θ between them:

$$I = \frac{p u}{2} \cos\theta \quad , \quad (6.1)$$

$$Q = \frac{p u}{2} \sin\theta \quad . \quad (6.2)$$

From Equation 6.1 the phase angle θ can be calculated:

$$10 \log_{10}(\cos\theta) = SIL - \frac{1}{2}(SPL + SVL) \quad . \quad (6.3)$$

Note that the $\frac{1}{2}$ in Equation 6.1 is not included in Equation 6.3 because SPL and SVL are effective levels. The reactive intensity level can now be calculated:

$$SQL = \frac{1}{2}(SPL + SVL) + 10 \log_{10}(\sin\theta) \quad , \quad (6.4)$$

which allows the real and imaginary parts of the impedance to be calculated:

$$10 \log_{10}(\text{Re}\{z\}) = SIL - SVL \quad , \quad (6.5)$$

$$10 \log_{10}(\text{Im}\{z\}) = SQL - SVL \quad . \quad (6.6)$$

The measurements were performed in a large hemi-anechoic room. The floor was a smooth rigid surface and the walls and ceiling were anechoic. For the impedance measurements the probe was positioned by hand. The power measurements were made in compliance with the international standards for measuring power using pressure measurements; however, the intensity probe was used. The probe was swept in a quarter of an arc of 2m in radius. The intensity was continuously averaged over the $12\frac{1}{2}$ minutes of this process. The source is rotated so the path of the probe relative to the source traverses a hemisphere

along a spiral path. The source which was used was omni-directional so that the rotation gave similar results.

A B&K reference sound source type 4205 was used for the measurement, Figure 6.15. This broad band noise source, which uses a loudspeaker, was chosen over the fan sources because of the large air motion around the fan. Also, the radiation surface of the loudspeaker is small, so the source is omni-directional and can be classified as simple. Therefore, the impedance measured at one point is sufficient to characterize the source impedance.

The acoustic impedance measurements were made at the point marked on the sketch of the source, Figure 6.15. This point was chosen as close to the center of the radiating surface as the probe could be positioned. The impedance and radiated power was measured as a function of source height above the floor. The source was raised 20cm, 40cm, and 80cm above the floor.

6.3.2. Analysis of the Results

The real and imaginary parts of the specific acoustic impedance measured in one-third octave bands centered from 63Hz to 5000Hz is shown in Figure 6.16. The results are very similar to those calculated for a small sphere with ka small, where a is the radius. At frequencies below 800Hz, where $ka = 1$, the impedance increases with frequency and the imaginary part is larger than the real part. The real and imaginary parts are equal at 800Hz. At frequencies above 800Hz the real part of the impedance stays constant and the imaginary part decreases. In Figure 6.16 the real and imaginary parts intersect at the band around 800Hz, which corresponds to a value for $a \simeq 7cm$. This is only 1cm smaller than the physical size of the source radiating surface. These results show that the source can be viewed as a simple source so that the impedance can be measured at one point.

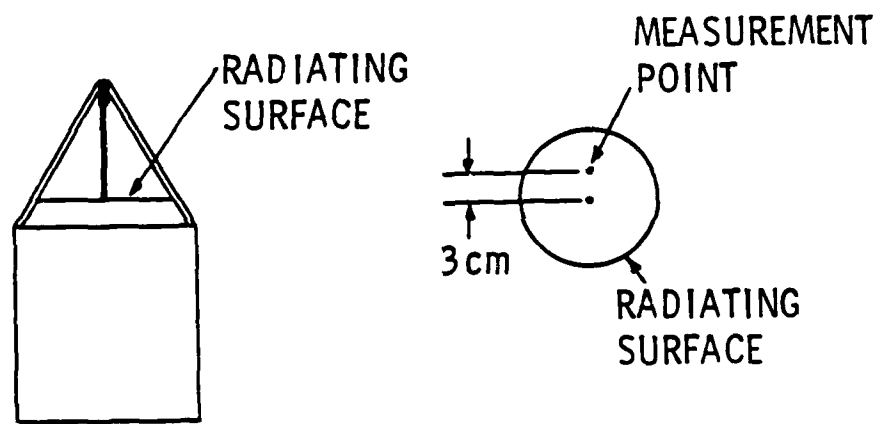


Figure 6.15 A sketch of the B&K reference sound source and the position of the measurement point.

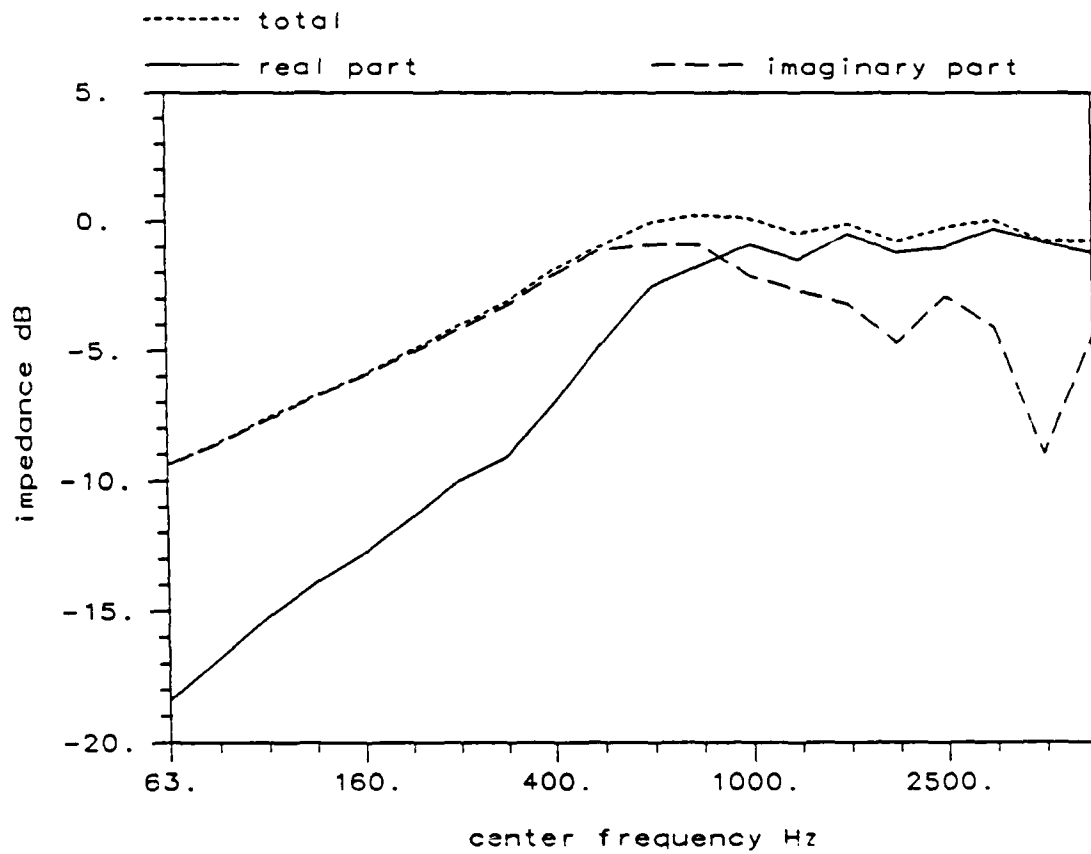


Figure 6.16 The impedance measured above the B&K reference sound source: the real part, imaginary part and the total magnitude.

Next the source was raised to different heights. Figure 6.17 shows the impedance normalized to the impedance of the source located on the floor. Similarly, the radiated power as a function of the source elevation referenced to the power of the source on the floor is plotted in Figure 6.18.

The overall shape of these curves shows the change in the radiated power corresponding to the change in the radiation impedance. Above 250Hz there is excellent agreement. Below 250Hz the deep minima are seen in both the power and impedance, but the change in impedance is much less than the corresponding changes in the output power.

The measured *SVL* varied only by $\pm 0.2dB$ for each source height. This variability is within the repeatability of the measurement, and therefore the source can be considered a constant velocity source. We can also conclude that the measured particle velocity amplitude was accurate and the discrepancy between the power and impedance changes cannot be explained by the variation in the *SVL*.

The discrepancy could also have been caused by positioning the probe too far from the source surface so that the measured impedance does not represent a good estimate of the impedance at the source surface. If the probe was not close enough then we would expect the largest discrepancies at high frequencies where the distance is acoustically large. Likewise, we would expect the most accuracy at low frequencies where the distance is acoustically small. However, the measurements above 250Hz were consistent between the power and impedance so the probe must have been close enough below 250Hz. Thus the distance of the probe from the source was also not the cause of the discrepancy.

The only other significant error is in the signal processing which calculates the sound intensity level. Differences between the *SPL* and *SIL* of 10dB to 15dB are beyond the dynamic range of the system. But, the *SPL* and *SIL*

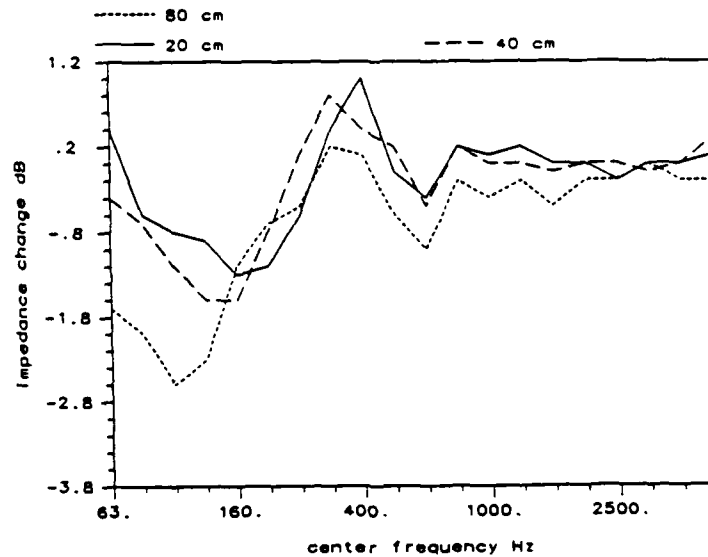


Figure 6.17 The difference in dB between the real part of the impedance measured with the source raised 20cm, 40cm, and 80cm above the floor and the source on the floor.

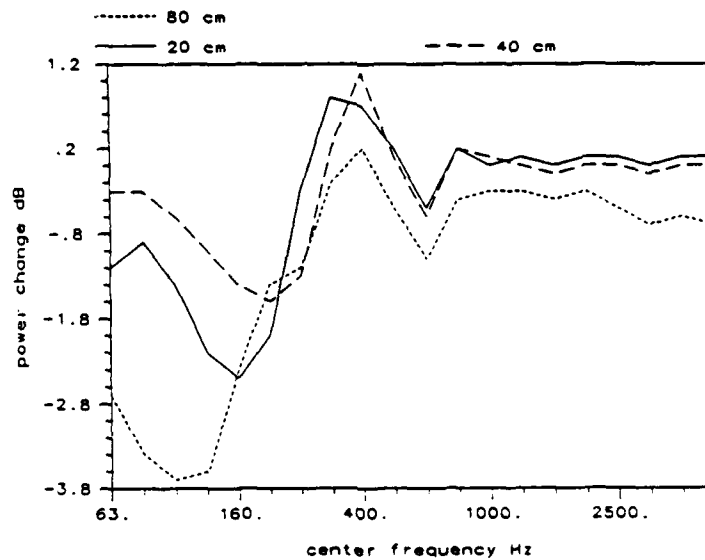


Figure 6.18 The difference in dB between the radiated power measured with the source raised 20cm, 40cm, and 80cm above the floor and the source on the floor.

around the source were within 3dB of each, so the intensity level was not beyond the dynamic range of the system. In general, phase mismatch between the two microphone channels causes the greatest errors at low frequencies. However, the power was measured accurately in the farfield, so the system can measure the *SIL* accurately below 250Hz. Thus the error was not caused by the phase mismatch between the two microphone signals.

The power measurements which were performed in the farfield differed from the impedance measurements which were performed in the nearfield, in that the level of the velocity out of phase with the pressure, U_r , was much larger in the nearfield. This is shown in Figure 6.16 where below 250Hz the imaginary part of the impedance is 5dB to 10dB higher than the real part, so that in the nearfield the particle velocity is nearly ninety degrees phase shifted with respect to the pressure. This corresponds to a high *SQL*. In contrast, above 250Hz the real part of the impedance is dominant so that the phase between the pressure and velocity is much smaller and consequently the *SIL* is measured accurately. Despite the high level of the *SQL* in the nearfield compared to the farfield the difference between the *SPL* and *SIL* remained constant in the nearfield and in the farfield and was only ± 1.5 dB.

Now consider how the analyzer processes the signals, Figure 6.19. There are two separate electrical circuits which calculate the pressure and velocity. The pressure and velocity signals are subsequently multiplied to form the instantaneous intensity signal. The instantaneous intensity signal is then time averaged to display the *SIL*. However, there are phase shifts introduced between the two circuits which calculate the pressure and velocity. This phase error will have different effects on the time averaged instantaneous intensity depending on the phase between the pressure and velocity.

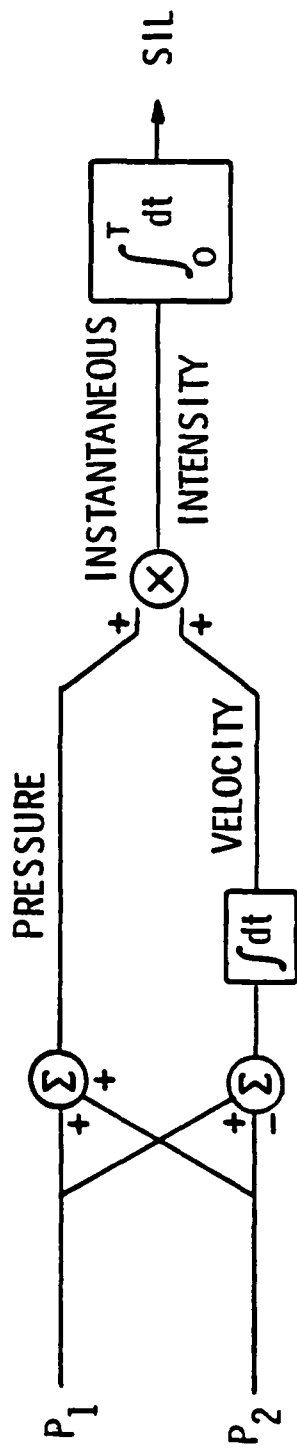


Figure 6.19 A schematic of the signal processing in a real-time analyzer which calculates the time-averaged sound intensity level.

When the *SQL* is very low the pressure and velocity are nearly in phase. Any phase error between the circuits calculating the pressure and velocity will have very little influence on the *SIL*. However, when the *SQL* is very high the pressure and velocity are nearly in phase quadrature, so small phase shifts introduced by the two circuits will greatly influence the *SIL*. This is exactly the behavior of the discrepancies between the power and impedance measurements.

Tests were performed with the analyzer by electrically creating signals which simulated high *SQL*. However, these were done only with a phase between pressure and velocity of fifty degrees. The analyzer accurately displayed the *SIL*. However, to simulate the errors encountered during the impedance measurements at low frequencies, greater phase shifts must be tested. Thus, when making intensity measurements with a real-time analyzer concern cannot be focused only on phase mismatches between microphones. The electronic circuits which separately calculate the pressure and velocity must also be accurately phase matched if measurements are going to be made where the reactive intensity is very high.

Chapter 7

EXPERIMENTAL ANALYSIS OF DIFFRACTION

7.1. Introduction

The details of diffraction are not easily understood because of the difficulty in exploring the nearfield, where the diffraction occurs. Acoustic intensity measurements provide a detailed visualization of diffraction regions. Consequently, the location of diffraction can be determined and the effects on the rest of the acoustic field can be seen. Three measurements presented in this chapter will be analyzed in a qualitative rather than quantitative manner. This is done to emphasize the visualization capabilities of the active and reactive intensity.

7.2. Diffraction in a Loudspeaker Nearfield

Loudspeakers are commonly analyzed as sources of sound. However, this chapter will focus on the diffraction in the nearfield of a loudspeaker because it degrades the loudspeaker radiation characteristics. The desired characteristic of a good loudspeaker is a uniform acoustic farfield. However, there are distortions of the sound radiation pattern that originate in the nearfield, thus the analysis should be performed in the nearfield where the sound is produced.

The loudspeaker is sketched in Figure 7.1. It was designed as a two way system with a 6dB per octave crossover at 600Hz. In the frequency range of the crossover the acoustic field is dominated by coupling and interference of the sound radiated by the woofer and tweeter. The measurements which will be discussed were made at 1500Hz and 2500Hz. This is far above the crossover frequency, so only the tweeter is active. Assuming the tweeter radiates like a piston of radius 3cm, then $ka = 1.37$ at 2500Hz. Thus, the radiation of the tweeter is essentially omni directional since the first zero in the main lobe occurs at $ka \approx 3.5$.

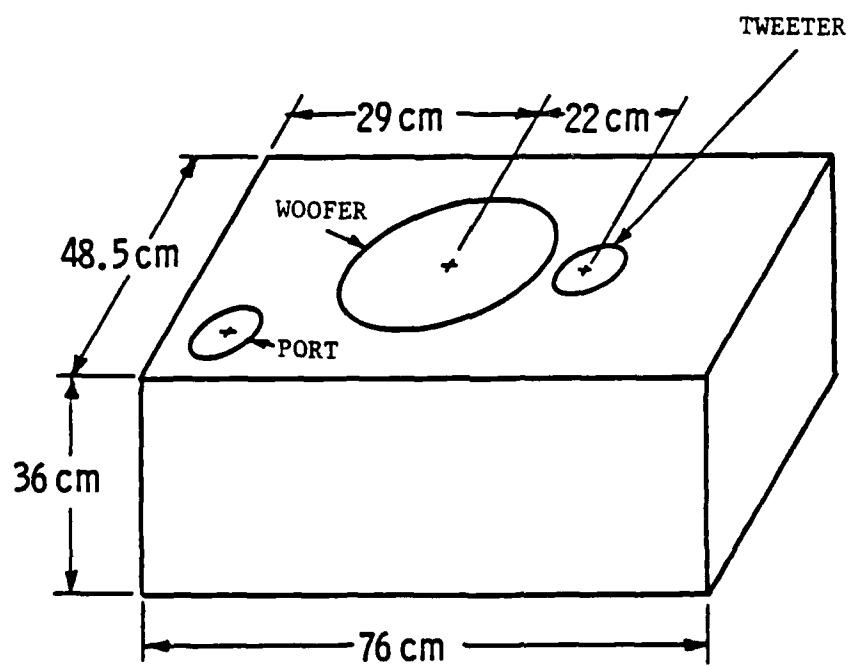


Figure 7.1 A sketch of the loudspeaker used for diffraction measurements.

Two measurement planes were used. A plane perpendicular to the loudspeaker surface through the center of the woofer and tweeter was chosen to characterize the radiation toward the farfield. This is a plane symmetric with respect to the sources so only two dimensions of the intensity was measured. Measurements were also made in a plane parallel to the loudspeaker surface to see the full interaction of the sources and box edges. This required a three dimensional measurement of the intensity which was made 3.5cm above the speaker surface.

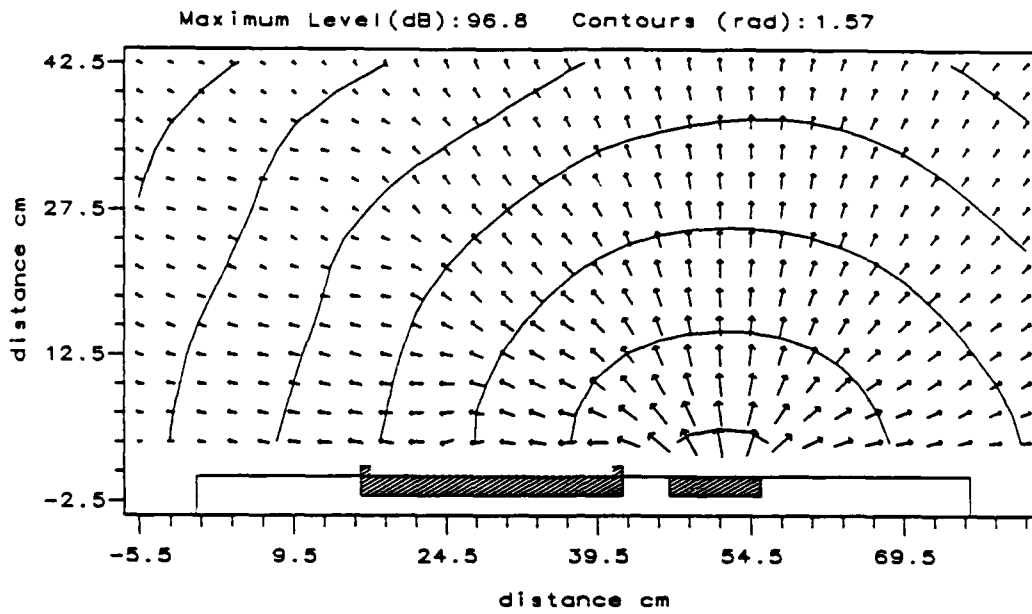
Diffraction will intuitively be most prevalent at impedance discontinuities. The most obvious areas on the loudspeaker are the outer edges of the box where there is a discontinuity between the wood surface and air. The other significant area is the edge of the woofer. The woofer edge protrudes 1cm above the box surface, but more significantly the woofer represents an abrupt discontinuity between the thin woofer cone and the rigid wood surface of the box. These measurements identify both discontinuities.

7.2.1. Diffraction Effects at 1500Hz

Let us begin with 1500Hz. The active intensity, Figure 7.2, shows that the wave fronts originate from the tweeter and propagate to the farfield as spherical waves. There is some distortion of the waves as they go past the woofer. The cause of the distortion is easily visualized in the reactive intensity.

The reactive intensity clearly points out of the woofer edge, Figure 7.2; consequently, there is a pressure maximum at the woofer edge, Figure 7.3. The kinetic energy associated with the velocity normal to the speaker, Figure 7.4, also has a local maximum at this point. The reactive intensity in the horizontal plane, Figure 7.5, also shows the pressure maximum above the woofer edge. Further, there is a pressure minimum and another maximum between this edge of the

ACTIVE INTENSITY & WAVEFRONTS



REACTIVE INTENSITY

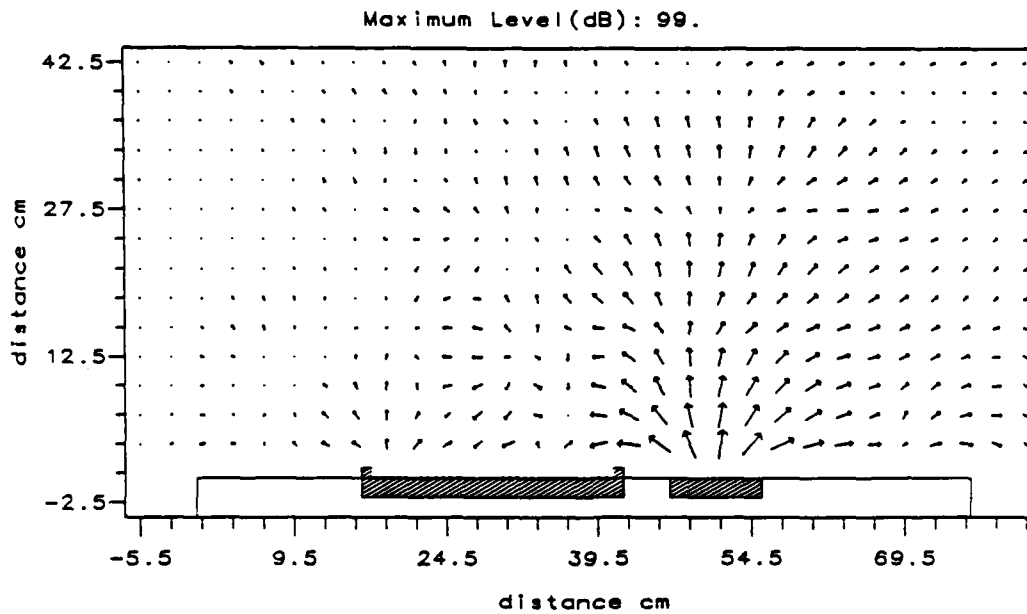


Figure 7.2 The active intensity and wave fronts and the reactive intensity measured at 1500Hz on a plane perpendicular to the loudspeaker surface.

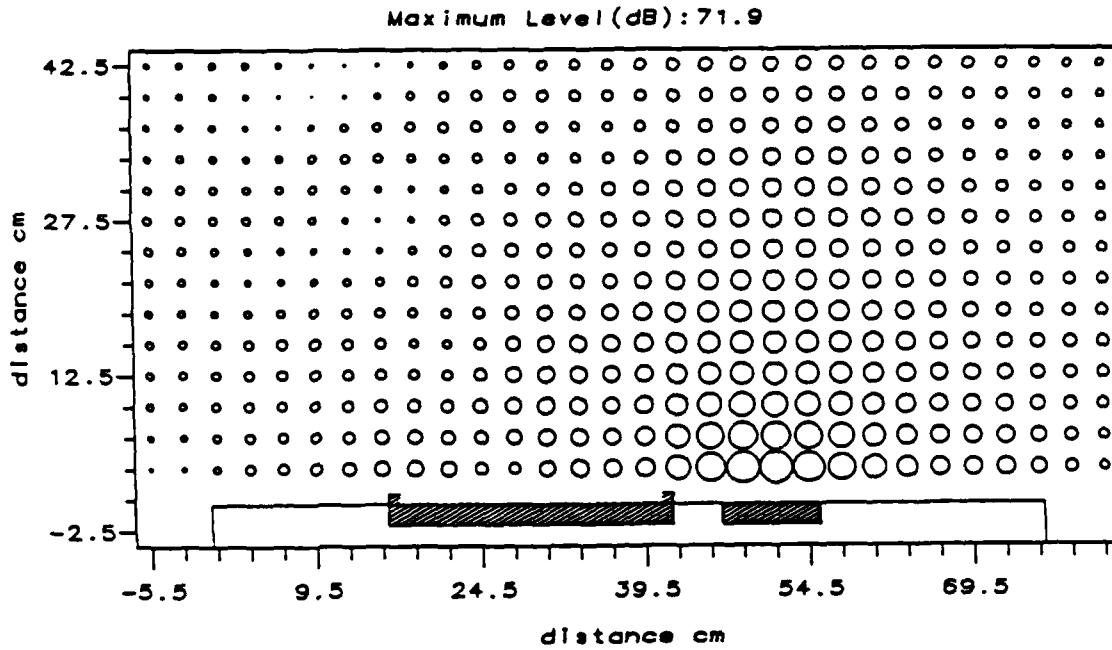


Figure 7.3 The potential energy measured at 1500Hz on a plane perpendicular to the loudspeaker surface.

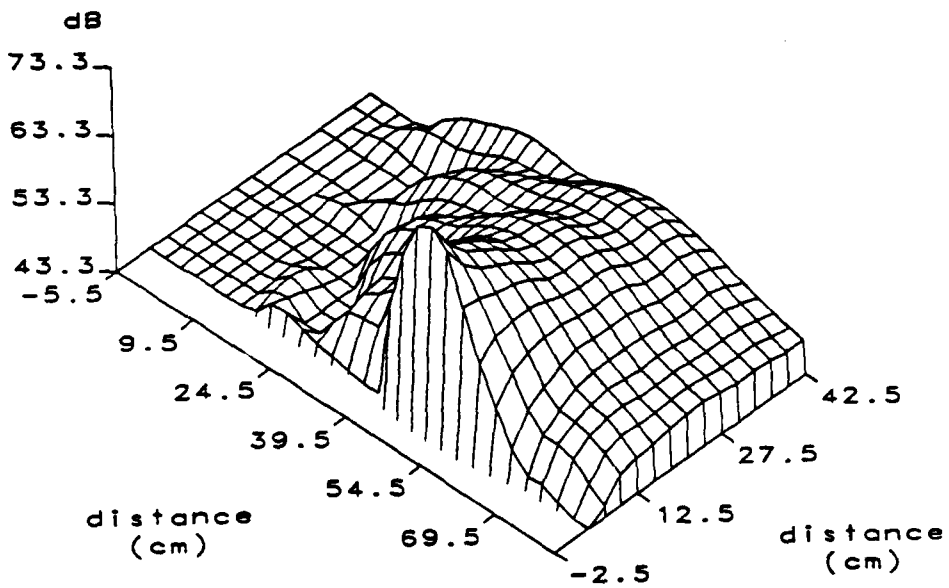
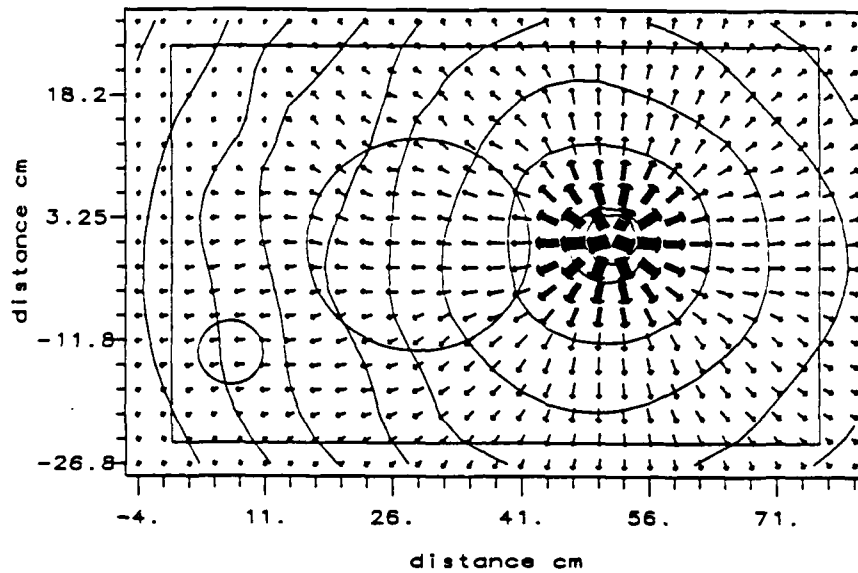


Figure 7.4 The kinetic energy due to the particle velocity normal to the loudspeaker surface, measured at 1500Hz on a plane perpendicular to the loudspeaker surface.

ACTIVE INTENSITY & WAVEFRONTS

Maximum Level (dB): 95.9 Contours (rad): 1.05



REACTIVE INTENSITY

Maximum Level (dB): 98.2

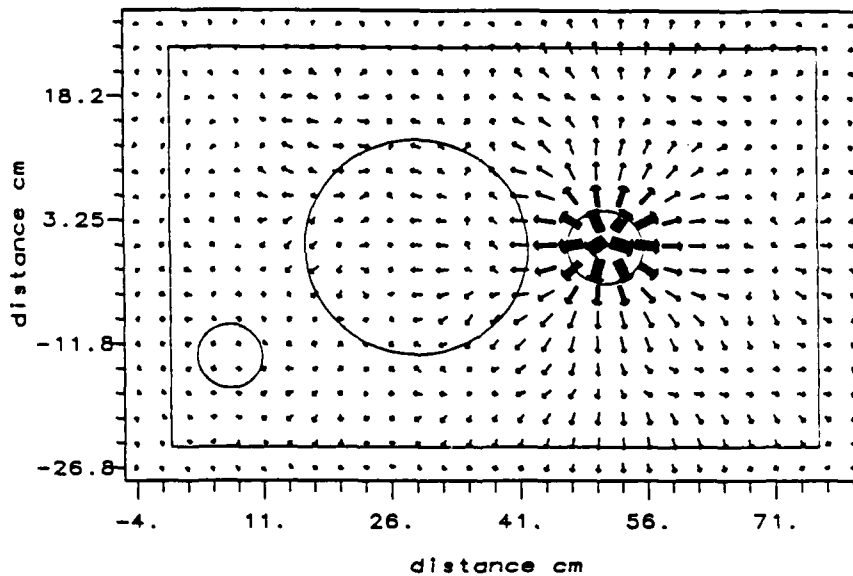


Figure 7.5 The active intensity and wave fronts and the reactive intensity measured at 1500Hz on a plane parallel to and 3.5cm above the loudspeaker surface.

woofer and the tweeter. Therefore there is a standing wave between the woofer edge and the tweeter caused by the direct wave from the tweeter interfering with the wave reflected by the woofer edge.

In Figure 2.5 and throughout the discussion of the tube and piston source measurements in Chapter 6, we saw that the reactive intensity provided invaluable insight. Likewise, in these measurements the reactive intensity in the nearfield reveals more important details than does the active intensity.

The effects of the box edge can also be seen in these measurements. This is most clearly shown in the measurements on the plane parallel to the box, Figure 7.5. The active intensity is not significantly effected by the box edge. However, the reactive intensity points out of pressure maxima, 3cm inside the edge, between the tweeter and top edge and the tweeter and right edge. The normal kinetic energy is also significant, Figure 7.6. There are regions of local velocity maxima just inside the box edge which are due to the diffraction at the box edge. These areas are not directly above the edge possibly because the measurement plane is 3.5cm (0.15λ) from the box.

The normal impedance shows some especially significant results, Figure 7.7. The real part of the normal impedance is clearly reduced by 3 to 4 dB beyond the box edge. This is a consequence of the change between the high impedance of the wood and the low impedance of the air.

The diffraction is seen as a 5 to 7 dB decrease in the imaginary part of the impedance around the box edge. The diffraction does not create or sink power, thus there is little change in the real impedance. Consequently, the peaks in the kinetic energy near the box edges are associated with the reactive intensity.

It should also be noted the kinetic energy maxima at the box edges are greatest at the portion of the edges closest to the tweeter, Figure 7.6. This is also seen as a slightly higher imaginary normal impedance at the same points.

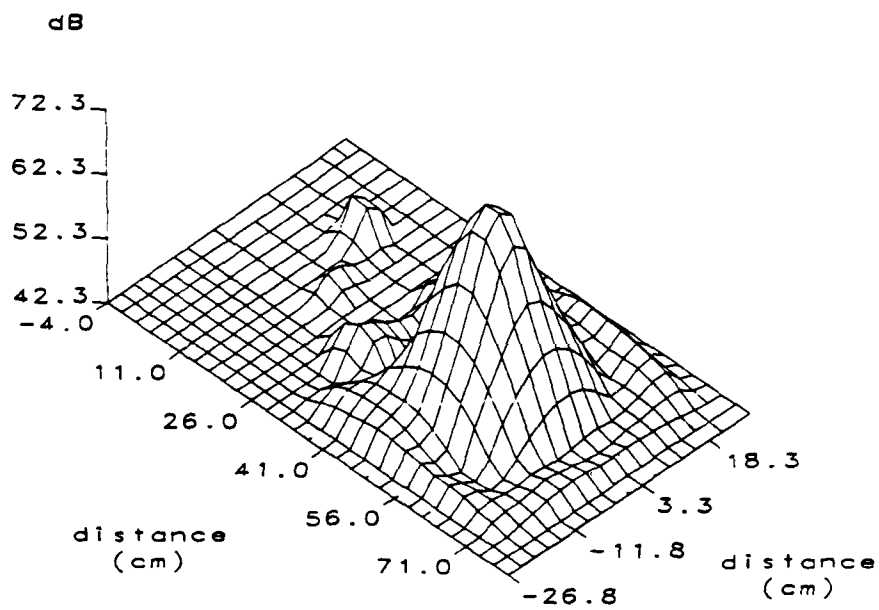
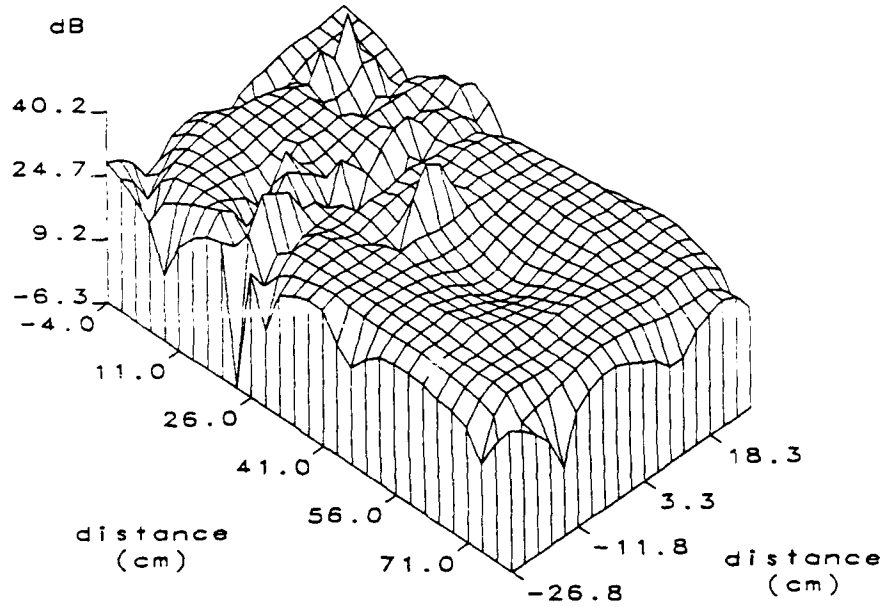


Figure 7.6 The kinetic energy due to the particle velocity normal to the loudspeaker surface, measured at 1500Hz on a plane parallel to and 3.5cm above the loudspeaker surface.

REAL NORMAL IMPEDANCE



IMAGINARY NORMAL IMPEDANCE

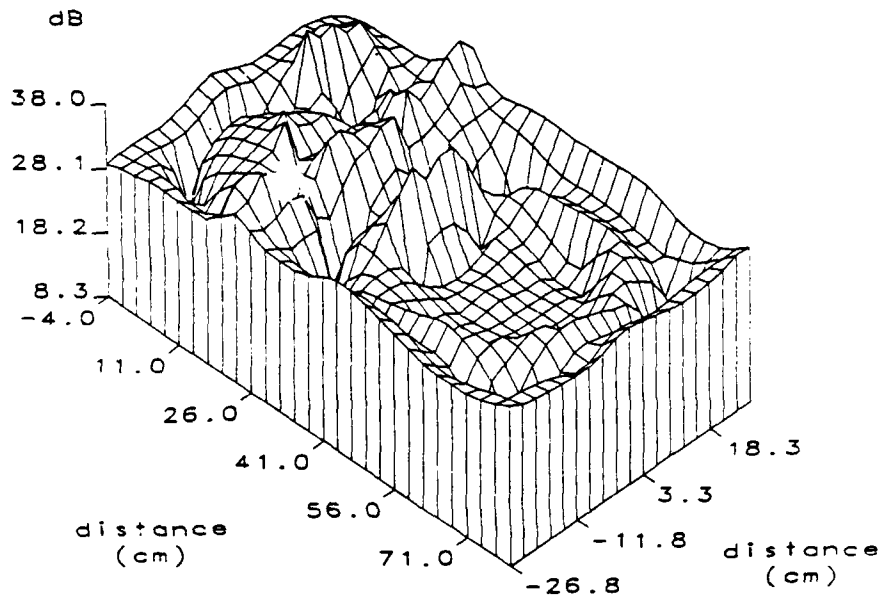


Figure 7.7 The real and imaginary parts of the impedance normal to the loudspeaker surface, measured at 1500Hz on a plane parallel to and 3.5cm above the loudspeaker surface.

This will be more effectively illustrated in the next section where comparisons of these measurements will be made with the measurements at 2500Hz.

7.2.2. Diffraction Effects at 2500Hz

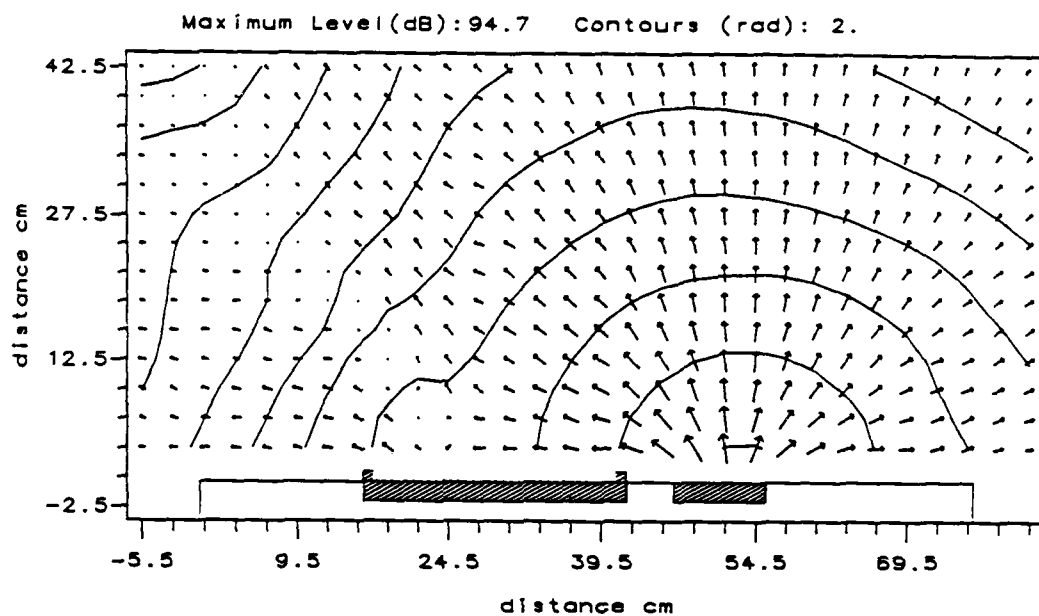
The consequence of the diffractions at 1500Hz do not significantly alter the wave front propagation, but is confined to disrupting the pressure distribution. At 2500Hz the same diffraction occurs, but has a significant impact on the wave front propagation.

First consider the vertical plane, Figure 7.8. The wave fronts are greatly distorted in a region extending from the woofer edge. The reactive intensity is once again pointing out of the woofer edge furthest from the tweeter, indicating a pressure maxima due to the diffraction at this edge. The potential energy, Figure 7.9, has a deep minimum beginning in the region between the woofer and the tweeter then extending to the farfield. The measurements in the horizontal plane clearly show the diffraction along with the standing wave between the woofer edge and the tweeter, Figure 7.10. However, the active intensity indicates that there is a wave radiating from the edge, later combining with the wave from the tweeter. The wave emanating from the woofer edge interferes with the waves from the tweeter causing the band of low pressure seen in the vertical plane.

One explanation for the region of low pressure could be the beam pattern of the tweeter. However, as already stated a piston of radius 3cm would have the first side lobe at $ka = 3.5$. But at 2500Hz $ka = 1.37$ so no side lobes in the beam pattern can occur. Also the active and reactive intensity clearly indicates that the interference is caused by the diffraction at the woofer edge.

The kinetic energy over the surface of the speaker reveals in great detail the areas of diffraction, Figure 7.11. There is a significant peak directly above the woofer edge and there are peaks at the box edges closest to the tweeter. At this

ACTIVE INTENSITY & WAVEFRONTS



REACTIVE INTENSITY

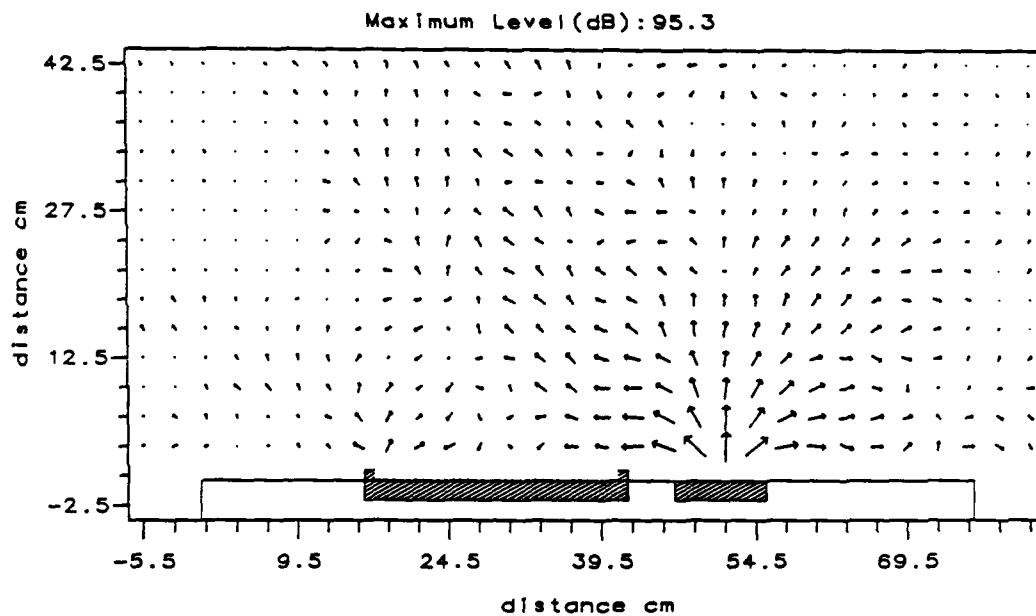


Figure 7.8 The active intensity and wave fronts and the reactive intensity measured at 2500Hz on a plane perpendicular to the loudspeaker surface.

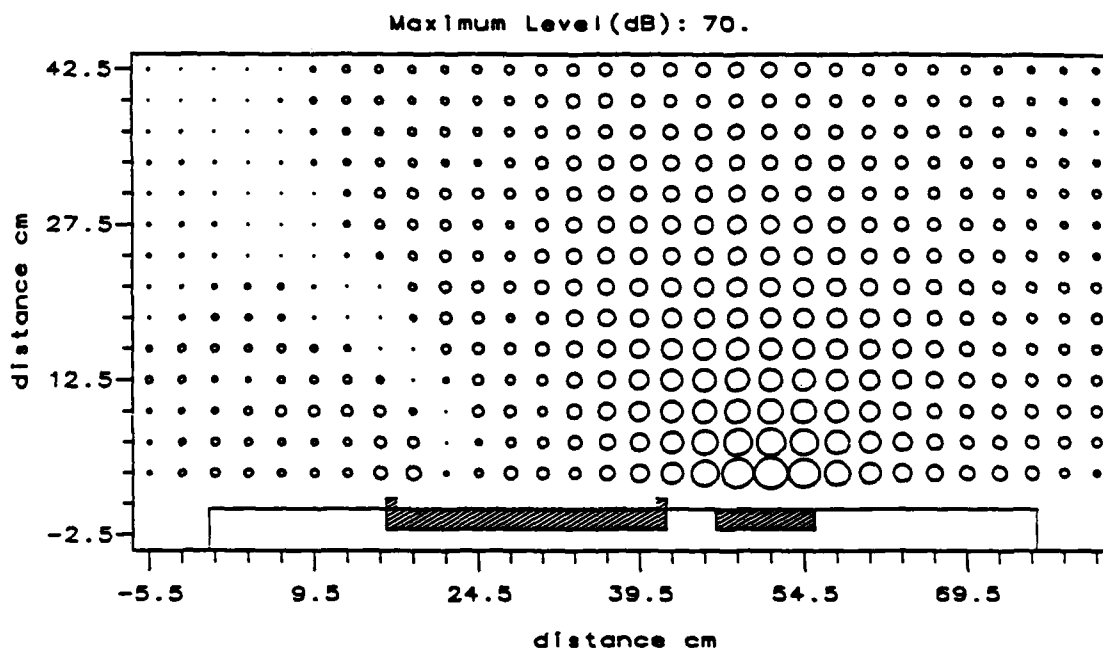
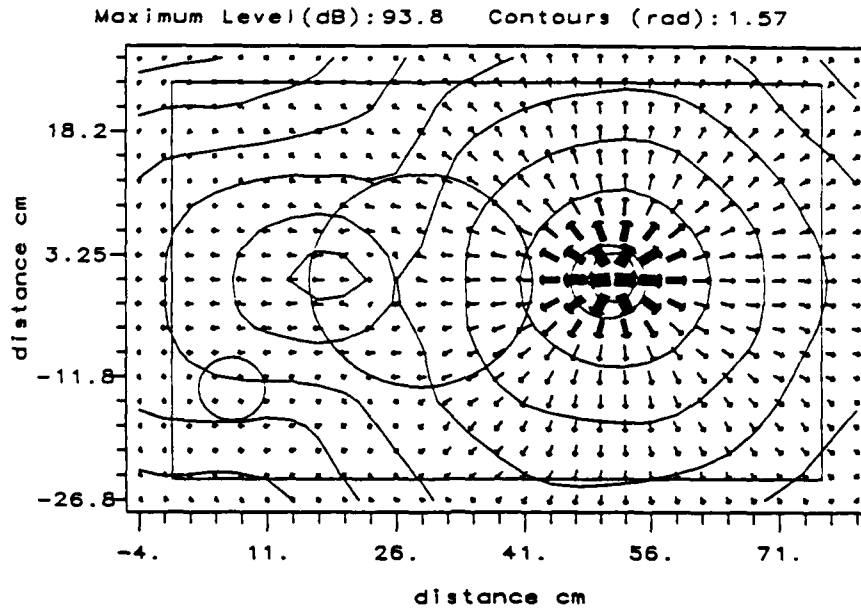


Figure 7.9 The potential energy measured at 2500Hz on a plane perpendicular to the loudspeaker surface.

ACTIVE INTENSITY & WAVEFRONTS



REACTIVE INTENSITY

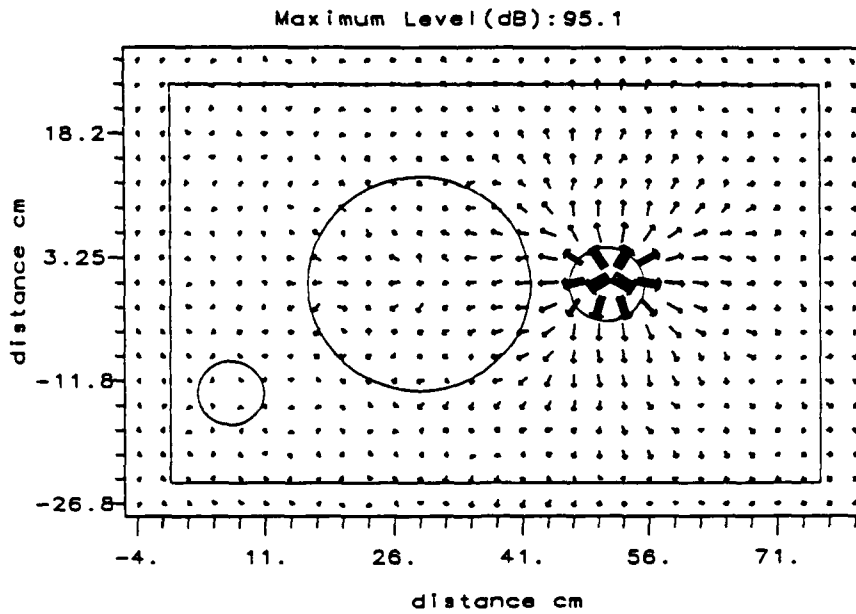


Figure 7.10 The active intensity and wave fronts and the reactive intensity measured at 2500Hz on a plane parallel to and 3.5cm above the loudspeaker surface.

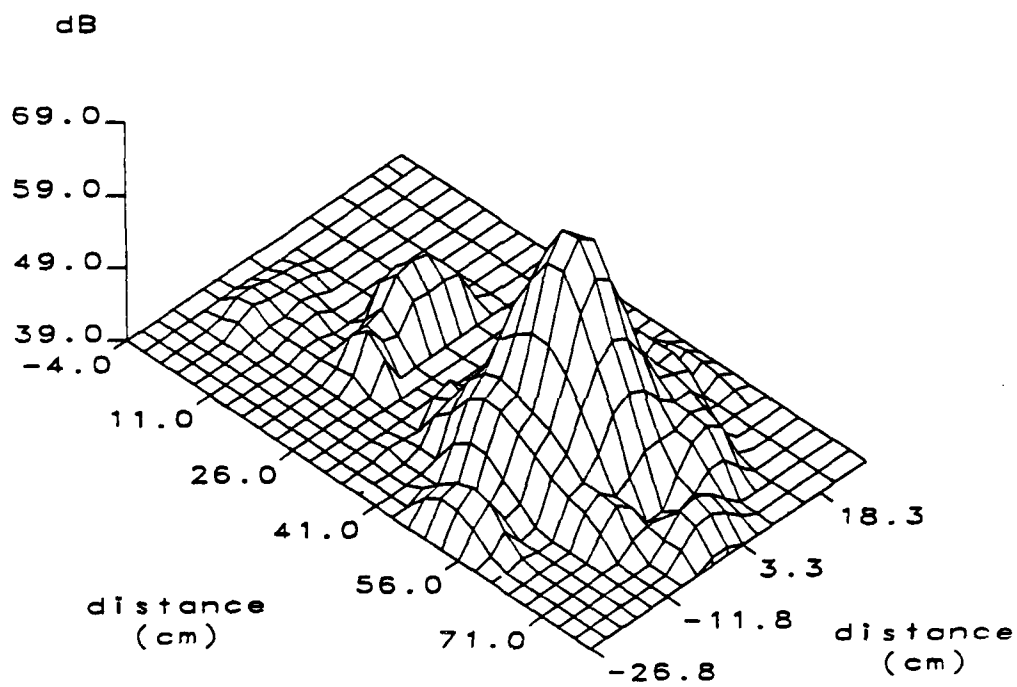


Figure 7.11 The kinetic energy due to the particle velocity normal to the loudspeaker surface, measured at 2500Hz on a plane parallel to and 3.5cm above the loudspeaker surface.

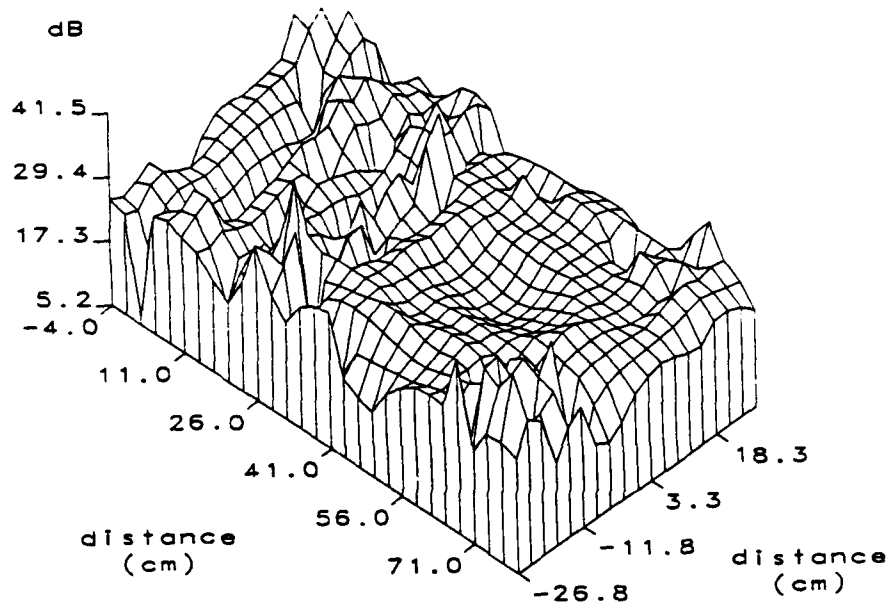
frequency the portions of the edges which have a large normal velocity are shorter in length than at 1500Hz. This seems to support the idea that the greatest effect of the edge is at points closest to the tweeter because of the decrease of energy with distance from the tweeter. Thus the diffraction at the box edge does not depend strongly on the incident angle with the edge.

At this higher frequency the impedance is less usable than at 1500Hz, Figure 7.12. This is partly due to the increased variation in the spatial pressure and velocity distribution. However, at 2500Hz the plane 3.5cm above the speaker is 0.26λ from the loudspeaker surface, as opposed to 0.15λ at 1500Hz. Consequently, this plane is acoustically more distant from the surface, thus imposing a limitation for the nearfield analysis. If the specific acoustic impedance is used to characterize a surface then the measurement must be acoustically close. This only significantly effects the impedance. The intensities and energy densities still provide sufficient information at this distance from the surface.

7.3. Nearfield of a Circular Disc

This example presents measurements which were made around a circular disc, with a piston source 1.5λ from the disc, Figure 7.13. Two different discs were measured: (1) a rigid disc constructed of $\frac{3}{4}$ inch thick particle board and (2) an absorptive disc constructed of 8cm thick fiberglass. The measurements were made on a plane perpendicular to the disc and intersecting the disc symmetrically. The source is included in the plane so that the intensity does not have components normal to the measurement plane. A more complete analysis of this configuration would include a three dimensional measurements in the disc nearfield, especially over the surface and edge of the disc. However, for the purposes which this example serves for this thesis, the analysis is confined to the two-dimensional

REAL NORMAL IMPEDANCE



IMAGINARY NORMAL IMPEDANCE

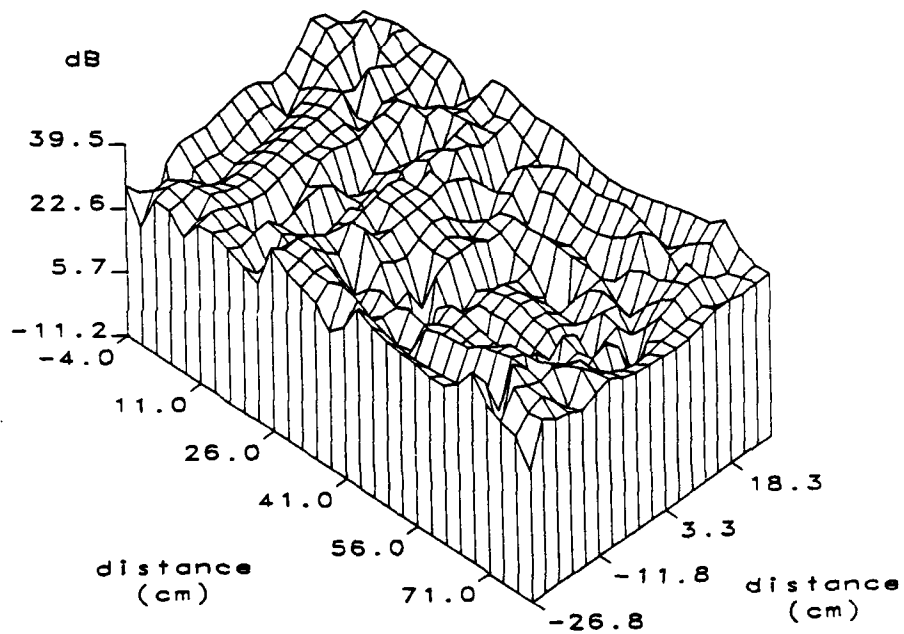


Figure 7.12 The real and imaginary parts of the impedance normal to the loudspeaker surface, measured at 2500Hz on a plane parallel to and 3.5cm above the loudspeaker surface.

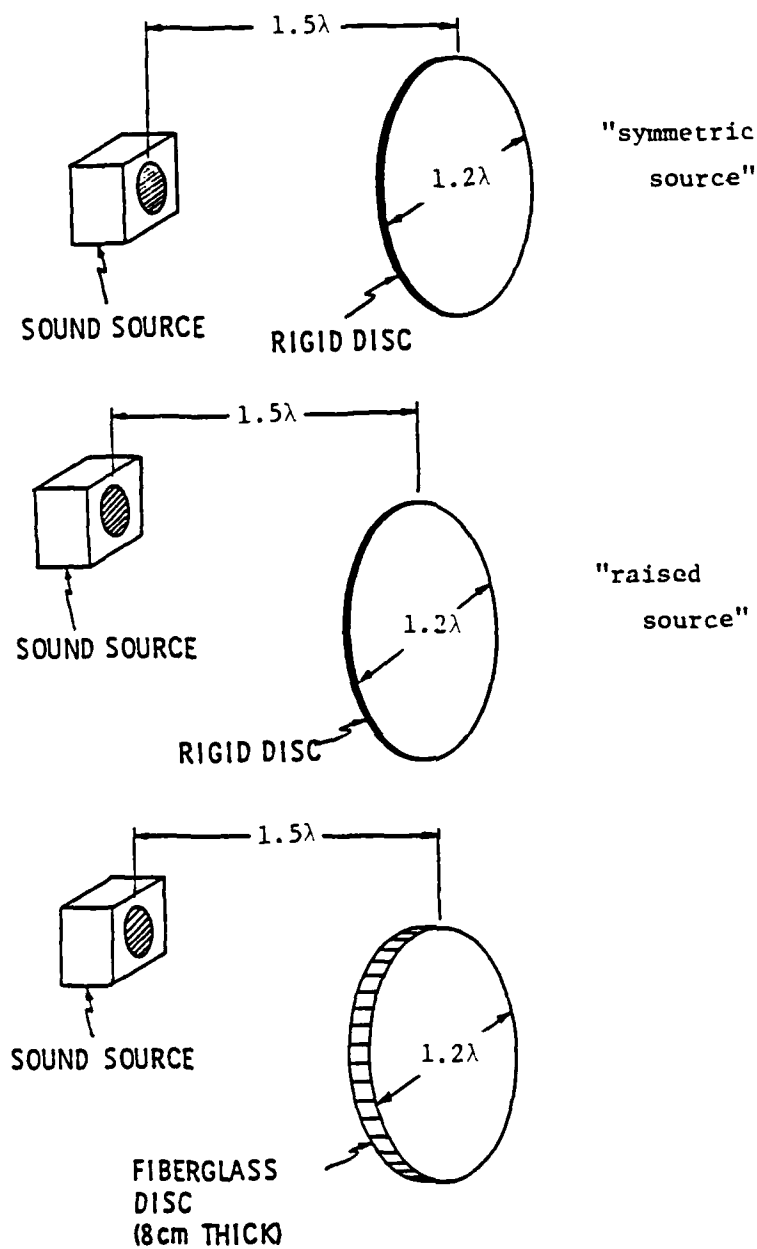


Figure 7.13 Sketches of the configurations for the disc diffraction measurements. The measurements were made at 1000Hz on a plane perpendicular to the disc and intersecting the source and disc symmetrically.

symmetric plane. The frequency is 1000Hz so that the relative disc size is 1.22λ and the measurement extends 0.8λ from the disc.

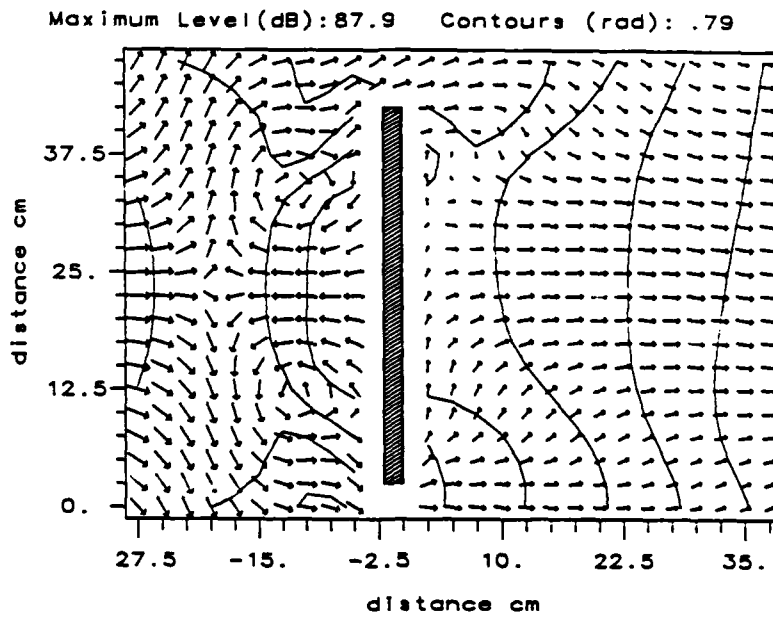
7.3.1. Rigid Disc

This first measurement demonstrates the beauty of the acoustic intensity measurement. For this example the source was positioned on the disc axis so that a full rotational symmetry was achieved. The active and reactive intensity are plotted in Figure 7.14 and the potential energy and phase speed are plotted in Figure 7.15. First look at the active and reactive intensity. There is no analytical solution to this source scatterer configuration in the nearfield. However, the active intensity shows the wave front propagation very clearly. The waves approach the disc then divert around the disc circling two points where the pressure is zero. These two formations are vortices which were explained in Section 4.5. The waves then combine on the shadow zone of the disc and propagate nearly as plane waves to the farfield.

The reactive intensity indicates a standing wave between the source and disc which arises from interference of the direct wave of the source and the wave reflected by the surface of the rigid disc. There is also a significant pressure gradient at the upper and lower edge of the disc facing the source. In the shadow zone there is a standing wave which consists of a horizontal pressure maximum and minimum caused by the interference of energy coming over the top and bottom of the disc. Consequently, the reactive intensity shows that the region on the source side of the disc has a vertical standing wave and in the shadow zone has a radial standing wave.

It was noted that there is a pressure maximum at the corners of the disc edge facing the source. The pressure maximum is seen in the reactive intensity which points away from these corners. The area to focus on is outlined on the

ACTIVE INTENSITY & WAVEFRONTS



REACTIVE INTENSITY

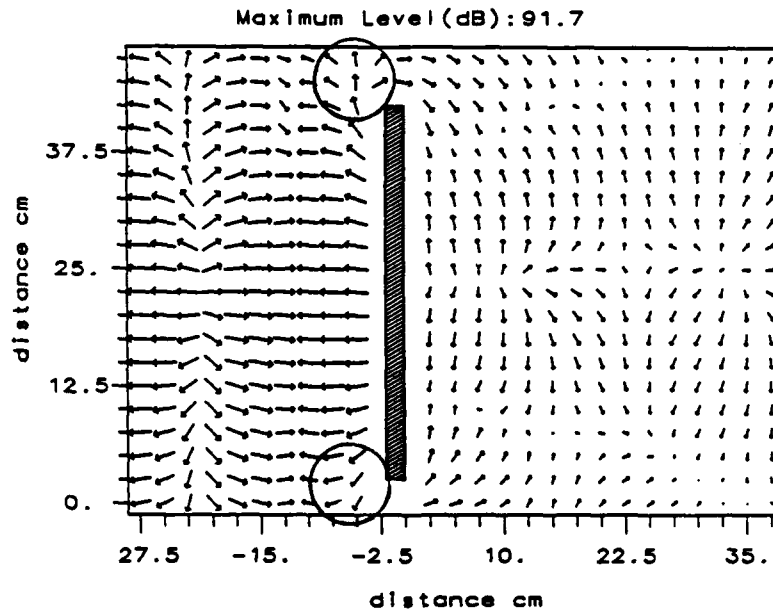
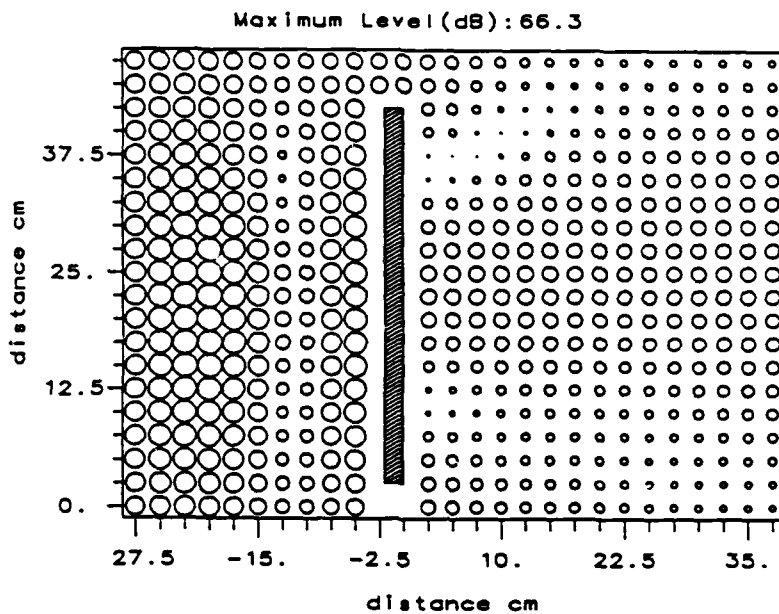


Figure 7.14 The active intensity and wave fronts and the reactive intensity measured at 1000Hz on a plane perpendicular to the rigid disc. The source is 1.5λ to the left, positioned symmetrically with respect to the disc center.

POTENTIAL ENERGY



RESULTANT PHASE SPEED

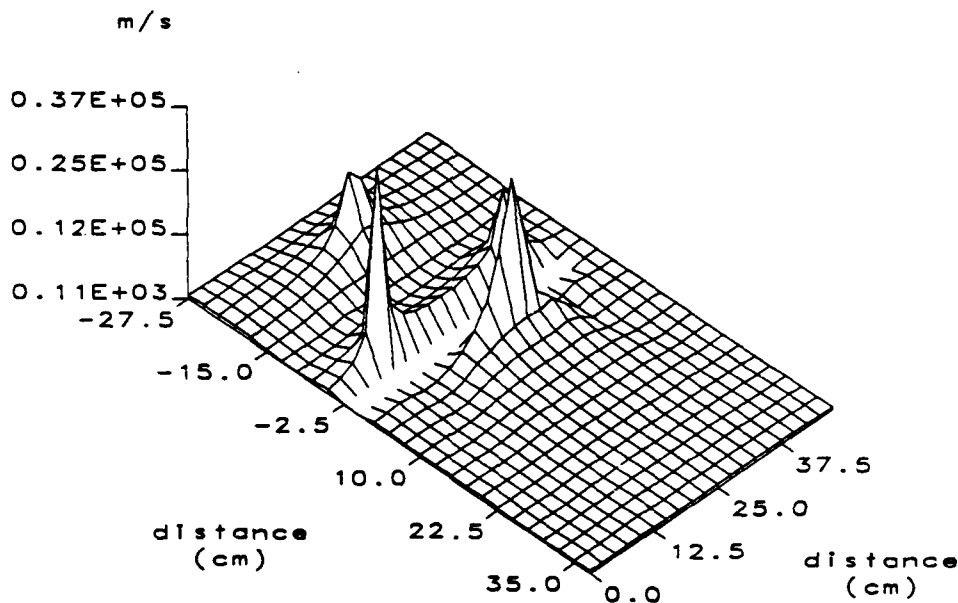


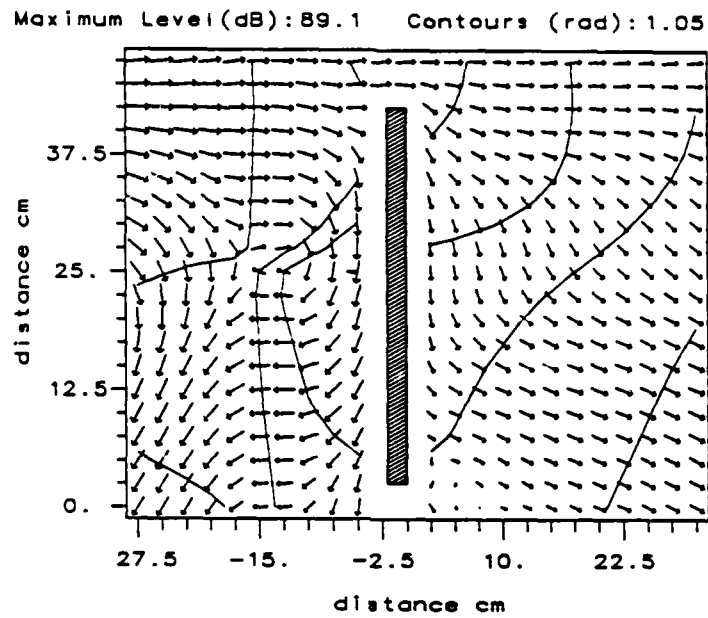
Figure 7.15 The potential energy and resultant phase speed measured at 1000Hz on a plane perpendicular to the rigid disc. The source is 1.5λ to the left, positioned symmetrically with respect to the disc center.

reactive intensity plot, Figure 7.14. The edge represents a sharp discontinuity between the rigid wood and the air. These measurements indicate that the effect of the discontinuity is most significant on the corners of the edge facing the source, compared to the corners of the edge facing the shadow zone. They also indicate that the wave propagation is not as dramatically effected as the pressure distribution so that the reactive intensity most readily identifies this diffraction effect. In essence, the kinetic energy associated with the diffraction is that which is due to the component of velocity which is out of phase with pressure, U_r . To control this diffraction in the nearfield it seems that the abrupt impedance change at the edge facing the incident sound needs to be reduced with absorption or by rounding the edge. This will have more effect than treating the edge in the shadow zone.

Measurements were also made with the source raised to the level of the disc top. The active and reactive intensity are plotted in Figure 7.16 and the potential energy and phase speed are plotted in Figure 7.17. As with the previous configuration there is a vertical standing wave between the source and the disc with a wave circulating a pressure zero point. Also, in the shadow zone there is a horizontal standing wave which is shifted because of the new source position.

Once again, the diffraction at the corners of the edges facing the source is clearly visible. The diffraction is best compared with the case of the symmetric source by using the acoustic impedance. Figure 7.18 contains the numerical values of the real and imaginary parts of the impedance close to the disc surface for the symmetric and raised source position. The real part of the impedance just beyond the disc edge is 1 dB lower compared to the level at the disc edge. For the symmetric source the imaginary part of the impedance just beyond the disc edge is 3 to 4 dB lower compared to the level at the disc surface. Similarly, with the raised source the imaginary part of the impedance decreases by 4 to 6

ACTIVE INTENSITY & WAVEFRONTS



REACTIVE INTENSITY

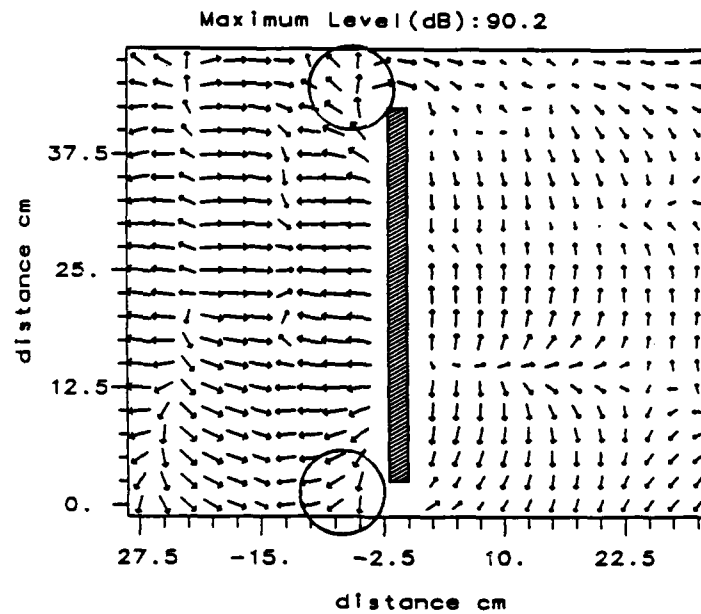
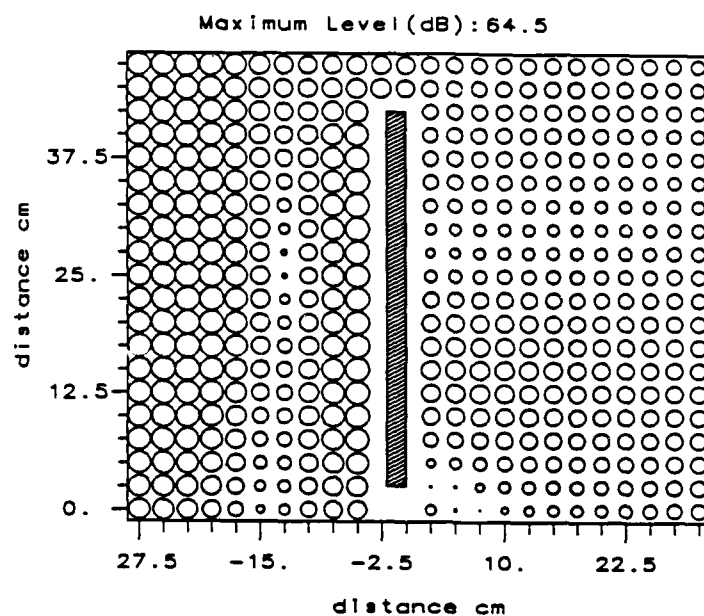


Figure 7.16 The active intensity and wave fronts and the reactive intensity measured at 1000Hz on a plane perpendicular to the rigid disc. The source is 1.5λ to the left, along a line extending from the disc top.

POTENTIAL ENERGY



RESULTANT PHASE SPEED

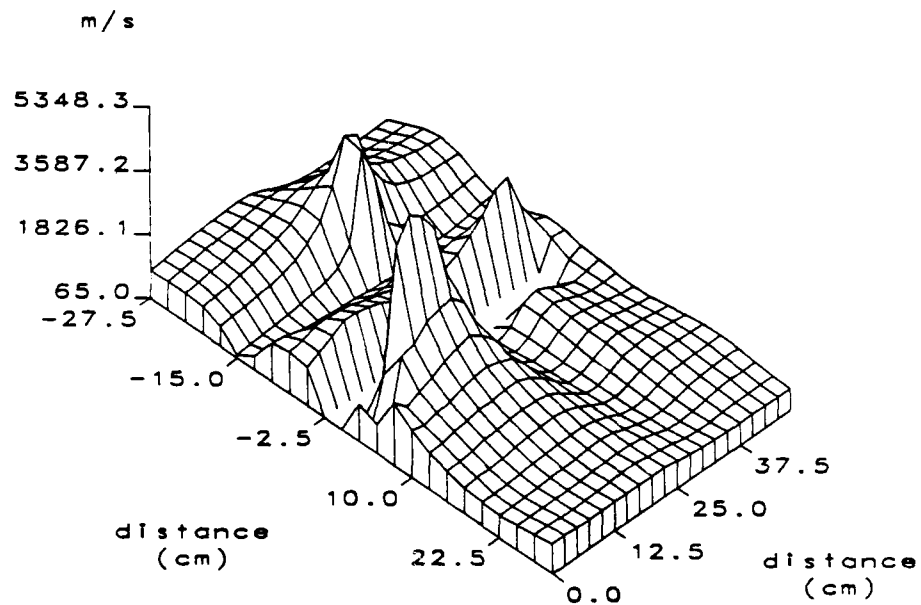
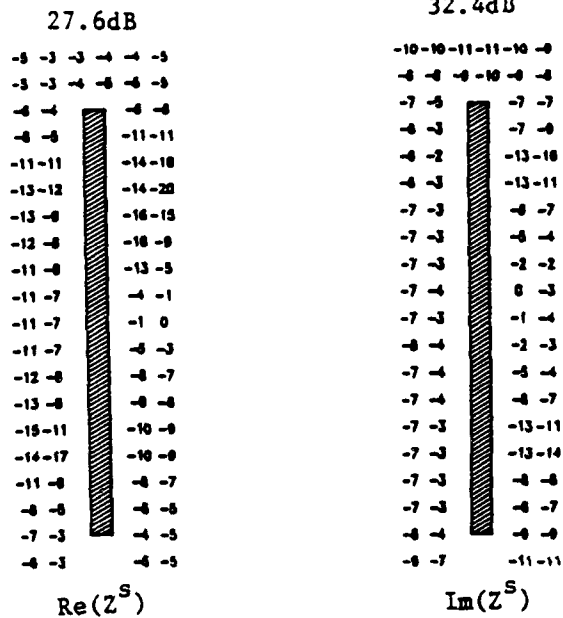


Figure 7.17 The potential energy and resultant phase speed measured at 1000Hz on a plane perpendicular to the rigid disc. The source is 1.5λ to the left, along a line extending from the disc top.

Symmetric Disc



Raised Disc

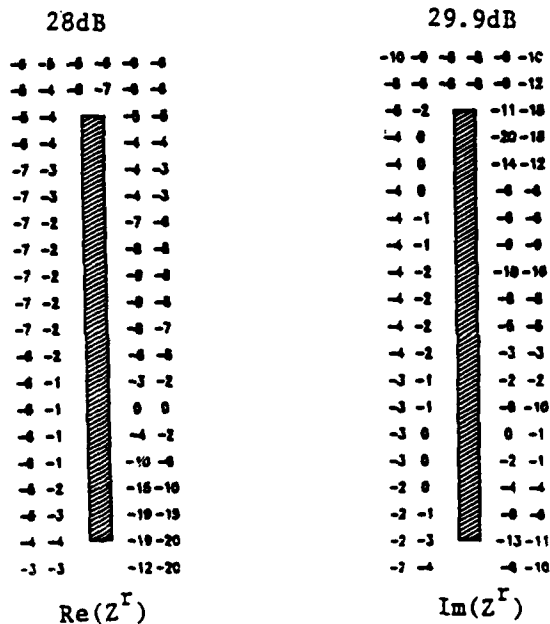


Figure 7.18

The real and imaginary parts of the total impedance around the disc. The top figures, Z^s , are for the rigid disc with the symmetric source position and the bottom figures, Z^r , are for the rigid disc with the raised source position. The numbers represent the dB level below the maximum level labeled above each plot.

dB beyond the top and 2 to 3 dB beyond the bottom. These results further show that the imaginary part of the impedance is greatly influenced by diffraction. Also there is more diffraction at the top of the disc than the bottom when the source is raised to the level of the disc top, and the diffraction with the symmetric source is between these two extremes.

The distance of the source to each edge is one possible cause of the variation of the diffraction at the two edges for the two source positions. When the source is raised to the level of the top edge, the distance of the source to the top edge is 51.5cm and to the bottom edge is 65.2cm. With the symmetric source position the distance to the two edges is 55.2cm. The amount of diffraction increases as the source to edge distance decreases. However, this is not a likely cause of the variation in diffraction. The various source distances would only change the amplitude of the incident wave; however, the impedance is not effected by the amplitude of the incident energy.

The appropriate explanation for the variation in the diffraction is the angle of incidence of the incident wave, which is the other major geometric variable in these measurements. The incident angle is 90 degrees with respect to the top edge with the source raised, 69 degrees with respect to both edges with the symmetric source position, and 52 degrees with respect to the bottom edge with the source raised. Thus, the diffraction increases as the incident angle increases toward 90 degrees. Physically this corresponds to a greater proportion of the incident energy being normal to the impedance discontinuity between the rigid disc and the air. These results are identical to those for the diffraction at the outer edge of the loudspeaker box.

This explanation can be further verified by comparing the direction of the active and reactive intensity at the various edges. First consider the top edge for the raised source. The wave fronts propagate past the edge, thus the active

intensity is perpendicular to the disc plane even above the disc top. However, the reactive intensity points away from the corner of the top edge facing the disc, thus the energy concentration created by the edge discontinuity must propagate away from the edge via the reactive intensity. For the symmetric source configuration there is a greater portion of the total energy parallel to the disc surface contained in the active intensity rather than the reactive intensity. Then with the raised source, the active intensity at the bottom edge is almost parallel to the disc surface so there is less energy associated with the reactive intensity due to the diffraction.

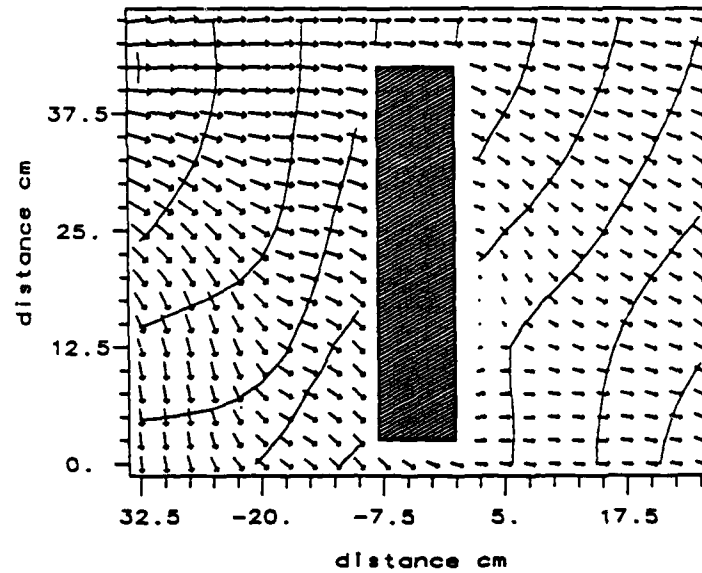
7.3.2. Fiberglass Disc in an Anechoic Room

The diffraction by a fiberglass disc was measured to show a strong contrast to the rigid disc measurements. The fiberglass disc was 8cm thick and of the same diameter as the rigid disc. The source was situated along a line extending from the top of the disc. The other parameters such as the frequency, source distance, and measurement plane were the same as with the rigid disc. The active and reactive intensity are plotted in Figure 7.19 and the potential energy and the phase speed are plotted in Figure 7.20.

First consider the region between the disc and source. The reactive intensity shows a standing wave, which has a minimum closer to the disc than the rigid case because of the impedance of the fiberglass disc. There are no pressure zeros so the active intensity does not indicate any vortices, but shows the power flux and wave propagation into the disc. Compared with the rigid disc, the active intensity level remains approximately the same, but the reactive intensity is reduced by 3 dB. It is interesting to note that the partial standing wave between the source and the disc is still present because the fiberglass does indeed reflect some energy.

ACTIVE INTENSITY & WAVEFRONTS

Maximum Level (dB): 89.7 Contours (rad): .79



REACTIVE INTENSITY

Maximum Level (dB): 87.3

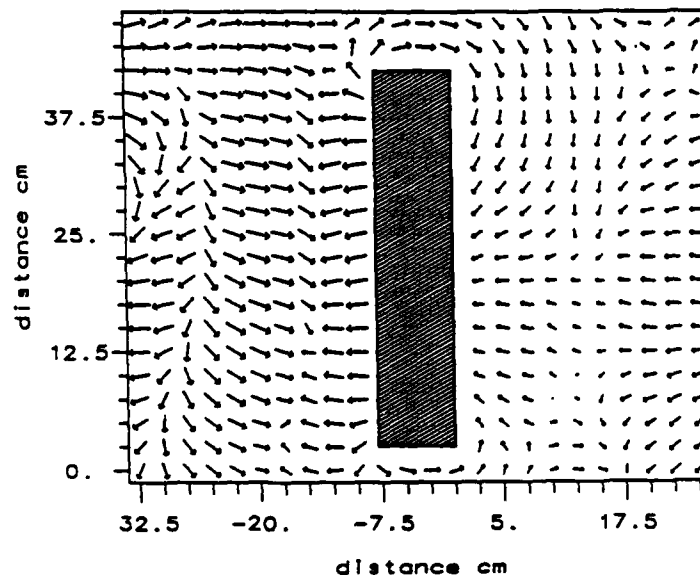
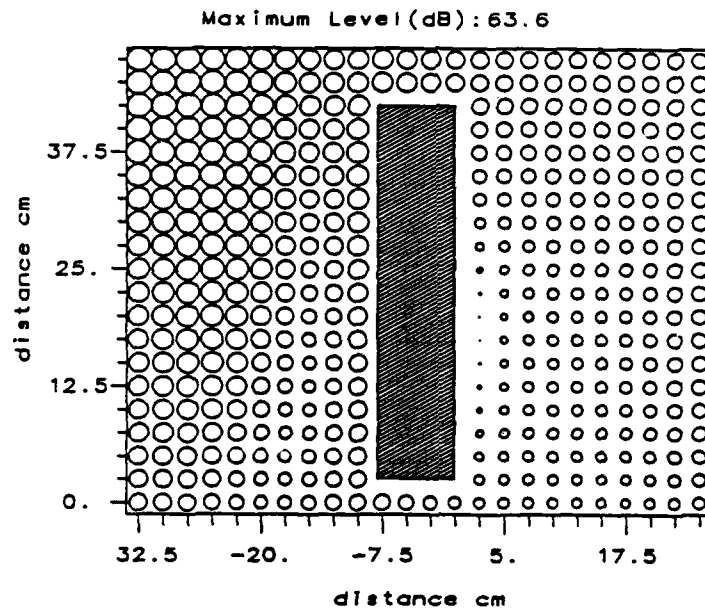


Figure 7.19

The active intensity and wave fronts and the reactive intensity measured at 1000Hz on a plane perpendicular to the 8cm thick fiberglass disc. The source is 1.5λ to the left, along a line extending from the disc top.

POTENTIAL ENERGY



RESULTANT PHASE SPEED

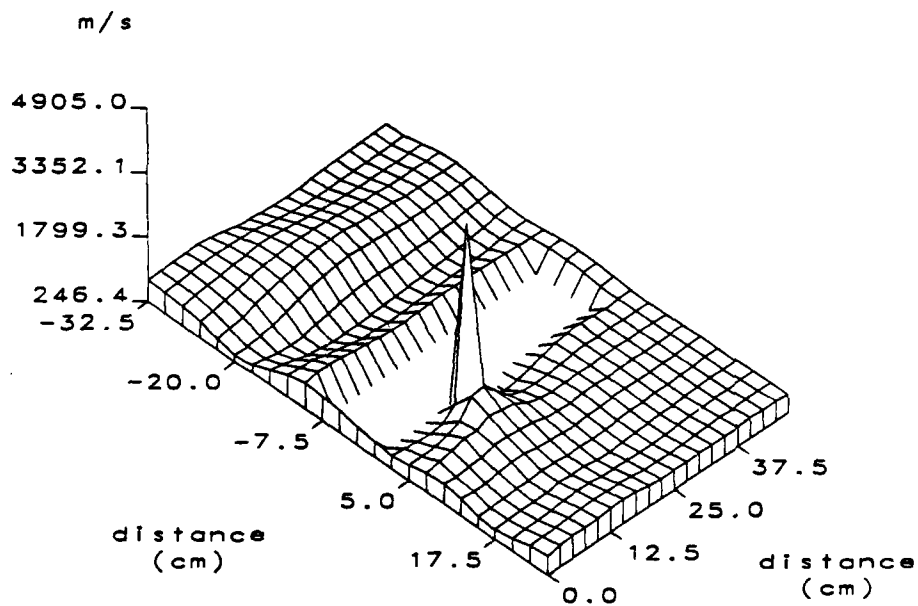


Figure 7.20 The potential energy and resultant phase speed measured at 1000Hz on a plane perpendicular to the 8cm thick fiberglass disc. The source is 1.5λ to the left, along a line extending from the disc top.

At the disc edge facing the source there is a diffraction which appears to be the same as that seen with the rigid disc. However, the reactive intensity indicates that the diffraction does not extend as far from the edge as with the rigid disc. This is expected because of the lower impedance of the fiberglass. The numerical values of the real and imaginary part of the impedance is plotted in Figure 7.21. There is a rapid change in the imaginary part of the impedance; therefore, the pressure maxima at the edge. However, this rapid change is now only 2 to 3 dB which is smaller than the 4 to 6 dB seen with the rigid disc.

In the shadow zone the data is greatly different for the fiberglass and rigid disc. This is most apparent in the reactive intensity which points into the fiberglass. Consequently, there is a pressure minimum at the surface of the fiberglass; and no horizontal standing wave. This is due to the attenuation of the energy propagating around the disc. The only significant energy propagation parallel to the disc surface is near the edges and is seen only in the reactive intensity. The active intensity is pointing out of the disc, which indicates that much of this energy comes from waves propagating through the disc.

There is a large pressure and active intensity minimum at the face of the disc slightly below the center in the shadow zone. However, there is a significant amount of reactive intensity so the pressure gradient is high. This pressure minimum shows that the energy is highly attenuated as it propagates around the disc. The minimum is below the disc center because there is more energy coming over the top of the disc which is closer to the source. It is very interesting to note that at this region where the pressure and active intensity have a low level, the mechanism for the energy removal is the particle velocity associated with the the reactive intensity which points into the fiberglass. This is reasonable if we remember that there is energy propagation even if the active intensity is zero, as was shown in Chapter 2.

7.3.3. Fiberglass Disc in a Reverberant Field

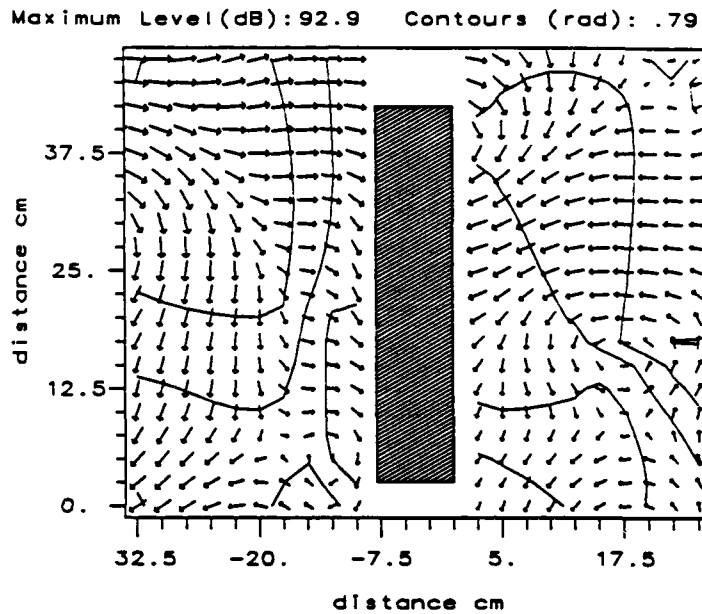
The measurements with the fiberglass were repeated with all the wedges removed from the room, thus creating a reverberant field. The reason for performing this measurement was to see what would happen with the energy associated with the active intensity which propagates away from the disc under anechoic conditions. The active and reactive intensity are plotted in Figure 7.22 and the potential energy and resultant phase speed are plotted in Figure 7.23.

Let us focus on two aspects of this measurement. First note that there is no significant diffraction at the disc edge. In the examples of the rigid disc we saw that the extent of diffraction at the top and bottom edge depended on the incident angle of the energy. In the reverberant room the energy is incident on the fiberglass disc edges at all angles so the diffraction is reduced.

The other important aspect of this measurement is the direction of the active intensity which points into the fiberglass. The reactive intensity indicates a build up of local energy due to the large spatial variation of the pressure in the reverberant conditions. Consequently, in these measurements the mechanism for energy propagation to the fiberglass resulting in energy dissipation is the active intensity.

7.4. Distinguishing Between Radiation and Diffraction

This last example investigates the acoustic field above a circular plate in the shadow zone of a rigid disc. The configuration is sketched in Figure 7.24. The plate is constructed of $\frac{1}{4}$ inch thick aluminum and is fixed at its edge. The plate was intended to be a rigid surface so that the diffraction around the rigid disc and the plate and supporting structure could be studied. However, the plate can be excited by the incident sound. The ensuing sound radiated by the plate vibration would disrupt the intended of investigation of diffraction alone.



REACTIVE INTENSITY

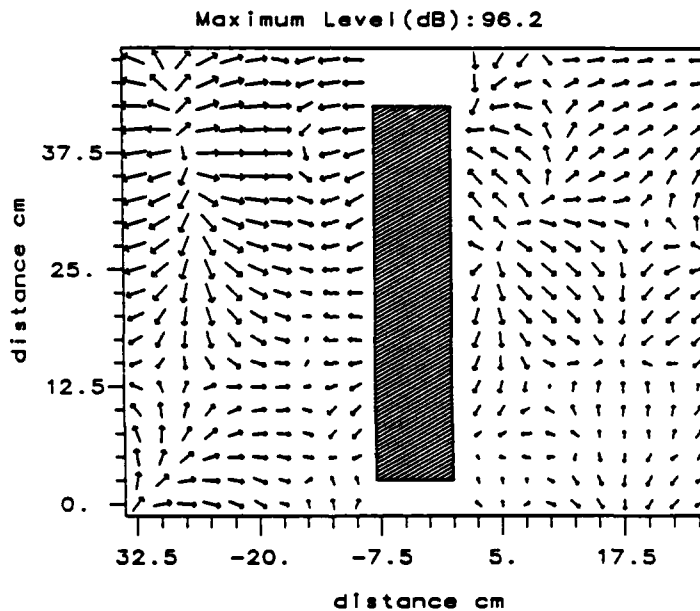
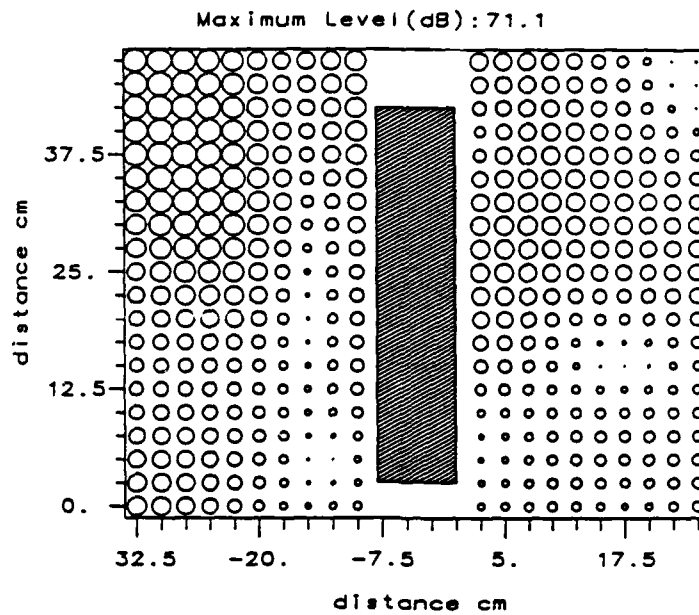


Figure 7.22

The active intensity and wave fronts and the reactive intensity measured at 1000Hz on a plane perpendicular to the 8cm thick fiberglass disc. The source is 1.5λ to the left, along a line extending from the disc top. The measurements were made in reverberant conditions.

POTENTIAL ENERGY



RESULTANT PHASE SPEED

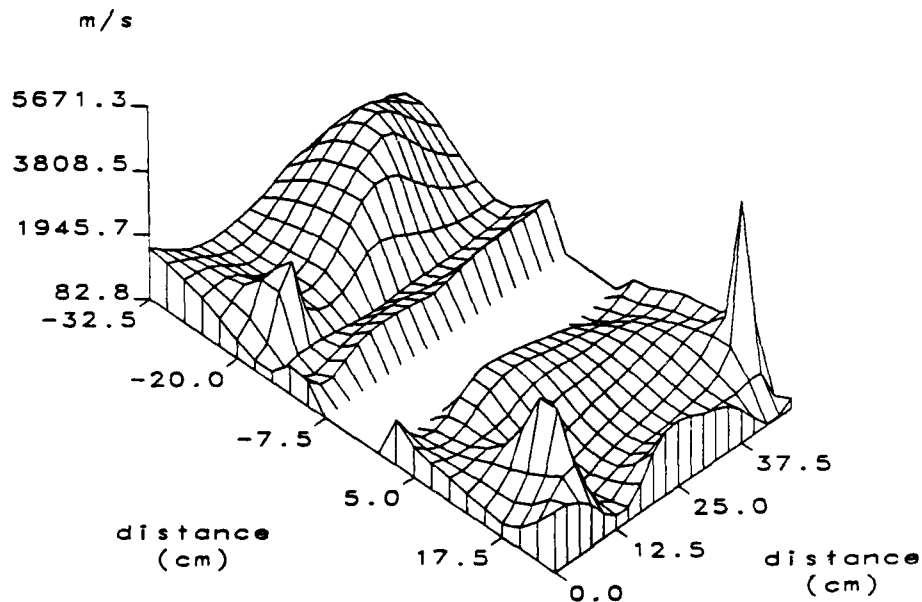


Figure 7.23 The potential energy and resultant phase speed measured at 1000Hz on a plane perpendicular to the 8cm thick fiberglass disc. The source is 1.5λ to the left, along a line extending from the disc top. The measurements were made in reverberant conditions.

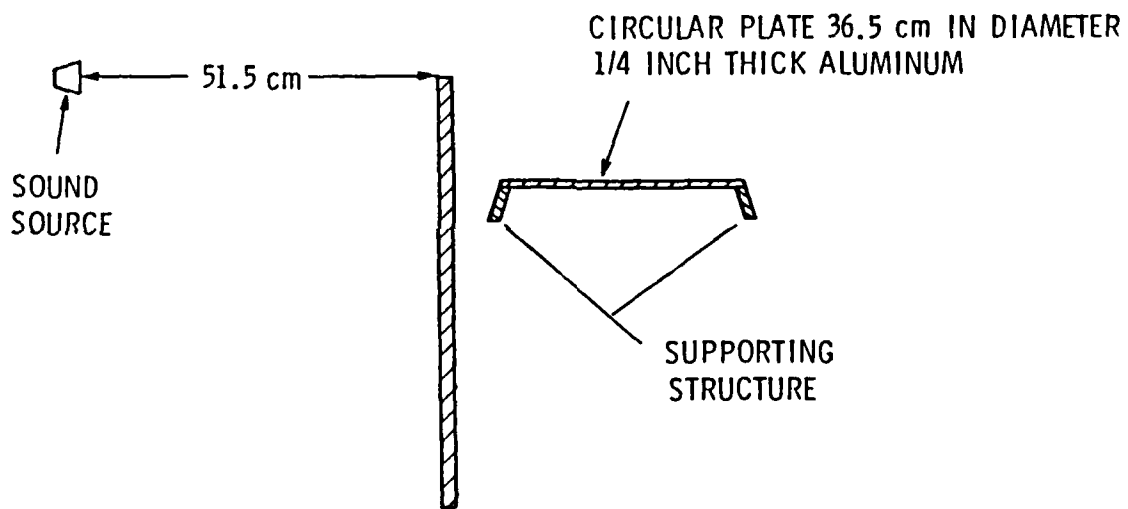


Figure 7.24

A sketch of the symmetric cross section of the measurement configuration with circular plate and supporting structure in the shadow zone of a rigid disc.

Consequently the following measurements were made to indicate the influence of the plate vibration on the acoustic nearfield of the diffraction.

The plate and supporting structure was placed near a loudspeaker radiating pink noise. The acceleration on the plate and the supporting structure, measured with an accelerometer, is plotted in Figure 7.25. The resonant response of the plate is 20dB to 30dB larger than the vibration of the supporting structure. Therefore, attention can be focused on the resonances of the plate because of the weak coupling between the plate and supporting structure. Constrained layer damping was applied to the plate, which reduced the vibration level at resonance frequencies by about 5dB.

To estimate the sound radiated by the vibration of the plate with the constrained layer damping, a crude measurement was made with the plate positioned behind the rigid disc, Figure 7.24. By placing a hand on the plate the vibration levels at resonance could be reduced by 10 dB. The pressure 2cm above the top plate was measured with a hand touching the plate. Then the hand was lifted off the plate but with the hand in essentially the same location so the diffraction was not altered. The small variation in pressure indicated that the radiated pressure at a resonance of the plate was 10 to 15 dB below the level of the diffracted field. The intensity measurements were performed at anti-resonances of the top plate vibration so it was considered safe to assume that the sound radiated by the sphere vibration is 20 to 25 dB below the level of the diffracted sound which we wanted to measure.

However, the intensity measurements lead us to believe that the vibration of the plate is indeed significant. This question is raised by the results at 1930Hz, Figure 7.26, and 2570Hz, Figure 7.27. These figures show an expanded section above the plate. The measurements were made on the symmetric axis of the

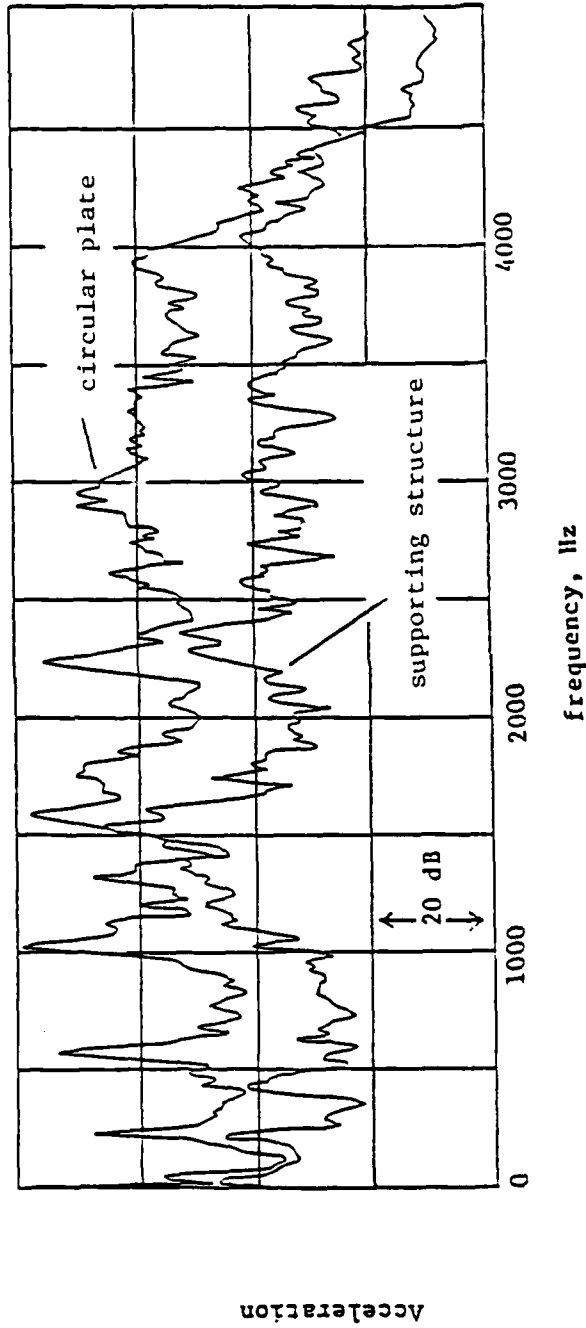


Figure 7.25 The response of the truncated sphere surface vibration when excited by pink noise from a loudspeaker 25cm from the truncated sphere.

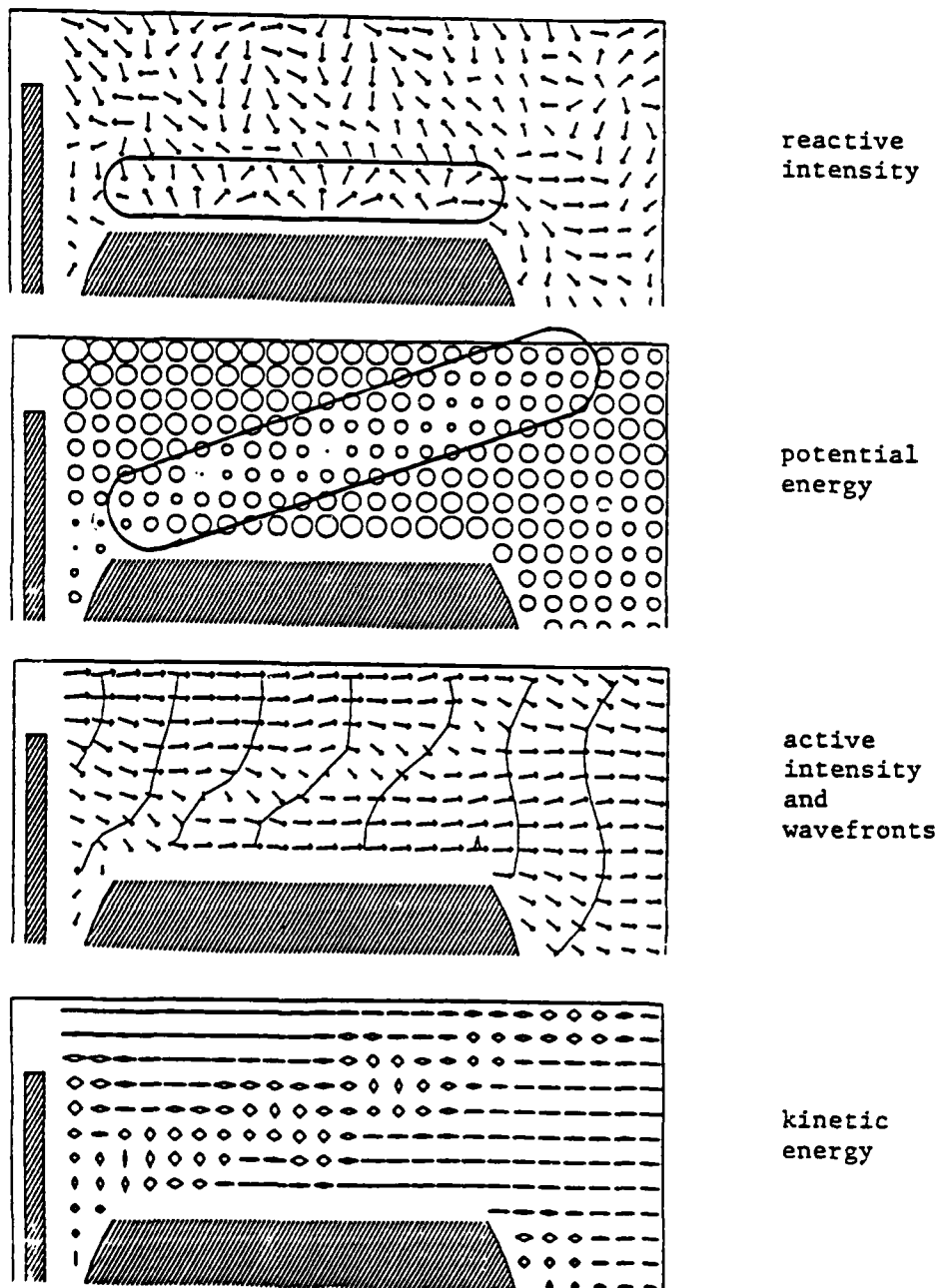


Figure 7.26 An expanded view of the measurement over the plate in the shadow zone of a rigid disc. The frequency is 1930Hz and the source is 53cm (3λ) to the left of the disc top.

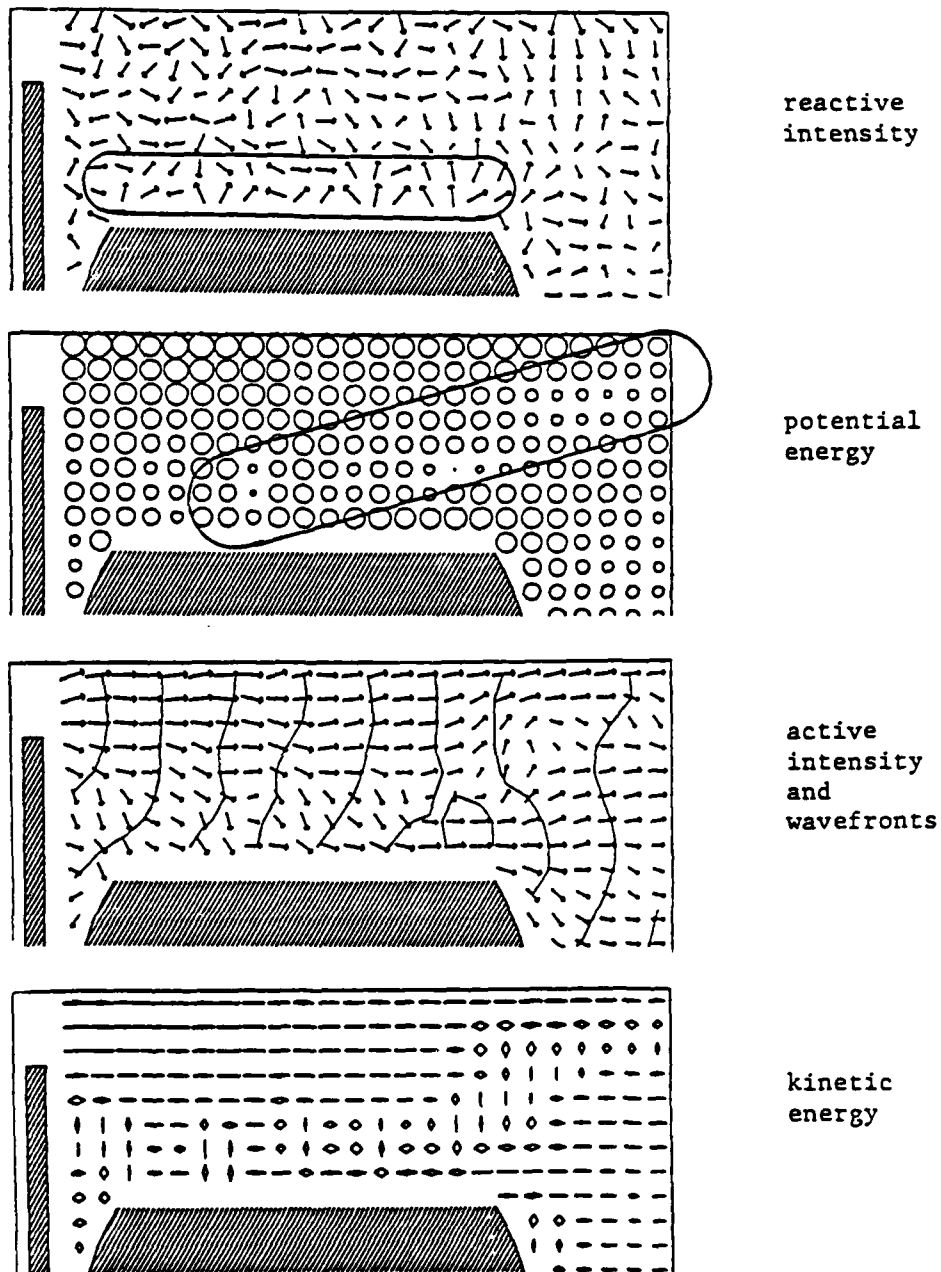


Figure 7.27 An expanded view of the measurement over the plate in the shadow zone of a rigid disc. The frequency is 2570Hz and the source is 53cm (4λ) to the left of the disc top.

source, disc, and truncated sphere which is a plane perpendicular to the face of the rigid disc and includes the source and slices the truncated sphere in half.

Careful inspection of the reactive intensity just above the top plate reveals areas of pressure maxima and minimum. These regions are circled in the plots. The reactive intensity has been proven useful by Degeorges and Tichy (1986), to locate areas of maximum vibration on rectangular plates so that the mode shape of the plate is readily visualized. In general, areas of maximum pressure directly above a vibrating structure will correspond to areas of maximum surface vibration. Thus, the reactive intensity pattern which is circled can be interpreted to indicate the modes of vibration of the top plate. The pattern is very symmetric with respect to the top plate so it seems very possible that a mode of the plate is significantly excited.

An alternative cause for this pressure distribution is to consider a simple model of the energy propagating over the top of the disc interfering with the energy reflected by the top plate. This is schematically drawn in Figure 7.28. This model does explain the pressure minima and maxima which are circled in the potential energy plots. However, the paths are not consistent with half wavelength distances which would cause the pressure reinforcement and cancellation which the reactive intensity indicates directly above the top plate. Thus this simplified explanation is inadequate.

The definitive measurement which should have been made was on a plane parallel to the top plate surface, which would have been a three dimensional measurement. This should indicate a mode shape of the top plate if there is significant vibration. However, this measurement could not be made for technical reasons. If the measurement indicates a mode shape then the active intensity can be used to calculate the power radiated by the top plate. For a preliminary indication Figures 7.26 and 7.27 can be used. At 1930Hz the active intensity

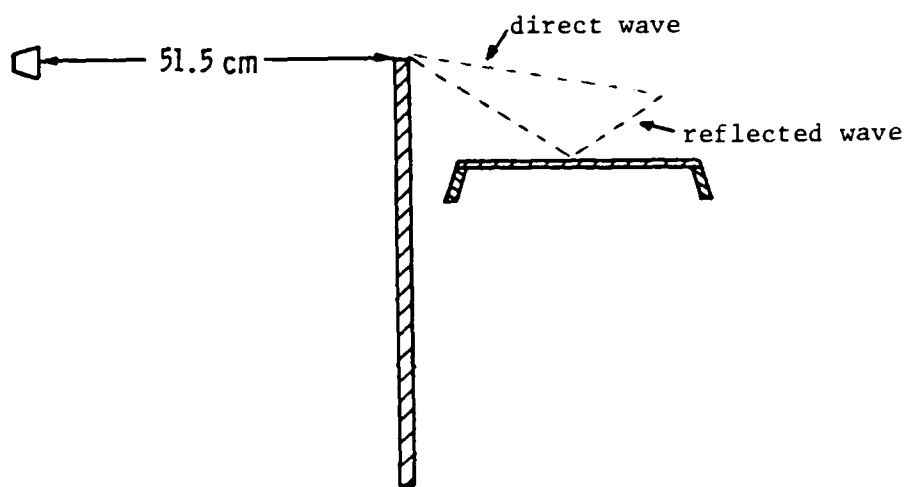


Figure 7.28 A schematic for interference of a direct wave over the disc top and a wave reflected from the truncated sphere top plate.

is parallel to the plate so there is only a negligible power flux from the plate. Likewise at 2570Hz a small amount of power goes into the plate, which would indicate that the plate is absorbing rather than radiating power. However at 2570Hz the closest measurement point is $\frac{\lambda}{3}$ from the plate surface so this may not be a valid indication of the power flux at the plate surface. These results lead to the conclusion that the plate is radiating no power.

Before concluding that the reactive intensity pattern is due to a diffraction effect, we must consider the nature of the plate vibration. The coincidence frequency of this plate is roughly 19,000Hz. The measurement frequencies are far below the coincidence frequency, so the plate is radiating very little power. Any acoustic energy radiated by the plate would be confined to the nearfield reactive intensity. This analysis agrees with the measurements. The radiated pressure may also be very small so that the simple measurement described earlier in the section would not indicate the extent of the plate vibration. However, as we have seen throughout this work, the reactive is sensitive to small pressure variations, so that in these measurements the reactive intensity indicates the extent of the non-radiating nearfield of the plate vibrations. Therefore, by considering the reactive intensity we can conclude that the plate is being excited by the incident sound field and cannot be assumed rigid.

Chapter 8

SUMMARY, CONCLUSIONS AND RECOMMENDATIONS

8.1. Summary and Conclusions

To effectively utilize the acoustic intensity in the nearfield, the physical interpretation of wave phenomena must be extended beyond the simple farfield or plane wave properties. The conceptions of wave motion are equally valid in the nearfield, but the wave shape and propagation speed vary. Consequently, a description of the energy propagation must include phenomena other than the motion of the wave front.

A general form was assumed for the pressure so that the intensity vectors could be linked to physical phenomena. The inter-dependance of the pressure amplitude and phase distribution are expressed by two non-linear differential equations. Since the waves, in general, travel at speeds other than c , there is a non-uniform pressure amplitude distribution which is described by the differential equations. The pressure gradient signifies that there is reactive intensity, thus the wave structure moves at speeds other than c , because there is energy propagating associated with the reactive intensity.

The energy propagation, in the direction of the instantaneous intensity, is in general not perpendicular to the wave fronts. Consequently, in general, the energy does not propagate with the wave fronts. This was clearly shown with instantaneous intensity flux lines with paths dramatically different than the wave front propagation. However, it is not practical to use the instantaneous intensity to investigate a sound field, because there is not one path on which the energy propagates at all times.

The time-independent intensity vectors were linked to fundamental concepts of wave motion. The active intensity is perpendicular to the wave fronts and the general phase speed is calculated from the active intensity and potential energy. Contrary to the farfield, the wave shape and speed changes as it propagates. The pressure amplitude variation in space is described by the reactive intensity which points in the direction of decreasing pressure.

The active intensity vortex is an interesting example which combines the concepts of energy propagation and wave front propagation. The vortex is centered at a point or line of zero pressure which also corresponds to a discontinuity in the pressure phase. At the phase discontinuity, different surfaces of constant phase intersect, so the vortex represents a wave propagating around the line or point of zero pressure. Three arguments were presented which concluded that the energy propagates through the vortex rather than being trapped by the vortex.

The capability of using the intensity measurements to analyze sound fields is the most important reason for developing the physical interpretations of the intensity vectors. The five measured examples explored several fundamental phenomena, i.e. sources, absorption, diffraction, source-resonator interactions, and the extended length of a resonating tube. The fundamentals of the phenomena are well understood. In the past these phenomena were not measured directly, but they were implied to be the cause of the results observed in the farfield. However, the nearfield measurements in this thesis gave a clear visualization of the phenomena and showed how the intensity measurements can be used to investigate more complicated phenomena.

The first measurement investigated the interaction of two pistons in a baffle with a resonating tube between them. The tube was tuned to a one-quarter wavelength resonance of 200Hz. Measurements were performed at two of the

tube resonances, 200Hz and 600Hz, and at a tube anti-resonance, 400Hz. The significant conclusions from these measurements were (1) the reactive intensity gave a visualization of the extended tube length, (2) a deep minimum in the imaginary part of the normal impedance identified the tube resonance, (3) sharp minima in the imaginary part of the normal impedance identified diffraction around the tube edge at the tube anti-resonance, and (4) a through analysis allowed absorption to be differentiated from sources.

The second source example investigated the variation in the radiated power of a simple source as a function of the height of the source above a rigid boundary. The measured radiation impedance basically agreed with the change in the radiated power. The few discrepancies which were observed between the power and impedance measurements were due to the pressure and velocity being nearly ninety degrees out of phase, which corresponds to a high reactive intensity. It turned out that the measurement error was not due to the phase errors in the probes, but due to the phase errors between the processing of the pressure and velocity in the real time one-third octave analyzer which was used for this one measurement.

This measurement was significant in two aspects because it pointed out the potential problem with using this type of instrumentation. A real time analyzer will often only display the pressure, active intensity, and the particle velocity. However, the reactive intensity and the real and imaginary parts of the impedance can be calculated from this limited information. The second important aspect was that with a real time analyzer the separate electric circuits which calculate the pressure and velocity need to be carefully phase matched. This is not a problem with FFT processing, and is only a concern with real time analyzers in the presence of high reactive intensity levels. This is significant because intensity measurements are most often made near to a sound source where the reactive

intensity is commonly 5dB to 10dB above the active intensity. Thus, care must be taken to insure phase matching throughout the real time analyzer if the analyzer is going to be used for nearfield measurements.

The next series of measurement investigated diffraction which can only be identified with nearfield measurements. Diffraction was localized in the nearfield of a loudspeaker using the reactive intensity and the imaginary part of the normal impedance. Diffraction was also studied at the edge of a circular disc. A rigid disc and an absorptive disc were contrasted along with two source positions. The combined analysis with the loudspeaker showed that the diffraction depended on the incident angle of the energy at the impedance discontinuity which caused the diffraction. More importantly, these measurements demonstrate that to localize diffraction, the measurements must be made acoustically close to a structure.

The final example further shows the need to use more than one quantity to entirely characterize the sound field. A plate like structure which was being excited by an incident sound field was analyzed. The reactive intensity indicated that the structure was vibrating in a mode, but the active intensity showed that no power was being radiated. However the measurement frequencies were far below the coincidence frequency of the plate, so the vibration radiates very little power. The reactive intensity identified the plate vibration because the energy was confined to the nearfield of the plate.

All the measurements demonstrated that the analysis of intensity measurements must consider all available quantities along with a detailed knowledge of the source being investigated. Table 8.1 summarizes how the active intensity, reactive intensity, energy densities, and specific acoustic impedance can be used to locate and distinguish between vibration sources, resonance, and diffraction.

Table 8.1 A summary of the distinguishing characteristics of active intensity, reactive intensity, potential energy, kinetic energy, and real and imaginary parts of the specific acoustic impedance near vibration sources, resonators, and diffraction.

Measured Quantity	Vibration Sources	Resonators	Diffraction
\bar{I}	local maximum points in or out	local maximum points in	not greatly altered
\bar{Q}	local maximum points out	local maximum points in	points out
V	local maximum	local minimum	local maximum
T	local maximum	local maximum	local maximum
$Re\{Z_n\}$	local minimum	local minimum	sharp change
$Im\{Z_n\}$	local minimum	deep minimum	sharp change

Most sound sources are more complicated than the examples used in this thesis. However, the conclusions can be used to suggest a procedure to investigate more complicated sources.

Using the above conclusions, let us consider a measurement which would be made on a motor. The motor and its surrounding structure have areas of vibration, resonance in the motor enclosure, and diffraction by the surrounding structure. These features all contribute to the sound radiated to the farfield, where the separate contributions of these features cannot be identified. However, in the nearfield the active and reactive intensity will locate each feature. Then the features can be classified as vibration sources, resonators, diffraction, or interference effects. With such detailed information the optimum procedure to reduce the sound radiated to the farfield can be addressed.

8.2. Recommendations for Further Work

This thesis has been confined to monochromatic sound fields to establish a clear understanding of the active and reactive intensity vectors for the simplest case. However, the majority of applications concern broad band and impulse sources. Also many of the measurements in industry are made in one-third octave bands and octave bands.

The interpretations of concepts such as impedance and wave propagation are not clearly defined in broad band sound fields. These concepts were studied in this thesis by explicitly expressing the time dependence of a monochromatic sound field. Thus, in a monochromatic sound field the time dependent phenomena such as wave propagation and energy propagation could be developed from the time independent quantities which are measured. However, with broad band sound this mathematical link between the time independent and time dependent descriptions is lost, because the time dependence cannot be recovered after time averaging in a broad band sound field. Therefore, the interpretations of the intensity vectors must be extended to include multi-frequency signals.

Even at single frequencies the instantaneous intensity is not a plausible means to describe the propagation of acoustic energy. The time independent active intensity represents the wave front propagation and the time averaged power flux, but it does not describe the path or speed of energy propagation to the farfield. The group velocity is used in multi-frequency fields to quantify the average speed of energy propagation, but it is derived for the time averaged farfield. Consequently, the knowledge of the group velocity needs to be further developed to incorporate the time dependent process of energy propagation and the energy propagation in the nearfield.

A very interesting application of the nearfield acoustic intensity measurements is to combine the analysis with the structural intensity measurements. By measuring the energy in both the structure and the fluid, the energy propagation within the structure can be understood along with the coupling to the acoustic field. Such a combined analysis would be invaluable for large structures such as airplanes and ship hulls. However, before the analysis can be used on complicated structures, simple panels with ribs and varying supports must be studied.

Nearfield analysis of simple structures has been recently published (Williams, Dardy, and Finke 1985; Williams, Dardy, and Washburn 1987); however, the reactive intensity and impedance was not considered. Although the time averaged power balance between the structure and the sound field is adequately described by the active intensity, the coupling between the structure and the sound will be strongly influenced by the reactive intensity. Consequently, the reactive intensity and impedance must be included in the analysis

Throughout the measurement examples the distance of the measurement plane to the surface being investigated had the greatest effect on the impedance measurements. This was especially important when the intent of the measurement was to represent the impedance at the surface. When the measurement distance was greater than $\frac{\lambda}{4}$ the impedance was greatly affected by the variations in the acoustic field above the surface. Consequently, the impedance on the measurement plane was not a good representation of the impedance at the structure surface. A greater number of measurements should be performed to establish the required measurement distance from a structure radiating sound for the measured impedance to be an accurate representation of the impedance at the structure surface.

The reactive intensity is mainly concentrated in the nearfield of an acoustic source, so that the power radiated to the farfield is quantified by the active

intensity alone. However, if an operator of a machine is in the acoustic nearfield then the reactive intensity may be significant. So this energy needs to be quantified in a convenient manner. Rather than expressing the output power of a source, a complex source strength combined with a directivity function may be more useful. This would quantify the power radiated to the farfield and the reactive intensity in the nearfield.

The pressure phase distribution can be calculated from the time independent active intensity and potential energy. The pressure amplitude and phase as a function of space can be used for acoustic holography. Thus holography measurements can be performed using a single intensity probe. Single pressure microphone holography can be performed, but the relative pressure phase at each measurement point must be carefully monitored with a reference microphone or with direct reference to the vibration of the source. Using the intensity technique no such monitoring is required.

A velocity sensitive probe would greatly increase the usefulness of the intensity technique because the signal processing would be much easier and a larger frequency range could be measured. There is one probe built by Norwegian Electronics which uses ultrasonic doppler shifts to measure the particle velocity. However this probe is large. Recent developments by Josserand and Maerfeld (1985) showed the use of a piezoelectric material, PVDF, for a velocity sensitive hydrophone, which simultaneously measures the pressure and velocity. This material also works in air. This is a very promising material and should be explored in greater detail.

Measuring the particle velocity directly with a laser should also be investigated. The laser only measures the particle velocity, but the pressure can be calculated using the equation of continuity which equates the pressure to the spatial derivative of the particle velocity. This is the direct analog of using the

Euler's equation to calculate the particle velocity from the spatial derivative of the pressure. The tremendous advantage of a laser based intensity system is that there is no probe which would disturb the acoustic field. Likewise, the measurements can be made much closer to a surface than the two microphone probe. Further, it is possible to simultaneously measure three spatial components of the particle velocity.

REFERENCES

- Biot, M. A., "General theorems on the Equivalence of Group Velocity and Energy Transport." *Physical Review*, 105(4), pp. 1129-1137 (1957).
- Bjor, O. H., "Sound Intensity Measurements in the Air and on the Surface." *Proc. 2nd International Congress on Acoustic Intensity, Senlis (France)*, pp. 11-16 (1985).
- Degeorges, J. F., and Tichy, J., personal communication (1986).
- Elko, G. E., "Frequency Domain Estimation of the Complex Acoustic Intensity and Energy Density." Ph.D. Thesis, The Pennsylvania State University (1984).
- Elko, G. E., "Simultaneous Measurement of the Complex Acoustic Intensity and Acoustic Energy Density." *Proc. 2nd International Congress on Acoustic Intensity, Senlis (France)*, pp. 69-78 (1985).
- Fahy, J. F., "Measurement of Acoustic Intensity Using the Cross-Spectral Density of Two Microphone Signals." *J. Acoust. Soc. Am.*, 62(4), pp. 1057-1059 (1977).
- Imaichi, K., and Ohmi, K., "Numerical Processing of Flow-Visualization Pictures - Measurement of Two-Dimensional Vortex Flow." *J. Fluid Mech.*, 129, pp. 283-311 (1983).
- Jackson, J. D., *Classical Electrodynamics*. John Wiley & Sons, New York (1975).
- Josserand, M. A., and Maerfeld, C., "PVF2 Velocity Hydrophones." *J. Acoust. Soc. Am.*, 78(3), pp. 861-867 (1985).
- Junger, M. C., "Energy Exchange between Incompressible Near and Acoustic Far Field For Transient Sources." *J. Acoust. Soc. Am.*, 40(5), pp. 1025-1030 (1966).

Kelly, J. J., "A Generalized Approach to Acoustic Intensity." Institute of Sound and Vibration Research, Memorandum No. 669 (May 1986).

Kristiansen, U. R., "A Numerical Study of the Acoustical Intensity Distribution Close to a Vibrating Membrane." *J. Sound Vib.*, (Letters to the Editor), 76(2), pp. 305-309 (1981).

Kurtze, U. "Zur Entwicklung eines Gerates fur Komplex Schallfeldmessungen." *Acoustica*, 20, pp. 308-310 (1968).

Lahti, T., "Application of the Intensity Technique to the Measurement of Impedance, Absorption and Transmission." *Proc. 2nd International Congress on Acoustic Intensity, Senlis (France)*, pp. 97-104 (1985).

Lamb, H., "On Group-Velocity." *Proc. London Math. Soc.*, 2(1), pp. 473-479 (1904).

Mann, J. A., Tichy, J., and Romano, A. J., "Instantaneous and Time-Averaged Energy Transfer in Acoustic Fields." *J. Acoust. Soc. Am.*, 82(1), pp. 17-30 (1987).

Morse, P. M., and Feshbach, H., *Methods of Theoretical Physics*. Vol. I and II, McGraw-Hill Inc., New York (1953).

Morse, P. M., and Ingard K. U., *Theoretical Acoustics*. McGraw-Hill Inc., New York (1968).

Pascal, J. C., "Measurement of the Active and Reactive Intensity in Various Acoustic Fields." *Proc. of the Conference on Recent Developments in Acoustic Intensity Measurements, Senlis (France)*, pp. 11-16 (1981).

Pascal, J. C. "Consequences de la structure rotationnelle des champs d'intensity acoustique." *Proc. 2nd International Congress on Acoustic Intensity, Senlis (France)*, pp. 97-104 (1985).

Pascal, J. C. and Lu, J., "Advantage of the Vectorial Nature of Acoustic Intensity to Describe Sound Fields." *Proc. of Internoise-84*, pp. 1111-1114 (1984).

Pierce, A. D. *Acoustics - An Introduction to its Physical Principles and Applications*. McGraw-Hill, New York (1981).

Rayleigh, L., *Theory of Sound*. Vol. 1, MacMillan and Co., London, (1926).

Romano, A.J., "Linear Systems Approach to Image Source Representations of the Sound Field in Enclosures." Ph.D. Thesis, The Pennsylvania State University (1986).

Schmidt, W., "Non-Contact Objective Quality Control by means of Intensity-Measurement-Techniques." Proc. 2nd International Congress on Acoustic Intensity, Senlis (France), pp. 369-373 (1985).

Schultz, T. J., Smith, P. W., Jr., and Malme, C. I., "Intensity Measurements in Nearfields and Reverberant Spaces." Bolt, Beranek, and Newman, Inc., Report No. 1135 (1964).

Schultz, T. J., Smith, P. W., Jr., and Malme, C. I., "Measurements of Acoustic Intensity in Reactive Sound Field." J. Acoust. Soc. Am., 57(6), pp. 1263-1268 (1975).

Skelton, E. A., and Waterhouse, R. V., "Energy Streamlines for a Spherical Shell Scattering Plane Waves." J. Acoust. Soc. Am., 80(5) pp. 1473-1478 (1986).

Skudrzyk, E., *Foundations of Acoustics*, Springer-Verlag, Wien, New York (1971).

Tichy, J. "Acoustic Intensity Measurements - A Review." Proc. AIAA/NASA 9th Aeroacoustic Conference, AIAA-84-2310 (1984).

Tichy, J., and Mann, J. A., "Use of the Complex Intensity for Sound Radiation and Sound Field Studies." Proc. 2nd International Congress on Acoustic Intensity, Senlis (France), pp. 113-120 (1985).

Waterhouse, R. V., "Vortex Modes in Rooms." J. Acoust. Soc. Am., 82(5), pp. 1782-1792 (1987).

Waterhouse, R. V., Crighton, D. G., and Ffowcs-Williams, J. E., "A Criterion for an Energy Vortex in a Sound Field." *J. Acoust. Soc. Am.*, 81(5), pp. 1323-1326 (1987).

Waterhouse, R. V., and Feit, D., "Equal-Energy Streamlines." *J. Acoust. Soc. Am.*, 80(2), pp. 681-684 (1985).

Waterhouse, R. V., Yates, T. W., Feit, D., and Liu, Y. N., "Energy Streamlines of a Sound Source." *J. Acoust. Soc. Am.* 78(2), pp. 758-762 (1985).

Whitham, G., "A Note on Group Velocity." *J. Fluid Mech.*, 9, pp. 347-352 (1960).

Whitham, G., "Group Velocity and Energy Propagation for Three-Dimensional Waves." *Comm. on Pure and Applied Math.*, 14, pp. 675-691 (1961).

Williams, E. G., Dardy, H. D., and Finke, R. G., "A Technique for Measurement of Structure-Borne Intensity in Plates." *J. Acoust. Soc. Am.*, 78(6), pp. 2061-2068 (1985).

Williams, E. G., Dardy, H. D., and Washburn, K. B., "Generalized Nearfield Acoustical Holography for Cylindrical Geometry: Theory and Experiment." *J. Acoust. Soc. Am.*, 81(2), pp. 381-407 (1987).